Czech Technical University in Prague
Faculty of Electrical Engineering
Department of Control Engineering

Detection and Estimation of Human Movement Using Inertial Sensors: Applications in Neurology

Doctoral Thesis

Otakar Šprdlík

2012

Ph.D. Programme: Electrical Engineering and Information Technology

Branch of study: Control Engineering and Robotics

Supervisor: Zdeněk Hurák

Acknowledgment

In the first place, I would like to thank my supervisor Zdeněk Hurák for giving me the opportunity to work in such an amazing field and for his advices, support, encouragement, and patience throughout all those years he had to wait for this thesis to materialize.

I give my thanks also to all other close colleagues from the University and from the Institute of Information Theory and Automation of the Academy of Sciences of the Czech Republic for discussions, creating good atmosphere, and some of them also for serving as subjects in a study presented in one of the chapters. Very inspiring and helpful were especially Petr Augusta and Sergej Čelikovský. They also encouraged me at right moments to continue with the work and finish this thesis.

Essential to my work was the tight cooperation with a team at Department of Neurology, Charles University 1st Medical Faculty and General Teaching Hospital in Prague, lead by professor Evžen Růžička. Conducting a research in an engineering discipline while staying in a close contact with practicing (and yet research-oriented) neurologists and rehabilitation specialists was an inspiring experience. Although I am thankful to numerous members of the department who helped me, I would like to express my special obligations to Evžen Růžička, Martina Hoskovcová, and Robert Jech for fruitful discussions and collaboration on our joint research papers. Needless to say that besides the numerous discussions I certainly benefited from collaboration with them through being granted an access to their equipment for motion tracking. Last but not least, I also appreciate the opportunity to join this team in other research ventures in the domain of Parkinson disease through a partial employment at the department towards the end of my dissertation period. Although closely related, this research is not covered by this thesis.

During this collaboration, I had an opportunity to meet Zdenka Uhríková – a Ph.D. student from Center for Machine Perception at my home university – who was also involved in the research of tremor quantification with the same team of neurologists, although she relied on processing image signals. Having similar background, I benefited much from discussions with her.

In my work, I also benefited from my Erasmus stay at Biomedical Signals and Systems Group at University of Twente, the Netherlands in the period December 2006 through March 2007. The focus of this research stay was on ambulatory monitoring in Parkinson's disease. Also my first thoughts and attempts leading to one of the thesis chapters (accelerometer calibration) originated in that time. Many members and students at the group deserve my thanks. In particular, I would like to acknowledge Peter Veltink and Ciska Heida who supervised my efforts there.

I give my greatest thanks to my parents and all the family for nice childhood, support, and patience, and to Lucie for being with me and for her lovely support and tolerance in the time of writing.

Financially, my research presented in the thesis was supported by Czech Ministry of Education under project 1M0567 (Center of Applied Cybernetics) and partially also by Grant Agency of the Czech Republic under the project 102/03/H116. Attendance at an international conference was supported by internal grant CTU0615413 of the Czech Technical University in Prague.

Contents

Notations

Here are described some essential terms used in the thesis. The table bellow shows abbreviations and widely used symbols.

Attitude is the orientation of an object in a selected reference frame. Mathematically, it is described by a parametrization of the rotation from the reference frame to a frame with the axes parallel to defined axes the object. Usually, an Earth surface-fixed reference frame is used. In some literature, the term attitude is used for what we call inclination or tilt.

Inclination (tilt) is the orientation of an object relative to vertical. In the inclination, there is less information than in the full attitude: the azimuth is missing. Mathematically, the inclination is described by the projection of a vertical vector to the frame defined by the object axes.

Pose is a term to cover the attitude together with position.

Gravitational acceleration, called in the thesis, is the acceleration of a free falling object on the Earth in vacuum. It is influenced dominantly by the gravity and also by the (fictitious) centrifugal force from the Earth rotation. Such convention is common in the field of tracking motion of humans or slow moving objects on the Earth, because it is not necessary to differentiate between the effects of the two phenomena.

Tremor is a *rhythmical, involuntary oscillatory movement of a body part.*

Physiological tremor *is present in every normal subject and every joint or muscle that is free to oscillate. Normal physiological tremor can just be seen with the naked eye.*

Pathological tremor is any tremor caused by a disorder. It may be manifested in different conditions, some of them are described in the following lines.

Rest tremor is *tremor that occurs in a body part that is not voluntarily activated and is completely supported against gravity (ideally, resting on a couch).*

Postural tremor is *present while voluntarily maintaining a position against gravity.*

Intention tremor is a *tremor during target-directed movements.*

Slanted text is a quotation from Deuschl et al. (1998).

Symbol	Meaning
EMG	Electromyography – measurement of the muscle electrical activity
EKF	Extended Kalman filter
FES	Functional electrical stimulation
f_s	Sampling frequency [Hz]
ϕ_m	Local magnetic inclination of the Earth magnetic field
g	Size of the gravitational acceleration on Earth ($\sim 9.81\,\mathrm{m\,s^{-2}}$)
IMU	Inertial measurement unit
$\mathcal{I}_n$	Identity matrix of size n
IQR	Inter-quartile range (3/4 quartile − 1/4 quartile)
PSD	Power spectral density
q	Quaternion
$\overline{q}$	Conjugate of quaternion q
Q	Covariance matrix of process noise, or quaternion multiplication matrix
R	Covariance matrix of output measurement noise, or rotation matrix
RMS	Root mean square
RMSE	RMS error
ROC	Receiver operating characteristic
T_s	Sampling period [s]
UKF	Unscented Kalman filter
$\times$	Cross product
$[a\times]$	Matrix of cross product of vector a: $a \times b = [a\times]\, b$
$\bullet$	Quaternion multiplication

Chapter 1

Introduction

1.1 Motivation and general introduction

Measurement with inertial sensors (accelerometers and/or gyroscopes) has been used in many applications through last decades. Navigation systems, airbag activation, car alarms, and camera stabilization are examples. One of the fields of application is medicine, where inertial measurements can supplement or replace other means of measurement or assessment for clinical diagnosis like video-based motion analysis, assessment of tremor and other symptoms by visual observation, or measurement of postural stability by posturographs. Since inertial sensors made with the micro-electro-mechanical systems (MEMS) technology are small components with low power consumption, they can be fixed easily to a human body part or to several places to acquire data related to the motion of the respective body segments. They can be essential parts of body-worn assistive devices for rehabilitation, movement data collection in daily life, or even restoration of a function lost due to an accident or disease.

In neurology, the analysis of human movements is an important part of the assessment. It helps to find the problems, quantify them, and to keep track of the disease development or treatment effect in time.

One typical target of the movement quantification in neurology is the assessment and monitoring in Parkinson's disease. The cause of the disease is still unknown but there is a reduction of dopamine in the substantial nigra of the brain causing large scale of disabilities of motor control (control of human movements by central nervous system). Most typical problems are rest tremor, bradykinesia (slowness of movements), hypokinesia (lack of voluntary movements), or rigidity (increase of resistance to joint movements). All these symptoms can be reduced by dopaminergic drugs (drugs increasing amount of dopamine in the substantial nigra) as levodopa. Drug's effect lasts in several hours after the intake, patient is said to be in the *on* state during the time of the effect – patient's motor control ability is increased, potentially to the normal function. The other time periods with the most severe above mentioned symptoms are referred as *off* state. As the disease develops and levodopa-based therapy continues, its efficiency decreases. Time of on state shortens, on/off fluctuations may occur, and abnormal involuntary movements (referred as levodopa-induced dyskinesias) of various character can emerge during the on state. Suitable adjustment of dosing minimizes occurrence of dyskinesias and duration of the off states. It demands good knowledge of patient's motor state and of the disabilities through time. Up to date, occa-

sional clinical diagnosis and home-filled diaries are the means of assessment. Self-assessment is subjective, does not describe the state in a detail, and it needs making notes in a consistent and reliable way. As an alternative, all-day measurements of patients movement can be performed and motor control state can be estimated from the signals. A flexible and feasible way is to measure accelerations and angular rates by small unobtrusive sensors fixed on the human body during whole day at home or even outdoor (Keijsers et al. 2003).

Essential tremor is another example. It is manifested typically only by the tremor itself. Connections to other possible problems are targets of many current investigations. Accurate quantification of the tremor and assessment of other movements may help in these efforts.

There are many other disorders which are or potentially can be the fields of movement analysis and therefore also of inertial measurements. These include disorders of balance, other types of tremor, disorders and injuries influencing the ability to walk, and others.

The objective of this thesis is to develop new and improve existing methods used in human motion assessment by inertial sensors for neurology application area. The developments shall be in the processing of the measured data by estimation methods. From the large field, tremor assessment and accelerometer calibration were chosen to be the subjects of development.

1.2 Contribution of the thesis

This thesis contributes to the field of the inertial measurements for human motion assessment especially in the accelerometer calibration and tremor assessment. Selected particular contributions follow.

- Design of a new criterion for ellipsoid fitting to be used in a procedure for accelerometer calibration from data collected in nearly static conditions.

- Comparison of several ellipsoid fitting methods mainly in situations when the collected data have only a limited range – simulating the probable situation in in-use accelerometer calibration: that the sensor is positioned only in a limited range of possible inclinations.

- Finding that even during a severe hand tremor it is possible to estimate the attitude by the inertial estimation with a certain accuracy.

- Proposal to estimate the center of rotation during hand tremor and finding that it may increase the accuracy of inertial estimation compared to the situation when no model of the motion used.

- Experimental determination of how big is the gravitational artifact in the oscillatory tremor acceleration signal when measuring at hands.

- Accurate regression of a visual tremor scoring done by trained clinicians using features extracted from the data captured with inertial measurement units attached to hands.

- According to my knowledge an original method to find the relative orientation of two attitude measurement systems.

1.3 Author's publications related to the topic of the thesis

At the beginning of my PhD studies, I focused on more topics of the field. One of them was the on-line detection of gait events with potential application in functional electrical stimulation (FES) for restoring some gait features in people with paresis of a part of the leg. More specifically, I focused on estimating gait events with the use of assumptions about the acceleration at heel (zero when standing, up at heel-off) but with the use of the sensors placed at shanks. An early attempt in the topic was presented in

> O. Šprdlík and Z. Hurák: Inertial gait phase detection: polynomial nullspace approach. In *Proceedings of the 6th IFAC Symposium on Modelling and Control in Biomedical Systems*. Reims, France, ISBN-10: 0080445306, 2006.

Although the topic stayed in my larger scope of interest, I partially skipped it in favor of other topics. However, gait phase detection was also part of my later work in a study of Parkinson's disease, but only using algorithms published by others. Also, I had this topic in mind when developing the here presented algorithm for the estimation of the center of rotation with the use of an inertial measurement unit.

In the meantime, the accelerometer calibration was in my focus as an essential step to get accurate data from the sensors. A study of a subset of the accelerometer calibration methods forms a part of this thesis. The methods taken into account have the potential to calibrate the accelerometer directly from the in-use data collected with the sensors placed on a human body and thus to be suitable for the use in ambulatory conditions. An earlier version of the study was presented as a part of

> O. Šprdlík and Z. Hurák: Ambulatory Assessment in Parkinson's Disease: Use of Inertial Sensors and Identification and Filtering Techniques. In *16th International Conference on Process Control*, 2007.

Approximately at that time, I was incorporated into a team working in a research of essential tremor and possible connected balance problems. My main task was to measure the tremor of the patients by inertial measurements units and to determine the tremor frequency and amplitude from them. At this point, I used the inertial estimation to find the gravitational and motion artifacts in the measured accelerometer data and to validate how these components can be useful in the assessment of the tremor severity and frequency. The results were presented at a conference technically co-sponsored by IEEE and then, substantially extended and hopefully in an improved form, in a special number of the Biomedical Signal Processing and Control journal. The paper is presented here in an edited form as one chapter.

> O. Šprdlík, Z. Hurák, M. Hoskovcová, and E. Růžička: Tremor analysis by decomposition of acceleration into gravity and inertial acceleration using inertial measurement unit. In *Proceedings of the 9th International Conference on Information Technology and Applications in Biomedicine*, 2009.

> O. Šprdlík, Z. Hurák, M. Hoskovcová, O. Ulmanová, and E. Růžička: Tremor analysis by decomposition of acceleration into gravity and inertial acceleration using inertial measurement unit. *Biomedical Signal Processing and Control* 6(3), 2011.

In the same study, video recordings were made in some of the subjects. The recordings were analyzed using algorithms by Zdenka Uhríková to estimate the tremor frequency. We validated the obtained frequencies using the accelerometer data:

> Z. Uhríková, O. Šprdlík, V. Hlaváč, and E. Růžička: Action tremor analysis from ordinary video sequence. In *Annual International Conference of the IEEE Engineering in Medicine and Biology Society*, 2009.
>
> Z. Uhríková, O. Šprdlík, M. Hoskovcová, A. Komárek, O. Ulmanová, V. Hlaváč, C. D. Nugent, and E. Růžička: Validation of a new tool for automatic assessment of tremor frequency from video recordings. *Journal of Neuroscience Methods* 198(1), 2011

The main results of the study – the clinical outcomes – have been presented at medical conferences but accompanied only by abstracts. A more detailed publication with a greater impact has been recently submitted to an international journal:

> M. Hoskovcová, O. Ulmanová, O. Šprdlík, T. Sieger, J. Nováková, R. Jech, E. Růžička: Disorders of balance and gait in essential tremor are associated with midline tremor and age. 2012. Submitted.

In the last two years, the team worked also on a study of falls in patients with Parkinson's disease. My task was to estimate various motion-related parameters from the *timed up and go* test performed by patients wearing inertial sensors. That included analysis of the gait and other movements done during the test. The methods were largely adopted from the literature with only some tunings and small changes, none of them seen by us up to now so significant to deserve a separate publication of the modified method. The data collection is done, the data are analyzed and statistically processed. Up to now, preliminary results have been presented at medical conferences but accompanied only by abstracts. Publications with full results and greater impact will be prepared.

1.4 Outline of the thesis

In the first part of the thesis, in chapters 2 and 3, short introductions are given to the studied fields. Chapters 4 to 7 provide the core of the thesis. Usually, they provide also the corresponding conclusions. Chapter 8 contains the general conclusion and suggestions for future work. It is followed by the list of referenced publications and by two appendices.

Chapters 2 and 3 provide short introductions to the inertial measurements and to the published approaches of their usage in neurology and rehabilitation. Reader with a knowledge of any of these fields may skip reading the corresponding chapter. However, the following chapters may refer to these introductory texts and also the reader may browse back for some definitions and naming. These chapters are intended to give only some basics of the fields. Later chapters 4 and 5 contain more detailed literature surveys of the corresponding fields: accelerometer calibration and tremor quantification by inertial sensors, respectively.

Chapter 4 provides a study of accelerometer calibration from the data measured in static or nearly-static (quasi-static) conditions. The core part of such a calibration is an ellipsoid fitting to the measured data. A new method is proposed and compared with several existing ones. The methods are used later in the other chapters for the calibration of accelerometer biases and gains, although the main feature compared among the methods – their performance in data distributed in a limited range – is not essential there.

Chapter 5 contains a study of human tremor quantification using different components of the accelerometer measurement and the gyroscope measurement as the signals to be related to the tremor intensity and frequency. The text corresponds to one of our published papers except for a few edits. Besides the accelerometer and gyroscope measurements, inertial estimation is used to decompose the accelerometer measurement to the gravitational and motion components. All such obtained signals are used to quantify the tremor and to predict a visual scoring assessment done by clinicians.

Chapter 6 consists of two parts, each describing one important method used in the following chapter. Although both the proposed procedures were motivated by the use in the next chapter, their application field may be potentially much larger. The first of them is dedicated to find the center of rotation in the case of an unknown rotation motion of an inertial measurement unit. The second method is proposed to find the relative orientations of two different technical systems for the attitude measurement.

Chapter 7 is dedicated to the accuracy of the inertial attitude estimation during tremulous motion. That way, achievable accuracy of the attitude estimation scheme from chapter 5 is estimated, although it is not its perfect validation. The phenomenon studied is the rotation motion, mainly its influence to the accelerometer measurement and how are different inertial attitude estimation methods able to deal with it. Numerical simulations of exact rotational motion and tremor mimicking by healthy humans are used. The methods of chapter 6 are used to enhance the attitude assessment in the tremor with a (partial) rotation character and to enable a validation against another attitude measurement system.

There are two appendices attached. The first of them contains only a short description of a non-core computation for saving the space in the main text. The second one is an additional list of publications regarding the assessment of tremor using motion measurement and a categorization of the publications according to several criteria. The attachment is intended to supplement the introductory texts on the tremor measurement given in the main part. A secondary objective is to relate the methods published in papers with my co-authorship to others, in the context of the few criteria.

Chapter 2

Introduction to Inertial Measurements and Estimation

2.1 MEMS based accelerometers

2.1.1 Principles and the state of fabrication

Accelerometer is a sensor dedicated to measure its own linear acceleration. The core of the sensor usually consist of a mass connected to the sensor's platform by a spring-damper link. When the sensor is accelerated the mass moves relatively to the sensor housing in the opposite direction than is the direction of the movement, see figure 2.1. The displacement of the mass proportional to the force of the spring element may be measured. Capacity measurement of the displacement if often used. It is then transformed to the sensor output (analog or digital), which is proportional to the acceleration. Nowadays, most of accelerometers are produced by the MEMS (Microelectromechanical Systems) technology reaching sizes of few millimeters and consumption of several hundreds of μA. There are accelerometers measuring acceleration in one, two, or all three axes.

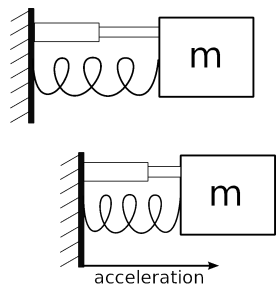

Figure 2.1: Accelerometer principle

2.1.2 What do they measure?

As noted above, the core of the accelerometer is the measurement of the forces between a mass and the housing to which the mass is connected. All phenomena causing these forces are identical with the specific force. Specific force (called also proper acceleration) is the difference between the instantaneous acceleration and free fall. In the case of a free fall, accelerometer measures zero. For a sensor being still at Earth surface, specific force is heading vertically up and has the size of the gravitational acceleration. The projection of the specific force to the sensor axes is measured. The measurement is

$$a_{\mathrm{m}} = R\left(\begin{bmatrix} 0 \\ 0 \\ \mathrm{g} \end{bmatrix} + a\right) \tag{2.1}$$

where R is the orientation matrix of the sensor in an Earth-fixed reference frame (base) having the third axis oriented vertically up, i.e. the rotation matrix of the rotation from the base to the local reference frame of the moving sensor. g is the size of the local gravitational acceleration (about $9.81\,\mathrm{m\,s^{-2}}$) and acceleration a is the instantaneous acceleration of the sensor with respect to the base expressed in the base coordinates. Coriolis effect due to the motion in the frame fixed to rotating Earth is neglected here.

The first part of (2.1) – $R\,[0 \;\; 0 \;\; \mathrm{g}]^{\mathrm{T}}$ – is called gravitational component or artifact in the text of the thesis. The second part – $R\,a$ in the sensor frame and a in the base-frame – is called motion acceleration or motion component.

2.1.3 Errors

Accelerometer output suffers from various errors, for example

- bias and gain error and their time drift, which is caused in a big part by temperature changes,
- nonlinearity,
- non-orthogonality and misalignment of sensor axes,
- zero-mean noise.

The nonlinearity is not marked and its compensation is not needed in most applications, otherwise its precise identification for applications demanding very high precision is not feasible without suitable equipment. Bias, gain error, non-orthogonality, and temperature drift can be calibrated more easily, but temperature sensor is needed for the partial drift compensation. The calibration procedure usually consists of putting the sensor to a number of orientations with respect to gravity. In such cases, only the gravitational component is measured by the accelerometer. That fact is used in geometrical calculations to estimate parameters of a model of the mentioned errors. See Ferraris et al. (1995) for a classical publication giving a complex procedure to estimate the parameters including the non-orthogonality. Some other approaches to calibration with possibility to applicate them directly to the in-use data are mentioned and/or described in chapter 4.

2.2 MEMS based gyros

2.2.1 Principles and the state of fabrication

Rate gyroscope (gyro) is dedicated to measure its own angular rate. Several principles have been introduced. For example laser gyros are often used in aviation navigation because of their accuracy. Vibrating mass gyros produced with the MEMS technology are small, low-power, but less accurate. They are based on the Coriolis effect. Nowadays, their power consumption is usually several mA per axis. That is somewhat more than for accelerometers, but still low and also usable in many battery-powered applications. The consumption limits them only in applications where long-term monitoring with the use of a very small battery is desired. Most of MEMS gyros produced until now have only one measurement axis, gyroscopes of several types have two of them. For years, making a 3D rate gyro from MEMS sensors implied usage of three single-axis gyros or one single-axis and one dual-axis gyro in a common bigger housing and – if not precalibrated by a producer – calibrating for misalignment caused by imperfect placement of the sensors into the housing. But recently, even 3D MEMS single-chip rate gyros of sizes of about 5×5 mm or lower have been made available (InvenSense 2011, Kionix 2011, VTI Technologies 2011).

2.2.2 What do they measure?

Angular rate is the quantity measured by the rate gyroscopes. But the angular rate is at each time instant measured in the instantaneous coordinates of the sensor. That means, the space angles (or other expressions of attitude) of the sensor cannot be computed by the simple numerical integration of the separate signals from the sensor axes. The instantaneous rate of change of the attitude do not depend only on the instantaneous angular rate as measured, but also on the instantaneous attitude itself:

$$\dot{R} = -[\omega_{\mathrm{S}}\times]R \qquad \text{or} \qquad \dot{q} = \frac{1}{2}[\Omega_{\mathrm{S}}\times]\,q \qquad \text{or} \qquad \dot{z} = -\omega_{\mathrm{S}} \times z, \tag{2.2}$$

where R and q are the expressions of rotation from a fixed (base) reference frame to the local reference frame of the moving sensor by means of a rotation matrix and quaternion, respectively. Vector z is a fixed vector in the base coordinates expressed in the sensor reference frame. Quantity ω_{S} is the rotational velocity of the sensor with respect to the base, expressed in the sensor coordinates. Matrix $[\omega_{\mathrm{S}}\times]$ is the matrix of cross product ($[\omega_{\mathrm{S}}\times]\,x = \omega_{\mathrm{S}} \times x$). Matrix $[\Omega_{\mathrm{S}}\times]$ is an antisymmetric 4×4 matrix constructed from ω_{S} in the following way (subscript S omitted).

$$[\Omega\times] = \begin{bmatrix} 0 & -\omega_1 & -\omega_2 & -\omega_3 \\ \omega_1 & 0 & \omega_3 & -\omega_2 \\ \omega_2 & -\omega_3 & 0 & \omega_1 \\ \omega_3 & \omega_2 & -\omega_1 & 0 \end{bmatrix} \tag{2.3}$$

The velocity ω_S is the quantity measured by rate gyroscopes, but involved by various errors.

2.2.3 Errors

Rate gyroscopes suffer from errors of all types described for accelerometers. 5. Moreover, the output can also be sensitive to linear acceleration a little, and the bias effects can be

more pronounced. The calibration of the gyroscope is different compared to accelerometers. Bias is determined very easily if it is possible to measure with the sensor being still. Then, the angular rates are zero and the gyroscope shall measure zero. The only errors in this case are the bias and zero-mean measurement noise. By averaging the measurement in a time interval, we get the bias. On the other hand, the other errors are more dificult to measure, because dynamic conditions are needed. That means, a special equipment inducing exact rotation velocities or their accurate measurement is needed. For the estimation of the gains only, it is possible to use a procedure including rotations of the gyroscope between well known orientations instead of an accurate angular rate reference.

2.3 Magnetometers

2.3.1 Principles and the state of fabrication

Magnetometers are devices used for the measurement of the intensity and/or the direction of the magnetic field. When only the Earth magnetic field is present, the device can be used as a magnetic compass. MEMS magnetometers are small devices of size of few millimeters and possess three sensitive axes. Therefore, full vector of the magnetic field is measured. The direction of the local Earth magnetic field is described by the local magnetic inclination ϕ_m and magnetic declination. Magnetic inclination is the angle between the horizontal plane and the field vector. Magnetic declination is the angle between the north direction and the horizontal projection of the magnetic field. For example in the middle Europe, magnetic declination is near to zero, while magnetic inclination $\phi_\mathrm{m} = 60$ to 70 degrees – the vector is heading at this angle down. Bot the values change in time as the Earth magnetic field changes. See NOAA National Geophysical Data Center (2012) for a magnetic field calculators showing the values at different places and times based on a model.

The magnetometer measurement of the Earth magnetic field is

$$m = R \begin{bmatrix} \cos\phi_\mathrm{m} \\ 0 \\ -\sin\phi_\mathrm{m} \end{bmatrix} \tag{2.4}$$

where R is the rotation matrix from a specific base coordinate system to the coordinate system specified by the sensor axes. The base coordinate system has the first axis heading to the magnetic north and the third axis heading vertically up.

2.3.2 Errors

Besides the noise, bias, gain error, non-linearity, and non-orthogonality, magnetometers suffer from magnetic disturbances in their neighborhood. The most marked disturbances belong into the two following groups,

- disturbances by magnetic materials fixed to the same moving body as the magnetometer,
- disturbances by magnetic materials not moving exactly with the sensor and by the magnetic field caused by non-constant electric currents.

The first group of the disturbances consists of hard-iron effects (permanent magnets) and soft-iron effects (materials deforming the Earth magnetic field). They cause additional bias

and additional gain error and rotation, respectively. Both the effects may be compensated, see e. g. Gebre-Egziabher et al. (2006). The second group can be compensated if the disturbances are known exactly, but that is normally not the case. Under some conditions, the disturbances may be estimated and compensated dynamically (Roetenberg et al. 2005).

2.4 Attitude estimation using inertial measurements

2.4.1 Purely rotational motion

If an accelerometer is still or it is only rotating around its center, the motion acceleration a in (2.1) is zero. Therefore, the accelerometer measures the projection of a vertical vector of size g to the coordinates of the sensor. The measurement itself or its low-pass component to reduce the noise may be used as a measure of the sensor inclination. When dividing the measurement by its 2-norm, we get a unit vector which is identical with the last column of the orientation matrix R in (2.1).

To get a full expression for the attitude, e. g. the orientation matrix or quaternion, an additional measurement is needed. One possibility is to use a magnetometer and its measurement model (2.4). There are different approaches how to fuse the two measurements. An intuitive approach which is a good choice especially if the accelerometer is really not accelerating in space, is to use the accelerometer to determine the inclination and the magnetometer only to add the missing information: the azimuth. Another possibility is to enable the magnetometer measurement to influence also other components of the attitude estimate, for example by a least squares fitting of the rotated accelerometer and magnetometer measurements to the known directions in the Earth-fixed reference frame. The task of this fitting is a simple example (only 2 measurements) of the general Wahba problem (Wahba 1966) and may be solved in a time-efficient way (Markley 2002).

2.4.2 Rotation and translation

If the sensor is translating and the motion is not a uniform linear motion then the accelerometer does not provide an accurate measurement of the inclination. That may be partially solved by an incorporation of a rate gyroscope measurement.

In the simplest approach, accelerometers are used for the inclination estimate at situations when no motion is detected. The situations may be recognized e. g. by zero angular velocity and still accelerometer measurement having 2 norm equal g. Between these static situations, the attitude or inclination is determined only by solving (2.2). Similar approach was used by Negård et al. (2005) for the on-foot navigation.

If the existence of the no-motion states is not guaranteed or the time between them is too long then the estimate from (2.2) fails to be good because it is not stable – the errors integrate in time, especially the biases. Then, the accelerometer must be used even though it does not provide a good instantaneous measurement of the inclination. For technical systems with known models and additional measurements of the internal states or speed or position, e. g. airplanes, the motion component of acceleration may be estimated well and subtracted from the accelerometer measurement to get a good inclination estimate. Similar approach is possible also for the human applications if more sensors are placed at several connected body segments and joint models are used (Hyde et al. 2008).

For monitoring of human motion by using only one inertial measurement unit (IMU) or more IMUs but placed at not directly connected segments, there is no exact model. Still,

the motion acceleration may be roughly estimated by a general dynamical model assuming it to have a character of a low frequency noise (Luinge and Veltink 2005). Zero-mean motion acceleration is assumed in such a case. This assumption is valid in normal situation when the subject is moving only by its own locomotion – if a body part accelerates, it must also soon decelerate. However, in many applications in the human motion or small flying devices, this model is not used and the whole accelerometer signal (Zhu and Zhou 2004) or its direction (Mahony et al. 2008) is directly used to provide the reference inclination measurement which influences the attitude estimate at low frequencies.

For fusing the gyroscope data with the accelerometer and magnetometer measurements, a dynamical filter is used – often a simple complemetary filter, or an observer for nonlinear systems, usually based on Kalman filtering principles. Additional quantities may be estimated to improve the accuracy in presence of some specific errors. That is often the case of the gyro bias (Luinge and Veltink 2005, Negård et al. 2005, Mahony et al. 2008).

2.5 Instrumentation

2.5.1 Available to us

In the first months of my PhD studies, I created a simple autonomous acceleration measurement unit consisting of a two-axis accelerometer ADXL202 (Analog Devices) and a small flash memory to store the measurements. The size of the device was about $50 \times 35 \times 15\,\text{mm}$ and the weight 16 grams (without battery). It was povered by a small external battery, and controlled by a single button used to start and stop measurements. However, I used it only for few first experiments. For most of the consecutive work and the results in the thesis, commertially available inertial measurement units (IMUs) were used. In particular, the series MTx produced by Xsens, The Netherlands. The IMU is a 3D accelerometer, 3D gyroscope, 3D magnetometer, and a temperature sensor contained in a single package of size $53 \times 38 \times 21\,\text{mm}$ and weight of about 30 grams (Xsens Technologies 2010). The measured data are calibrated for in-factory determined biases, gains, nonorthogonalities, and temperature drifts. Therefore, the data are well calibrated except the additional drifts not covered by the temperature compensation.

The IMUs contain also proprietary Xsens attitude estimation algorithms fusing all the measurements. The results may be sent on-line in the form of quaternion, rotation matrix, or Euler angles from the IMU besides the measured data. Alternatively, the same algorithms implemented in supplied software may be applied offline in PC to raw data acquired from the IMUs.

The MTx devices are produced and sold in several variants with different sensor ranges and communication interfaces. There are two possibilities how to connect the MTx devices to PC which collects data,

- direct connection of single MTx to PC via RS232/USB converter and the USB ports of the PC,
- connection of several MTx to Xbus Master device via the proprietary serial line Xbus and connection of Xbus Master to PC via USB port or Bluetooth wireless connection.

For most of the time of my PhD studies, two devices supporting the first type of communication were available. They were used in the study in chapter 5 and for short validation measurements in section 6.1. When connected to PC independently, both the

Company, Device	Size (mm)	Magn.	Fusion
Analog Devices			
www.analog.com			
ADIS16367	$23 \times 23 \times 23$	-	-
ADIS16334	$33 \times 22 \times 11$	-	-
ADIS16400	$23 \times 23 \times 23$	X	-
InterSense			
www.intersense.com			
NavChip	$24 \times 13.5 \times 9.1$	-	-
InvenSense			
invensense.com			
MPU-6050	$4 \times 4 \times 0.9$	-	X
MPU-9150 (to be available)	$4 \times 4 \times 0.9$	X	X
ST Microelectronics			
www.st.com			
LMS330DLC	$5 \times 4 \times 1.1$	-	-

Table 2.1: Combo-devices: Single-package electronic parts including a 3D gyroscope and 3D accelerometer. **Magn.:** also 3D magnetometer included. **Fusion:** included a platform for fusion of the sensor data for gesture recognition and/or other applications.

sensors provide own timing. To ensure synchronous sampling and starts of measurements in the study of the essential tremor, I constructed a device which generates a clock signal of a specified frequency and this signal is sent to both MTx to force common timing. The device provides also synchronous measurement of pressure by a force sensing resistor (FSR) which can be used for example to determine the moments when a patient touches a target by a finger in a test for the intention tremor.

Later, five devices enabling the second type of communication (via Xbus) were available at Neurological Clinic of Charles University and General University hospital in Prague. These devices are used primarily in a study of gait and other movements of Parkinson patients which is not the core of this thesis, but they were also used for the measurements in chapter 7.

2.5.2 On the market

Only few alternatives to the above described system were available in the first years (about 2006). One big alternative was to produce own dedicated measurement system, but that would lead to additional time burden. Besides taking care of the communication and powering, the construction of full IMU implied until recently a careful mounting of a set of single sensors and a bulky calibration.

During few last years, also devices combining 3-axis accelerometers and 3-axis rate gyroscopes became widely available, see table 2.1. They are usually precalibrated from factory for misalignments and sometimes also the temperature bias drifts are partially compensated. The devices are in fact IMUs, but they need additional interfaces to communicate with PC or to store the measured data. But still, they make the construction of a ready-to-use IMU more easy. For Analog Devices ADIS line, only few examples are listed from a wide range of products. The line is focused more on technical applications and provide low gyroscope measurement ranges (less or equal 300 °/s) and therefore has limited usability

in human motion applications, except ADIS16367 (1200 °/s). By comparing the available datasheets at the time of writing, the larger devices (ADIS and NavChip) tend to have better gyroscope accuracy.

Ready-to-use wearable IMUs are produced by several companies. The commercially available devices are listed in table 2.2. The information was get from public materials on the Internet, for MTx partially also from own experience. The columns of the table have the following meaning:

Size: Maximum dimension of IMU excluding cables and connectors. Kinesia device consists of two parts connected by a short and flexible cable: sensor unit and control unit.

Weight: Weight of IMU excluding cables.

Accel., Gyro, Magn.:
X – the measurement unit contains the sensor and can provide the data from its measurement;
x? – the sensor is included in IMU and used to estimate the attitude, but it is not stated if also the sensor measurements can be provided.

Fusion: IMU contains a build-in attitude estimator fusing the measured data.

Cable: IMU can send the data on-line by a wired connection.

Wireless:
X – each IMU can send the data on-line by a wireless connection;
x – IMUs send the data by a cable to a central unit, which can send them to a computer by a wireless connection.

Storage: IMU contains a build-in memory to store the measured data for later transfer to a computer.

Synchr.: How many IMUs can be connected and synchronized using a provided central device. Two numbers signalize the possibility to use two central devices synchronously.

A number with '?' – how many IMUs can be connected for simultaneous data acquisition using a provided device, but it is not stated explicitly if the data acquisition is synchronized;

x – synchronization is possible only by a user-provided external synchronization signal;

start – only the start of the measurement can be synchronized via a cable connection, then each IMU uses its own internal clock.

Frequency: Maximum acquisition frequency (internal sampling frequency may be higher).

Company, Device	Size (mm)	Weight (grams)	Accel.	Gyro	Magn.	Fusion	Cable	Wireless	Storage	Synchr. (devices)	Frequency
Xsens											
www.xsens.com											
MTx-28A (RS232/USB)	53	30	X	X	X	X	X	-	-	x	orient.: 256 Hz; data: 512 Hz
MTx-49A (Xbus)	53	30	X	X	X	X	X	x	-	10+10	1 unit, data: 512 Hz; 5 units, raw data, Bluetooth: 100 Hz
MTw	58	27	X	X	X	X	-	X	-	32	1 unit, 120 Hz; 6 units 75 Hz
McRoberts											
www.mcroberts.nl											
DynaPort	88	55	X	-	-	-	?	-	X	-	100 Hz
Hybrid	87	74	X	X	-	-	?	X	X	start	100 Hz
InterSense											
www.intersense.com											
InertiaCube2+	37	17	x?	x?	x?	X	X	-	-	?	180 Hz
InertiaCube3+	39	17	X	X	X	X	X	-	-	?	180 Hz
Wireless InertiaCube3	43	20	X	X	X	X	-	X	-	?	1 unit: 180 Hz; 4 units: 120 Hz
InertiaCubeBT	60	67	x?	x?	x?	X	-	X	-	?	180 Hz
GLI Interactive											
www.motionnode.com											
MotionNode	35	10	X	X	X	X	X	x	-	20?	100 Hz
Microstrain											
www.microstrain.com											
3DM-GX3 -25	44	18	X	X	X	X	X	-	-	-	1 kHz
Movea											
www.movea.com											
MotionPod	31	14	X	X	X	X	-	X	-	32?	200 Hz up to 5 units
CleveMed											
www.clevemed.com											
Kinesia	15+80	5.7+85	X	X	-	-	-	X	X	-	128 Hz

Table 2.2: Wearable IMU devices available on market. For the exact description of the columns, see the text starting at page 13

Chapter 3

Brief Survey of Methods of Human Motion Assessment based on Inertial Sensors

This is a very brief overview of the instrumented assessment of movement, symptoms of neurological disorders or overall patient's motor state using body-worn inertial sensors. The survey is far from being complete – both the details about the single assessments and the listed possible assessments are limited. Other areas of use of inertial sensors in human movement assessment and monitoring include the quantification of dyskinesias (non-rhythmical involuntary movements) in Parkinson's disease or monitoring of proper conduction of rehabilitation exercises.

3.1 Activity monitoring

Activity monitoring is a method for discrimination of movement activity from rest, for classification of activities, or for quantification of general movement intensity.

This field can be divided into two parts, although many works deal with both of them:

- Quantification of the activity of the subject in long time intervals by means of percentage of time spent moving, or by mean movement intensity, or by some combination of them, e. g. percentage of motion time together with the intensity averaged only during the intervals when movements were detected.
- Discrimination of different body postures or different movement activities.

To the first point, several strategies were proposed to assess the total amount of patient's activity by measuring his motion: most simple actigraphs just counting threshold crossings of accelerometric signal, or some way of representing mean measured acceleration in a frequency band (Dunnewold et al. 1997, Mathie et al. 2003), or mean amplitude of acceleration derivative (Keijsers et al. 2006) or angular rate (Salarian et al. 2007b) during specified time periods or only in their parts when a movement was detected. The methods may be used to monitor people with movement problems or neurological disorders, e. g.

Parkinson's disease, people recovering from an injury or disease, or elderly. Such calculated features can be used also to estimate the energy expenditure (Bouten et al. 1994). All these methods represent rather general activity and "mean" intensity of one's movements than direct measure of any symptoms of a neurological disease. Although the outcomes often correlate reasonably with clinical scores of bradykinesia and hypokinesia in Parkinson's disease (Salarian et al. 2007b), they are still very dependent of one's daily routine, kind of activities intentionally performed during assessed time segment, and there are large inter-individual differences.

Detection of body postures, that means the discrimination between standing, sitting, and lying, or more detailed positions, gives some information about the person's activity and may form a part of a method for the assessment of some specific activity or symptom (Prill and Fahrenberg (2006), Zwartjes et al. (2010)). Several methods were proposed to do the detection. The most typical is just thresholding of the estimated inclinations of one or more body segments (Veltink et al. 1996, Dunnewold et al. 1998, Lyons et al. 2005). Typically, a trunk sensor is used to discriminate between lying and other positions and a thigh sensor is used to discriminate between standing and sitting. Najafi et al. (2003) and Salarian et al. (2007a) did not use a sensor on thigh. Instead, they used a detection and classification of the sit-to-stand and stand-to-sit transitions from simple signal features of other sensors, mainly the sensor at trunk.

Similar approaches were applied to discriminate not only between the statical body postures but also between several dynamical activities. They use predefined feature ranges (Veltink et al. 1996, Bussmann et al. 2001), or distances from values precollected in a standardized protocol (Foerster and Fahrenberg 2000), or classifiers learned with precollected larger training data (Bao and Intille 2004, Zwartjes et al. 2010). To include the classification of dynamical activities, also few other signal features were used, for example rectified and averaged high frequency components of signals for detection of motion of a body segment, or functions indicating peaks in data or in frequency spectra typical for walking.

See Godfrey et al. (2008) and Yang and Hsu (2010) for more detailed reviews of activity monitoring methods. The first one provides more details about the methods and the second one is a little more recent. Both of them reffer also to a number of commercially available activity monitoring systems.

3.2 Tremor detection and quantification

Tremor is a well observable and easily instrumentally detectable symptom of neurological disorders due to its alternating character. This is true especially for the rest tremor or postural tremor, where the body segment does no other marked motions except the tremor. Moreover, if a specific tremor type is searched for, only limited frequency band can be investigated (e. g. 3–8 Hz for the tremor in Parkinson's disease).

Many researchers detected and quantified tremor using miscellaneous instrumentation including motion-capture systems, tablets, electromyogram (EMG) recordings, and inertial sensors. The inertial sensors are most suitable for an ambulatory assessment due to their size, especially in case of a long-term monitoring. They are also a good choice for short-time assessments at clinics, although EMG may provide better measurement of the frequency of the pathological neuron firing. Especially if the body segment is loaded by a mass, the frequency spectrum of the accelerometer or other motion sensor may manifest two significant peaks, one of them connected to the pathological central oscillator and the

second one at a lower frequency depending on the mechanical properties of the segment and the mass (Hallet 1998).

Hand tremor is the usual subject of the studies. For sensor placement, wrists are commonly used for ambulatory monitoring (van Someren et al. 1998, Salarian et al. 2007b) due to the facility and acceptability. More distal segments are usually used for short-time assessments (hand back, a finger). Leg tremor was also detected and quantified (Sander et al. 1998, Zwartjes et al. 2010).

A 3D trajectory of tremor was not computed from the inertial measurements. Usually some not very complicated signal processing is applied directly to the measured quantities (acceleration or angular rate) or their integrals: Threshold crossing detection in filtered data (van Someren et al. 1998, Caligiuri and Tripp 2004), identification of autoregressive (AR) model of tremor time series (Timmer 1998, Salarian et al. 2007b), or direct spectral or frequency analysis via FFT (Foerster and Smeja 1999, Hoff et al. 2001) have been used. Comparing reported sensitivities and specificities of tremor detection during daily life activities using sensors at wrists, method of Salarian et al. (2007b) using rate gyroscopes and identification of AR model was somewhat more successful than van Someren et al. (1998) and Hoff et al. (2001) (noted by Salarian et al. (2007b)), but each verification was done with time series from different trials.

In the mentioned methods, tremor is usually quantified by the amplitude or power of acceleration or angular velocity. Sometimes (e. g. Pullman et al. (1994), Elble (2003)), the amplitude of velocity or displacement is estimated. Burkhard et al. (2002) reported strong negative dependence of spatial amplitude and tremor frequency in healthy subjects asked to simulate parkinsonian tremor. Using this observation and the fact that acceleration and velocity are more related to power and energy we guess that acceleration or velocity may be in fact more suitable for comparison of tremor intensity than spatial amplitude. On the other hand, the spatial amplitude is more related to the existing visual assessment techniques and likely it is more related to the severity of the real impairment: what is the preciseness of the affected hand and how visible is the tremor.

See section 5.1 for an overview with more details especially regarding the type of inertial sensor used and the presence of the gravitational artifact in the accelerometer measurement. See appendix B for more technical details and more referenced works: It contains a categorization of published papers on tremor quantification by movement measurement. The categorization is based on sensors used, their placement, amplitude and frequency extraction, and few other criteria.

3.3 Gait analysis

Many approaches have been published to analyze human walking, particularly its temporal, and sometimes also spatial parameters. Switches or pressure sensors under feet are sometimes used, for laboratory analysis it is possible to use 3D camera systems, and there is also possibility to use leg-worn or trunk-worn inertial sensors. Many of the methods were developed primarily for on-line detection of gait events (heel-off, terminal foot contact, heel strike, etc.) and to be used in a feedback for a functional electrical stimulation (FES) of lower leg or whole leg of patients with drop-foot problem or other leg paresis (Lyons et al. 2002). Other approaches are intended primarily to monitor gait parameters during a long period or during clinical assessment trials. Due to the character of the applications, an off-line analysis is enough. Gait parameters (cadence, step length, etc.) or the distance

walked are typically needed. Sometimes, also other details like joint angles of the position of the center of mass are of the interest.

For the timing detection it is possible to use shoe insole sensors of the pressure. Inertial sensors bring the possibility to estimate also spatial parameters and to place the sensors also to other places than under the feet. That may be helpful for example in case of the stimulation of peroneal nerve (Lyons et al. 2002): The stimulation electrodes are placed at upper part of shank and inertial sensors can be placed just next to them.

The methods of the gait event detectors based on inertial sensors differ based on the core ideas used. One possible approach is to assume that the foot or the position of the ankle is still or does not move much during the stance phase with the heel on the ground. Such approach may be used with the sensors at feet (Pappas et al. 2004) or by estimating the ankle acceleration by sensors placed on shanks (Willemsen et al. 1990). Another possibility is to work with the inclination angle of the lower leg or with the corresponding angular rate: When walking forward, the inclination of the shank is changing from forward lean to backward lean during most of the swing phase which lasts from the terminal foot contact to the next heel strike. During the stance phase, the shank inclination is changing in the opposite direction. A concrete used signal originating from a shank-mounted sensor may be the inclination as measured by an inclinometer (Dai et al. 1996) or accelerometer, or the angular rate measured by a rate gyroscope (Salarian et al. 2004).

Sensors placed at trunk are attractive because of easy fixation, especially at waist level, and because they may be also used for the detection of body positions (see section 3.1) and balance assessment (see section 3.6). Vertical and anterior-posterior accelerations of the trunk typically exhibit two periods during one gait cycle, because two steps (left and right) are performed during the cycle. For the detection of steps, the fact that peaks in the signals are present at the heel strikes may be used (Zijlstra and Hof 2003, Moe-Nilssen and Helbostad 2004). For the discrimination between the left and right steps, the acceleration in the medio-lateral axis (Zijlstra and Hof 2003) may be used. However, both the accuracy of step detection and of step quantification tend to be lower than with using sensors at legs.

The above referred works use various detection algorithms based on human knowledge about the signals at different gait events and phases. Alternatively, it is possible to use a machine learning method directly to the measured or slightly preprocessed data, e. g. Williamson and Andrews (2000) with shank-mounted accelerometers.

Inertial sensors are not used only for the detection of gait events and phases, but also to estimate the length of steps or consequently the distance walked. They may be estimated for example by double integration of foot acceleration (Negård et al. 2005) or by geometrical calculations using known lengths of legs or leg segments and the angular amplitudes of the leg motion (Salarian et al. 2004, Moore et al. 2007). Zijlstra and Hof (2003) uses a trunk sensor to estimate the step length. Known leg length and an estimate of the vertical trunk displacement from the accelerometer were used to estimate the step length.

Gait freezing and festinations are symptoms of the Parkinson's disease. Both can be observed not only in medication *off* state, but also during *on* state. The occurrence of freezing in the off state is higher than in the on state, but it may be reduced by the subthalamic nucleus stimulation (Davis et al. 2006). Several authors used instrumentation to detect freezing. Han et al. (2003) and Moore et al. (2008) used accelerometers placed above ankle. Hausdorff et al. (2003) used force sensors under the feet. All the groups used the fact that most freezing episodes are not pure akinetic states, but tremulous leg motion occurs due to patient's effort to move. The motion has typically not as sharp frequency spectrum as parkinsonian tremor (Hausdorff et al. 2003).

See Lyons et al. (2002), Kavanagh and Menz (2008), and Rueterbories et al. (2010) for reviews of the field. Lyons et al. (2002) focused specifically on the correction of the drop-foot problem and the on-line gait phase detection usable for the purpose. The two later reviews consider also the off-line processing and gait analysis. Kavanagh and Menz (2008) focused mainly on accelerometers, other sensors are hardly mentioned. They address especially the different goals and results of the studies which use accelerometers for gait analysis. Rueterbories et al. (2010) focused mainly on the sensor placement, sensor type, and the numbers of the sensors used and sensor axes processed in the published papers.

3.4 Rising from a chair

Timing aspects and difficulties of standing up have been reported as highly correlated to Parkinson disease stage and treatment (Bloem et al. 1997). Some of investigators used instrumentation to estimate the duration of the transition: Bloem et al. (1997) with a camera system, Giansanti and Maccioni (2006) with an accelerometer and gyroscope, Janssen et al. (2008) with a uniaxial accelerometer. Only thresholds of acceleration and/or angular rate variation were used to detect the start and the end of the movement – steady posture before and after the transition is needed. Giansanti and Maccioni (2006) needed the posture to be steady only relatively to the motion during the transition. Janssen et al. (2008) used only the measurement in the sagital direction, therefore the system was sensitive especially to the forward bending of the trunk but not to the motion in other directions. By the above methods, only the transitions conducted in well defined conditions may be detected and quantified, determining these methods practically only to clinical assessment where they may substitute time measurement by stop-watches and potentially also to add other quantities to describe the transition.

A little different approach to detection and assessment of standing up was proposed by Najafi et al. (2002) and altered by Salarian et al. (2007a). The algorithms were proposed to be used not only for the assessment of separate standing up but foremost to detect the transitions in general conditions during daily life. They used features of the measured signals typically observed in sit-to-stand and stand-to-sit trials, mainly the inclination angle in sagital plane estimated from the trunk angular rate. Finally, by Salarian et al. (2007a), the detection was implemented mainly as a detection of signal maxima and minima of specified polarities and amplitudes greater than thresholds. The approach was successful with some tolerance when detecting the transitions during trial simulating life conditions.

3.5 Timed up and go test

The timed up and go test (TUG) is a simple test to assess the mobility of a subject by measuring the time of the conduction of the following sequence:

- Get up from a comfortable sitting in a chair,
- walk 3 meters,
- turn back,
- walk back to the chair,
- turn again and sit down.

Recording of the time to perform the test was proposed by Podsiadlo and Richardson (1991) to simply and reliably asses the mobility of elderly people. Since then, it was used in a vast number of studies involving elderly, patients with Parkinson's disease, hemiplegics, and other people having problems with mobility. The strong points of the method are that the test is easy to perform and reconstruct, and that it consists of several different activities in which the people with reduced mobility may have problems: getting up from a chair, walking, turning around. The performance is aggregated into one measurement: the overall time measured by a stopwatch. Recently, several papers proposed to use motion sensors to automatize the time measurement and to add other quantities as measures of the mobility, giving more information from one conduction of the test. Above all, durations of the separated phases of the test are measured and the separated tasks evaluated, some of them using the methods described in the previous sections.

Higashi et al. (2008) used rate gyroscopes at trunk and legs and an accelerometer at trunk. They evaluated the time of TUG and times of its main phases and few simple parameters like RMS of the measured acceleration. The algorithm was used in a pilot study involving 20 hemiplegics. Ten of them were able to conduct the test by themselves, the others needed an assistance. Times of the walking phases of TUG and features of lateral and vertical acceleration differed significantly between the groups.

Marschollek et al. (2009) used an accelerometer placed at waist level. Without describing the methods in detail, they state to estimate the energy expenditure and several gait parameters from the measured acceleration. The study involved 110 geriatric patients divided into two groups based on the evidence of in-hospital falls: 26 fallers and 84 non-fallers. The mean step length differed significantly between the groups and there was also a borderline difference in the pelvic sway during walking and the TUG duration.

Weiss et al. (2010) used also an accelerometer placed at waist. They estimated the overall TUG time, durations of the sit-to-stand and stand-to-sit transitions and several other parameters of the two transitions. Seventeen Parkinson's disease patients and fifteen controls were involved in the pilot study. The groups differed significantly in most of parameters. Many sit-to-stand and stand-to-sit parameters shown the difference at a higher significancy level than the TUG time.

Salarian et al. (2010) and Zampieri et al. (2010) used more sensors and more detailed features derived from the signals. A modified TUG execution was used – the walking distance was prolonged to 7 meters. Salarian et al. (2010) used seven inertial measurement units placed at different body segments, four of them at legs. Zampieri et al. (2010) used five units, two of them at legs. They assessed both the gait and the transitions, while the other studies usually focused only on one them. Moreover, via sensors at wrists the arm swing during gait was assessed. The pilot study involved 12 patients with only mild-to-mid-stage Parkinson's disease and 12 controls. The duration of the modified TUG did not differ between the groups significantly, nor the duration of the standard TUG (Zampieri et al. 2010). However, several detailed parameters differed significantly: walking cadence, arm swing, trunk rotation speed during walking, time and speed of the 180 degrees turning at the distant end of the walkway, and the duration of the stand-to-sit transition.

3.6 Balance

Decreased stability in standing or walking is a symptom found in many disorders, namely in Parkinson's disease and after damages of the vestibular system. The balance, or postural

stability, is usually assessed using standardized physical tests conducted and evaluated by a physician or physiotherapist. The test may comprise of quiet standing in different conditions: eyes opened/closed, hard/soft plate below feet, standing with different leg positions or at only one leg, etc. The different conditions are used to separate the influence of the differents parts of the systems used in the human balance control: visual feedback, vestibular system, foot pressure sensing. Also dynamical conditions are sometimes used, e. g. pushing the subject, moving with the board on which the subject stands, or tandem walking – putting a heel just in front of the toe of the second foot and so on.

For a quantitative analysis, force plates are widely used to measure the center of pressure (COP) during a static test or when moving the board under the feet. The measurement provides 2D position of COP: medio-lateral and anterior-posterior. Several features of COP time course are then used to quantify one's performance, e. g. RMS of COP position or the length of the trajectory during a certain time interval. The motion of COP is related to the motion of the center of mass (COM), but it is different because of the dynamical forces.

Accelerometry was proposed to measure the motion of a point near to the COM – the lower back. One problem of using a single accelerometer at lower back is that because of the unknown character of leg and pelvis movements the gravitational and motion artifacts cannot be separated and therefore the motion cannot be reconstructed accurately. Moe-Nilssen (1998), Moe-Nilssen and Helbostad (2002) used the presumption that the tilt is constant or changes only very slowly during quiet standing and static walking and all the changes of acceleration in the two directions are from linear forward-backward and left-right motion only. On the contrary, Mayagoitia et al. (2002) assumed in quiet standing that the motion is pendulum-like, slow, and not very high, and therefore, the motion of the sensor may be described only by the changes of the tilt (inclination) and by the known distance of the sensor from the ground. The inclination is calculated with the assumption that the triaxial accelerometer measures just the gravity. To estimate COM from accelerometer measurements, a more complex model taking advance of more sensor units placed on the body may be also accompanied (Betker et al. 2006).

In the aforementioned publications, the methods of Moe-Nilssen and Mayagoitia were used successfully to discriminate different conditions or different patient groups. Moreover, methods similar to the method of Moe-Nilssen (1998) were evaluated by cross-correlation with standardized clinical functional balance tests (O'Sullivan et al. 2009) and force-plate measurements Whitney et al. (2011).

3.7 General patient's state in Parkinson's disease evaluated in daily life conditions

Activity monitoring, tremor detection and other quantities (for example, gait parameters) have been used to classify time periods to *on* and *off* states in Parkinson's disease. (Hoff et al. 2004, Keijsers et al. 2006, Salarian 2006). The most detailed assessment of particular symptoms and parameters before the classifier training was done by Salarian (2006). The output of their method is not only the result of classification (on/off), but it is also accompanied by the assessment of particular symptoms giving more information about the patient's state.

Chapter 4

Accelerometer Calibration from In-Use Data

An older version of this chapter was presented at a conference as a part of Šprdlík and Hurák (2007)

4.1 Introduction

This chapter is motivated by the use of inertial navigation methods for the analysis of symptoms and deals with in-use calibration of accelerometers using a detection of quasi-static states. Several methods for estimation of sensor parameters from data captured during nearly static conditions are given and compared in simulations.

Outputs of micro-machined inertial sensors (accelerometers and rate gyros) are subject to different kind of errors. Some of them can be fully or partially compensated by single calibration procedure (misalignment of axes, cross-axis sensitivity, gyroscope sensitivity to acceleration). Others vary throughout time (especially biases). Although sensor manufacturers achieve better and better characteristics, the drifts should be compensated for, especially in applications where sensor displacement is estimated by double integration of motion acceleration in a global reference frame.

Absolute majority of assessment methods for human movement quantification do not use inertial navigation. Its drawback may be mainly its higher computational demand but we suppose that quantities which may be estimated much better with calibrated sensors, e. g. position or velocity, may be more easily interpreted than the measured quantities. Moreover, the assessment methods based on position may be compared to the methods based on movement monitoring using motion capture systems.

When sensors are fixed to human body, it is impossible to perform their calibration by a standard calibration procedure requiring a special equipment or at least rotation of sensor in several directions and letting it still without any motion in each position.

There are different methods to approach the in use estimation of inertial sensor parameters which change slowly. One group of algorithms is based on Kalman filtering: Sensor parameters or their estimate errors are dealt as filter states added to nonlinear Kalman filter observing sensor orientation or simplified linear Kalman filter observing error of orientation estimate see e. g. Luinge and Veltink (2005) (only gyroscope bias is estimated

in this case) or Batista et al. (2011) (dynamic accelerometer bias estimation). Addition of sensor parameters to the Kalman filter increases number of its states and therefore also the computational burden especially if the number of estimated parameters is high. Sensor parameters are usually actualized in each filter step, that is in fact unnecessary because they change very slowly.

An alternative approach to accelerometer calibration was proposed by Lötters et al. (1998). It is based on detection of quasi-static states, i. e. situations when sensor does not move or its motion is very slow. The detection uses the assumption that it is unlikely in human motion to achieve constant nonzero acceleration. Accelerometer bias and gain are estimated from accelerations measured in quasi-static states using the fact that then the amplitude of the measured acceleration is near to gravity.

Similar approach was used also for the magnetometer calibration (Gebre-Egziabher et al. 2006). Also different ellipsoid fitting algorithms were proposed for the calibration (Šprdlík and Hurák 2007, Pylvänäinen 2008, Bonnet et al. 2009). Generally, an ellipsoid fitting may be used for a 3D sensor of any time-invariant physical field (Pylvänäinen 2008, Bonnet et al. 2009).

Next sections briefly refer to published approaches to ellipsoid fitting and 3D accelerometer calibration using a detection of quasi-static states. Then, some properties of the algorithms are discussed and modified approaches are proposed and compared in simulations.

4.2 Problem formulation

Accelerometer calibration procedure is split to two problems,

1. detection of quasi-static states,

2. estimation of sensor parameters from data measured in quasi-static states.

We suppose that misalignment of sensor axes is pre-calibrated. Therefore, we restrict the sought parameters to biases and sensitivities only. In an ideal case accelerations measured in static conditions lie on an ellipsoid with the center defined by the accelerometer bias, axes parallel to the accelerometer axes, and semi-axes lengths equal to sensitivities of the accelerometer axes to gravitational acceleration. In reality, measured points do not lie exactly on the ellipsoid because of the sensor noise and non-ideal quasi-static conditions. Moreover in human applications, often only part of the ellipsoid is covered by quasi-static data – for example trunk is typically approximately in vertical position during most of the daytime and therefore sensor placed on trunk may capture only limited range of orientations. See left part of figure 4.1 for principal 2D sketch of situation. Nonorthogonality of the sensor axes leads to the need to identify also the orientation of the ellipsoid axes. As we used only sensors precalibrated from the production, we assumed the sensor axes perfectly orthogonal.

If the accelerometer bias o and sensitivity s are known, calibrated acceleration a may be computed from measured values v,

$$a_j = \frac{v_j - o_j}{s_j},$$

where $j \in \{x, y, z\}$.

4.3 Methods

The estimator is divided to two parts. The first one is a detector of quasi-static states and the second one fits an ellipsoid defined by accelerometer parameters to the data measured in quasi-static states.

Lötters et al. (1998) used detection function

$$d_1 = \mathrm{LPF}\left(\mathrm{REC}\left(\mathrm{HPF}\left(\mathrm{Size}(v)\right)\right)\right),$$

where $\mathrm{Size}(v)$ stands for $\sqrt{v_x^2 + v_y^2 + v_z^2}$. Symbols LPF, REC, and HPF mean Low-pass Filter, Rectification, and High-pass Filter, respectively. Output of this function is compared to threshold to detect type of state. Value of d_1 is unlikely to be near zero during most of human movements.

Next possibility is to shift computation of vector size up in the hierarchy, for example

$$d_2 = \mathrm{LPF}\left(\mathrm{Size}\left(\mathrm{HPF}(v)\right)\right),$$

or even to add the gyroscope output to the detection scheme (Saxena et al. 2005). In systems with high sampling frequency, standard deviation of signal may be estimated in periods of suitable length and then compared to threshold.

Although detection of quasi-static states is important part of the estimator we do not deal it deeply here and focus more on the ellipsoid fitting part of the procedure. The detection signals d_1 and d_2 depend not only on the amplitude of the motion but also on its direction relative to vertical line. Detection signal d_1 may also underestimate the rotation component of the sensor motion and thus theoretically classify some rotational movements as quasi-static states if the center of rotation is near to the sensor. Therefore, in the example below we rather choose the estimates of acceleration and angular rate standard deviations computed in short data segments. Segments of length 0.3 second at sampling frequency 50 Hz were used in the example in section 4.6.

Used ellipsoid fitting methods are described bellow.

4.3.1 Method 1

The first of the used methods was introduced by Lötters et al. (1998) and used by Saxena et al. (2005) for accelerometer calibration and similar equation was used also by Gebre-Egziabher et al. (2006) for magnetometer calibration. In the literature, a least squares optimization procedure was proposed which uses the following function,

$$h(v_i, p) = \sqrt{\left(\frac{v_{x,i} - o_x}{s_x}\right)^2 + \left(\frac{v_{y,i} - o_y}{s_y}\right)^2 + \left(\frac{v_{z,i} - o_z}{s_z}\right)^2},$$

where parameter vector $p = [s_x \; s_y \; s_z \; o_x \; o_y \; o_z]^{\mathrm{T}}$ and i is the number of the measurement. If the measurement v_i and the gain-offset model of accelerometer measurement are exact, the function equals one

$$h(v_i, p) = 1\,[\mathrm{g}]$$

The optimization procedure finds p using h as a model and 1 as measurement. Optimization is iterative – each iteration is done by linearization of $h(v_i, p)$ at point specified by previous estimate of p and then finding the optimal change Δp with minimum variance estimator. See Lötters et al. (1998) for more details.

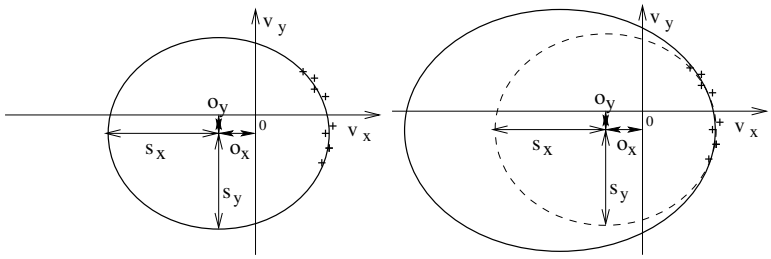

Figure 4.1: 2D sketch of ellipsoid defined by accelerometer parameters and inaccurate estimate from measured quasi-static outputs v of accelerometer.

A drawback of this approach is the fact that the function scales the errors of the measured acceleration (v) relative to the estimated sensitivity (s). Therefore the results with greater sensitivities may be preferred in some situations. In situations when too small part of the ellipsoid is covered by measured quasi-static points, the estimated ellipsoid has longer semi-axis in the direction of missing data (see the right part of figure 4.1 for principal sketch) or even the algorithm diverges producing greater and greater ellipsoid in each iteration.

4.3.2 Method 2 (Algebraic fit with constraint)

A large group of fitting methods for nonlinear models is formed by algebraic fitting methods. They minimize quadratic error of an equation describing the model. Even the previous method belongs to this group. For a general conic surface, an equation in the form

$$F(A, b, c, v) = v^\top A\, v + b^{\mathrm{T}} v + c = 0 \tag{4.1}$$

may be used.

In some cases, a non-elliptic conic (paraboloid, hyperboloid) may be found when minimizing the norm of F and the data come from only a small part of the ellipsoid and are corrupted by noise and other errors. In the case of accelerometer calibration, only an ellipsoid is desired as the result of the minimization. For 2D case – ellipse fitting – there is a simple solution with the use of a quadratic constraint in the minimization (Fitzgibbon et al. 1999). The minimization with the quadratic constraint is solved by the solution of a generalized eigenvalue problem. Grammalidis and Strintzis (1998) proposed to use the same method for 3D ellipsoids. They proposed to set a constraint for parameters corresponding to two of the three axes. Although an ellipsoid is not guaranteed in the 3D case, it is found in many cases when other type of conic would be estimated if no constraint has been used.

As the original method was developed for general ellipsoids but only estimates of center position and lengths of semi-axes are needed in our case (the ellipsoid has its axes parallel to system axes), we simplified the method. See the paper by Grammalidis and Strintzis (1998) for description of the original method. Simplifications are straightforward: Matrix A is diagonal in our case,

$$A = \mathrm{diag}(a_{11}, a_{22}, a_{33}).$$

To specify an ellipsoid, the three diagonal terms must have the same polarity. With a quadratic constraint, e. g. $a_{11}\, a_{22} = 1$, we can force two selected terms to have the same polarity.

4.3.3 Method 3 (Consistent)

Least squares algebraic fitting of ellipsoids is inconsistent: If a set of measured points is generated as a set of points on ellipsoid plus centered, independent, identically distributed errors, then the estimated ellipsoid does not converge to the original ellipsoid as the size of the sample grows to infinity. Even geometric fitting – minimization of geometric distances from measured points to the ellipsoid (see bellow) – is inconsistent.

Consistent estimator based on the algebraic LS estimator has been proposed by Markovsky et al. (2004, 2006) for normal distribution of errors. The Adjusted Least Squares (ALS) estimator has been proposed for a general ellipsoid. We made its reduction to ellipsoids with axes parallel to system axes. Short description of the algorithm follows.

Parameter vector

$$\beta = (a_{11}\ a_{22}\ a_{33}\ b_1\ b_2\ b_3\ c)$$

of eq. (4.1), where $A = \mathrm{diag}(a_{11}\ a_{22}\ a_{33})$, is estimated in both method 2 and 3. Accelerometer parameters s and v can be computed directly from the vector.

Algebraic LS fit without constraints may be computed forming vector

$$y = (v_x^2\ v_y^2\ v_z^2\ v_x\ v_y\ v_z\ 1)^{\mathrm{T}}$$

for each point, matrix of all data is then formed

$$Y = \begin{bmatrix} y^{(1)\mathrm{T}} \\ \vdots \\ y^{(N)\mathrm{T}} \end{bmatrix},$$

finally $\beta_{ls} = V_{min}$ ...singular vector corresponding to the smallest singular value of Y. Alternatively

$$\psi_{\mathrm{ls}}^{(i)} = y^{(i)} y^{(i)\mathrm{T}}, \quad \Psi_{\mathrm{ls}} = \sum_{i=1}^{N} \psi_{\mathrm{ls}}^{(i)} = Y^{\mathrm{T}} Y.$$

Parameter vector is then proportional to eigenvector corresponding to the smallest eigenvalue of Ψ_{ls}.

Adjusted procedure uses correction $\Delta\psi_{\mathrm{als}}^{(i)}$ to make the estimator consistent under the assumptions noted above.

$$\psi_{\mathrm{als}}^{(i)} = y^{(i)} y^{(i)\mathrm{T}} + \Delta\psi_{\mathrm{als}}^{(i)}, \quad \Psi_{\mathrm{als}} = \sum_{i=1}^{N} \psi_{\mathrm{als}}^{(i)}(v_i)$$

Parameter vector is computed in the same way as for LS estimate based on finding eigenvector of Ψ. Singular value decomposition of data matrix Y cannot be used in this case because matrix $Y^{\mathrm{T}}Y$ is corrected (not the data matrix itself).

Correction matrix for the case of ellipsoids with axes parallel to system axes is

$$\Delta\psi_{\text{als}}^{(i)} = \begin{bmatrix} 3\sigma^4 - 6v_x^2\sigma^2 & \sigma^4 - \sigma^2(v_x^2 + v_y^2) \\ * & 3\sigma^4 - 6v_y^2\sigma^2 \\ * & * \\ * & * \\ * & * \\ * & * \\ * & * \end{bmatrix}$$

$$\begin{bmatrix} \sigma^4 - \sigma^2(v_x^2 + v_z^2) & -3\sigma^2 v_x & -\sigma^2 v_y & -\sigma^2 v_z & -\sigma^2 \\ \sigma^4 - \sigma^2(v_y^2 + v_z^2) & -\sigma^2 v_x & -3\sigma^2 v_y & -\sigma^2 v_z & -\sigma^2 \\ 3\sigma^4 - 6v_z^2\sigma^2 & -\sigma^2 v_x & -\sigma^2 v_y & -3\sigma^2 v_z & -\sigma^2 \\ * & -\sigma^2 & 0 & 0 & 0 \\ * & 0 & -\sigma^2 & 0 & 0 \\ * & 0 & 0 & -\sigma^2 & 0 \\ * & 0 & 0 & 0 & 0 \end{bmatrix},$$

where above v indexes $^{(i)}$ are omitted, σ is the standard deviation of the error, and * stands for symmetric element. See Markovsky et al. (2004) for details about construction of correction matrix.

General drawback of using this approach is the potential non-normality of the error in the case of quasi-static states and its unknown variance. Only some estimate of the variance may be used in the real situation.

4.3.4 Method 4 (Distance along ray)

In this method distances from measured points to specific points on ellipsoid are minimized in LS sense. The points g_i lie at places where rays from the ellipsoid center o to the measured points v_i cross the ellipsoid. They may be found in a closed form:

$$g = o + \frac{v - o}{\sqrt{\left(\frac{v_x - o_x}{s_x}\right)^2 + \left(\frac{v_y - o_y}{s_y}\right)^2 + \left(\frac{v_z - o_z}{s_z}\right)^2}},$$

where indexes i of the points were omitted at g and v.

Similar approach using the same points g on the ellipsoid was proposed by Calafiore (2002) for general ellipsoid fitting, motivated mainly by applications in graphics and computer vision. He proposed to use the metrics specified by semi-axes lengths for criterion. That may lead to similar problems as described for the method 1. Therefore we rather used directly the metrics of the measurements.

In our case, Gauss-Newton iterative method was used to find a solution minimizing the distances of g and v. However, also a semi-definite programming problem formulation for the similar fitting exists (Calafiore 2002).

4.3.5 Method 5 (Geometric fitting)

Method for fitting ellipses by minimizing the sum of squares of geometric distances from measured points to the ellipse (Gander et al. 1994) was modified to allow fitting of 3D ellipsoids:

Points on ellipsoid nearest to measured points can be parametrized by two angles, φ_1 and φ_2. Then, the difference of a measured point and the nearest one on the ellipsoid is

$$d = \begin{bmatrix} v_x - o_x - s_x \cos\varphi_1 \cos\varphi_2 \\ v_y - o_y - s_y \sin\varphi_1 \cos\varphi_2 \\ v_z - o_z - s_z \sin\varphi_2 \end{bmatrix},$$

where indexes i of the points were omitted at d, v, φ_1, and φ_2.

The problem is that the optimization criterion (sum of squares of distances) in this representation depends not only on the bias and sensitivity but also on values of $\varphi_{1,2}$, that have to be found by the optimization algorithm too. Therefore $6 + 2N$ variables are used for N measured points. This fact makes the method computationally ineffective especially for large samples of measured data. We used Gauss-Newton method to minimize the sum of squares of the second norms (lengths) of d_i. It converges to a local minimum and may diverge in some cases, especially if the initial estimate is far from reality.

An alternative approach to cope the parameter number explosion in this nonlinear geometric fitting is to use iterative scheme with algebraic fits using weighting dependent on the distance from the estimated center (Gander et al. 1994).

4.4 Simulations

Ellipsoid fitting algorithms were tested in simulations. "Measured" values of acceleration were generated from a part of the original ellipsoid by adding Gaussian noise to the points on ellipsoid which were generated as random points distributed uniformly in polar coordinates with one pole in the center of the used part (cone) of the ellipsoid.

Cones were specified by angles θ from 10° to 180° (full ellipsoid). Small angles simulate conditions when a body segment has little variation of inclination for a long time and therefore only limited range of points is available. Two different positions of the center of the used part of ellipsoid were considered:

- Orientation 1 at one of ellipsoid axes (this simulates for example the most obvious placement of sensor on trunk – one axis approximately vertical in standing and sitting). Axis Z of the accelerometer was used.

- Orientation 2 at the same angular distance from all axes (about 54.7°) – this orientation of sensor axes relative to dominating direction of gravity was found to achieve better estimation results by Lötters et al. (1998).

See figure 4.2 for an example of simulation data generated in a cone with the axis in orientation 2 and angle 30 degrees (diameter 60 degrees).

Three different standard deviations of additive error were used (0.01, 0.05, and 0.4 $\mathrm{m\,s^{-2}}$). Four different numbers of points were used (10, 40, 200, and 1000). For each combination (orientation/standard deviation/sample size) ten instances have been generated. Initial sensitivity estimate was $9.81\,[\mathrm{m\,s^{-2}}]$ in all axes in all cases, initial bias was set to zero. Real sensitivities varied up to 0.21 and biases up to $0.5\,[\mathrm{m\,s^{-2}}]$ from the initial ones.

For iterative algorithms (methods 1, 4, and 5), the stopping condition was change of biases and sensitivities lower than 10^{-5} of the previous estimate of sensitivities (i.e. approximately $10^{-4}\,\mathrm{m\,s^{-2}}$). Maximum number of iterations was set to 100.

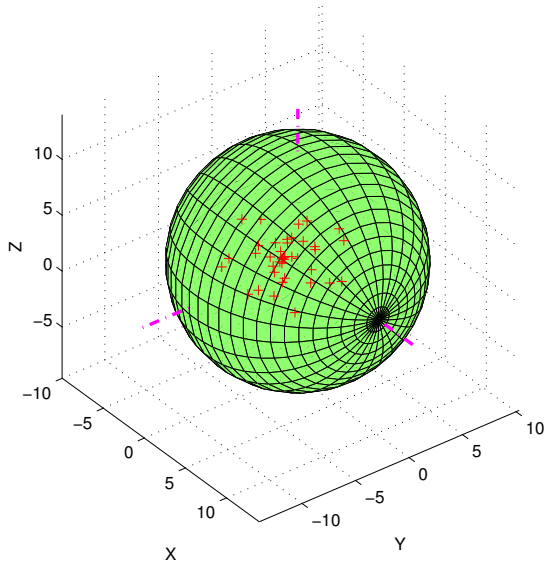

Figure 4.2: Example of simulation data spread in a cone with the axis in orientation 2. Units $\mathrm{m\,s^{-2}}$. The ellipsoid is given by the accelerometer bias and gains used in the simulation.

Method 2 was used with two choices of quadratic constraint. One of them (2a) involved two axes which are horizontal in orientation 1. The second constraint (2b) involved one vertical and one horizontal axis in orientation 1.

4.5 Simulation results

Errors of estimated ellipsoids were transformed to relative errors of acceleration estimated using the ellipsoid parameters in the same way as in Lötters et al. (1998),

$$err_{s_i} = \frac{|\hat{s}_i - s_i|}{s_i} \cdot 100\,\%, \quad err_{o_i} = \frac{|\hat{o}_i - o_i|}{s_i} \cdot 100\,\%,$$

where s is actual sensitivity, $\hat{s}$ is estimated sensitivity, o is actual bias, $\hat{o}$ is estimated bias.

See figures 4.3–4.4 for mean errors over several instances of task. Each figure represents different combination of standard deviation and sample size, results for sample size 200 are not displayed to save space. In the left column of each figure results for orientation 1 (one of axes parallel to typical direction of gravity in local coordinates) are displayed and for orientation 2 in the right column.

Rows correspond to different methods. Each small graph shows error versus size of cone covered by measured points. If value is not displayed, it is greater than 100 %, iterative algorithm diverged, or other cone (not ellipsoid) was returned.

Accuracy of estimate increases with increasing range of orientations and is better if no sensor axis is approximately parallel to the direction of most of the measured points.

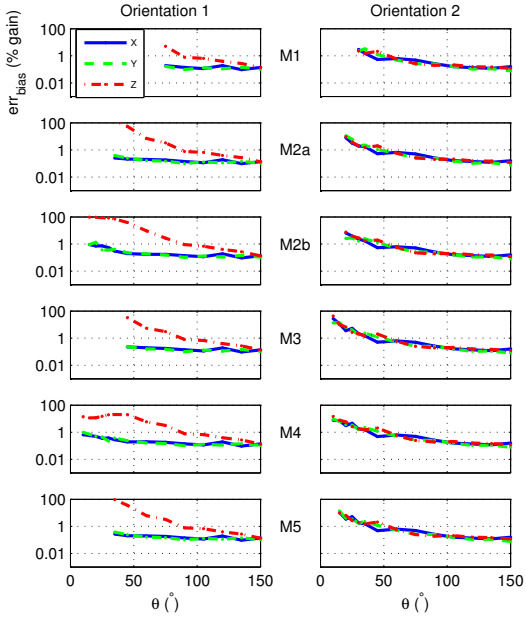

(a) 40 acceleration points

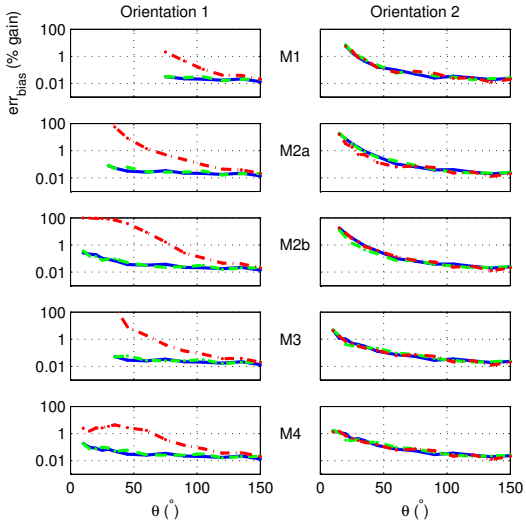

(b) 1000 acceleration points

Figure 4.3: Relative errors of accelerations caused by error of gains estimated by the described methods versus space angle of quasi-static accelerations. Results for orientation 1 are at the left column, for orientation 2 right. Standard deviation $\mathbf{0.05}\,\mathrm{m\,s^{-2}}$ of the error of the acceleration points was used.

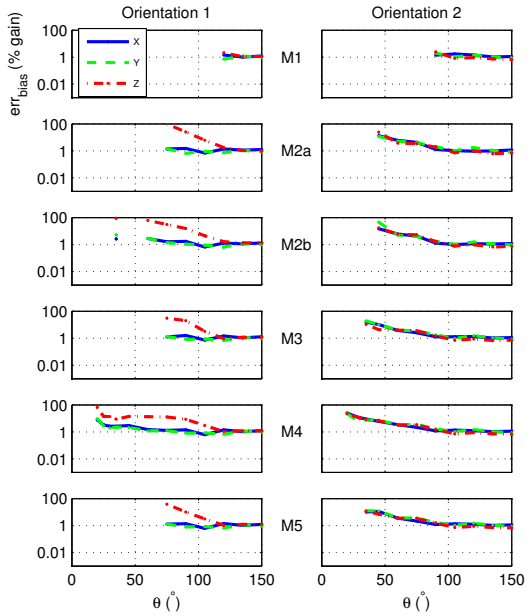

(a) 40 acceleration points

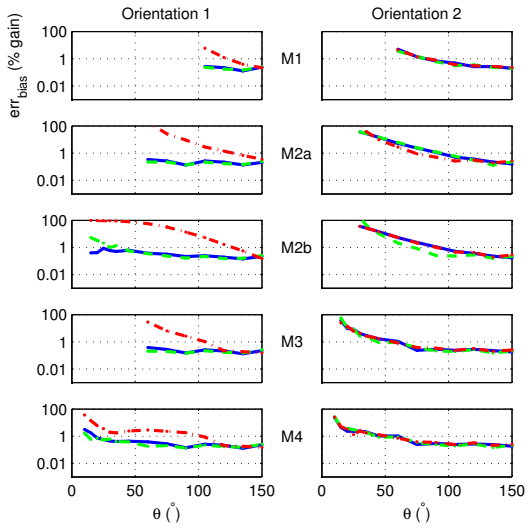

(b) 1000 acceleration points

Figure 4.4: Relative errors of accelerations caused by error of gains estimated by the described methods versus space angle of quasi-static accelerations. Results for orientation 1 are at the left column, for orientation 2 right. Standard deviation $\mathbf{0.4}\,\mathrm{m\,s^{-2}}$ of the error of the acceleration points was used.

SD [$m\,s^{-2}$]	N	Orientation 1 θ		Orientation 2 θ	
0.01	10		–		–
	40		–		–
	200	25°	M4 < M2b	10°	M3,M4,M5 < M1,M2
		30°	M2a,M4,M5 < M2b,M3		
		35°	M2a,M4,M5 < M3 < M2b		
		45°	M2a,M3,M4,M5 < M1,M2b		
		60°	M2,M3,M4,M5 < M1		
	1000	10-15°	M4 < M2b	10-15°	M3,M4 < M1 < M2
		20-25°	M4 < M2	20°	M4<M1,M2; M3<M2
		30°	M4<M2a<M2b; M3<M2b		
		35°	M2a,M3,M4 < M2b		
		45°	M2a,M3,M4 < M2b < M1		
		60°	M2,M3,M4 < M1		
0.05	10		–		–
	40	60°	M3 < M2b	20°	M3,M4,M5 < M2
	200	10-30°	M4 < M2b	10°	M4 < M3,M5
		35°	M4 < M2	15-30°	M3,M4,M5 < M1,M2
		45°	M2a,M4,M5<M2b; M4,M5<M3		
		60°	M2a,M3,M4,M5 < M2b		
		75°	M2a,M3,M4,M5 < M1,M2b		
		80°	M1,M2a,M3,M4,M5 < M2b		
		90°	M2a,M3,M4,M5 < M2b		
	1000	10-35°	M4 < M2	10°	M4<M3
		45°	M4 < M2a,M3 < M2b	15°	M3,M4 < M2
		60°	M3,M4 < M2a < M2b	20°	M3,M4 < M1,M2
		75°	M3,M4 < M2a < M2b < M1	25-35°	M1,M3,M4 < M2
		90°	M3,M4 < M2 < M1	45°	M3,M4 < M2
0.4	10		–		–
	40	35°,90°	M4 < M2b	60°	M4 < M2
	200	30-45°	M4 < M2b	25-30°	M4 < M3,M5
		60°	M4 < M2b,M5	35°	M4 < M3,M5 < M2
		75°	M4,M5<M2; M4<M3	45°	M3,M4,M5 < M2
		90°	M3,M4,M5 < M2	60-75°	M3,M4,M5 < M1,M2
		105°	M4,M5<M2a<M1,M2b; M3<M1,M2b	90°	M3 < M2
		120°	M1,M2a,M3,M4,M5 < M2b		
	1000	20-45°	M4 < M2b	15-25	M4 < M3
		60°	M4 < M2,M3	30-45°	M3,M4 < M2
		75°	M4 < M3 < M2	60°	M3,M4 < M1,M2
		90°	M3,M4 < M2a < M2b	75-90°	M3,M4 < M1 < M2
		105°	M3,M4 < M2a < M1,M2b	105°	M3,M4 < M1,M2
		120°	M3,M4 < M1,M2a < M2b		
		135°	M3,M4<M2; M1<M2a		
		150°	M3,M4 < M2a		

Table 4.1: Comparison of mean errors of the used methods on simulation data. **Notation:** M1,M2<M3,M4 means that mean errors of methods M1 and M2 in 10 samples were lower than mean errors of M3 and M4, all comparisons with P<0.05. SD – standard deviation of error of data points; N – number of data points; θ – angle defining the cone of data points. For orientation 1, M2 means M2a,M2b.

	10 p.	40 p.	200 p.	1000 p.
	time [ms]			
M 1	4	8	23	160
M 2a	0.3	1	3	33
M 2b	0.4	1	3	40
M 3	4	7	17	65
M 4	9	24	87	355
M 5	9	29	1140	?

Table 4.2: Mean computation time versus method and sample size. The computation time of method 5 (geometric) for 1000 points was about 1 minute. Due to the time burden, the method was not used for all the 1000-point datasets from the simulations.

	10 p.	40 p.	200 p.	1000 p.
	mean number of iterations			
M 1	3.8	3.5	3.7	3.7
M 4	5.3	4.9	4.6	5.0
M 5	14.5	13.8	13.9	?

Table 4.3: Mean number of iterations versus method and sample size. Due to the time burden of method 5, it was not used for all the 1000-point datasets from the simulations.

The benefit of orientation 2 was already reported by Lötters et al. (1998) for method 1, results verify it also for other methods of ellipsoid fitting.

Method 1 needed greater range of orientations to converge and to give an ellipsoid as result than other methods. Other methods gave results also for lower ranges of orientations, although for the lowest numbers of measured points, they did not give very clear improvement of accuracy. With increasing sample size the accuracy increased especially for methods 3, 4, and 5 – see figures 4.3 and 4.4 for methods 3 and 4 applied to samples of 1000 points and table 4.1 for comparison of mean errors with samples of 200 and 1000 points. For orientation 2, only results of M2a are shown as M2. For M2b, the results were mostly the same. Results are not shown for situations when some of two compared methods did not find an ellipsoid solution for some of the 10 samples and for situations when both of two compared methods had the mean errors greater than 10%. Method 2a (axes bind by the constraint are horizontal in the central position of orientation 1) gave in orientation 1 usually better results than methods 1 and 2b. Method 2b in orientation 1 gave results also for very low ranges, but it had the biggest errors, even in case when method 1 gave a result too.

Computational demand of our implementations of the methods was measured as mean time of run over all instances in set specified by method and number of points. An ordinary laptop with 2.3 GHz 2-core processor and 64-bit Linux operating system and 64-bit Matlab® was used. Instances where the method diverged were excluded as well as all instances with the cone angle lower than 45° to reduce the influence of divergences which were quite common for the low angles. See table 4.2 for results.

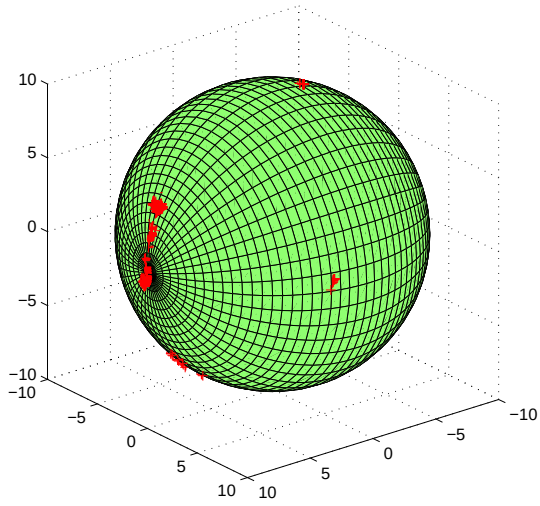

Figure 4.5: Collection of quasi-static states and estimated ellipsoid. Units $\mathrm{m\,s^{-2}}$.

4.6 Real data example

Calibration procedure has been applied to inertial data measured at a human subject. The subject wore an inertial measurement unit MT9 by Xsens on sternum. First, he reached several positions – standing, sitting, lying at different sides. See figure 4.5 for set of quasi-static states collected from sternum-placed accelerometers and for ellipsoid defined by sensor parameters estimated by method 4.

Nonlinear unscented Kalman filter has been built for estimation of sensor orientation from calibrated accelerometer and gyroscope data (gyroscope bias is estimated as mean output value in quasi-static periods during short measurement trial) using ReBEL toolkit (OGI School of Science & Engineering 2008) for nonlinear filtering. See chapter 5 for more details about almost same algorithm except that here, the magnetometer measurement was not used. Orientation is used for transform the acceleration measurement to global frame. Gravitational component is subtracted and Displacement is estimated by double integration.

Since no heading reference is used, the azimuth component of orientation is estimated with strong drift which also corrupts estimate of displacement in horizontal plane. On the other hand the vertical component of acceleration has a stable estimate. Relative vertical displacement of sternum estimated as the double integrate of the vertical acceleration component during a part of the same measurement session is shown at figure 4.6. Two sit-to-stand and stand-to-sit transitions were performed during the trial.

4.7 Discussion and conclusions

Several ellipsoid fitting methods for accelerometer calibration from data measured in quasi-static states have been described. They include a partially new method minimizing distances along rays from the center of the estimated ellipsoid. The methods were compared in simulations where the measurements in quasi-static states were substituted by random numbers.

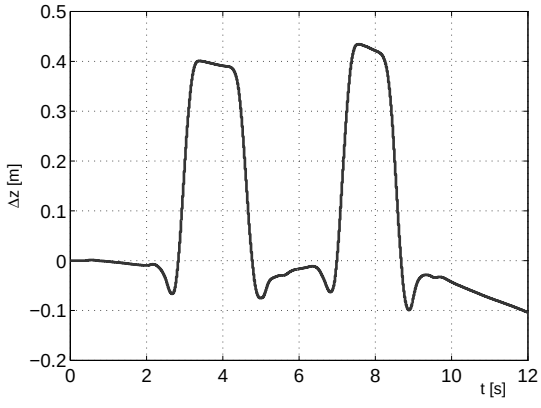

Figure 4.6: Estimated relative vertical displacement of sternum during transitions between sitting and standing

In the conducted simulations, the accuracy of all of the methods was similar when the points were accurate (simulating well static conditions) and covered a large part of the ellipsoid defined by calibration parameters (simulating a wide range of positions of the body segment with the accelerometer). Increased number of points lead to increased calibration accuracy for all the methods.

Method 3 (consistent) gave one of the best results but it uses corrections of data matrix based on assumptions on noise (zero mean, normal distribution, known variance). In the reality, real quasi-static data are used, that may be far from fulfilling the criteria due to the presence of slow movements. In such a setting, method 3 may by of low utility.

From the studied ellipsoid fitting methods, method 4 (distance along ray) gave usually one of the best results. It has a slower computation but still probably feasible for most applications.

From the simulation results it appears that if an algebraic method has to be used and it is known that there will be a low range of measured points and one of the axes will be usually approximately vertical, using a quadratic constraint binding the two approximately horizontal axes may help (see method 2a in orientation 1).

As a possible future development of the methods, modification to adaptive procedure which will forget old and incorporate new data may be done to enable estimation of time varying parameters and use of inertial navigation methods anytime during long measurement trials with patients. Quasi-static states may be of different level, therefore they may be given different weights depending of estimated level of their staticity (Saxena et al. 2005). Weighting can be applied into most of ellipsoid fitting methods.

Iterative methods shown to be slower than one-step methods. But in case of adaptive estimation, if it will be implemented such that the used sample of quasi-static data changes only a little at each adaptation step, then a limited number of iterations or even only one iteration shall be enough at each adaptation step, so the disadvantage may be reduced. Moreover, relative change 10^{-5} which we used as the stopping condition for the iterative methods may be unnecessarily strict.

Chapter 5

Tremor Quantification with the Help of Separating Gravitational Artifact of Measured Acceleration

This chapter was created by an edit of the accepted author manuscript of Šprdlík et al. (2011) [1]. An older version of a significant part of the study was presented at a conference (Šprdlík et al. 2009).

Decomposition of acceleration was investigated as an alternative to commonly used direct spectral analysis of measured acceleration or angular velocity for tremor quantification. An orientation estimation algorithm was devised to decompose the measured acceleration into the gravitational artifact and the motion acceleration caused by sensor motion in an Earth-fixed reference frame. Resulting signals, beside the measured acceleration and angular velocity, were used to assess tremor amplitude and frequency by spectral peak detection. The algorithm was tested on experimental data from a clinical study including patients with essential tremor. The testing comprised of the classification of measurements to come from a patient or a healthy control and of the regression of the visual assessment of tremor amplitude. Small improvements in performance measures were achieved by using the decomposed acceleration. The regression accuracy was comparable to the accuracy achieved in other works. The influence of sensor calibration and connections of results to an analytic approach were analyzed briefly.

5.1 Introduction

Tremor is defined as a rhythmical, involuntary oscillatory movement of a body part (Deuschl et al. 1998). Its quantification is necessary for clinical monitoring as well as for studies of movement disorders featuring tremor (Louis and Pullman 2001). Clinical examination with various rating scales has been the most frequently used approach, although inertial sen-

[1] This chapter contains additionally paragraph 5.3.1 with median found amplitudes and tremor frequencies. Table 5.7 was reduced compared to the manuscript. The notation and naming were slightly changed.

sors have also become widely used in research studies. Direct spectral analysis of signals measured by accelerometers has mostly been employed. This, however, may lead to several problems including the contamination of the measured linear acceleration by the variable projection of gravity, which implies the deterioration of a simple estimate of displacement (or its amplitude) using double integrated acceleration, as used for instance by Louis and Pullman (2001), Elble (2003). A component of the gravitational artifact may have a frequency that is double of the frequency of tremor due to the non-linear properties of the periodic alternate movement with a rotational character (Elble 2005). However, similar frequency doubling may be present even in the movement acceleration.

These problems can be reduced by a suitable arrangement of the test procedure and a choice of the most suitable sensor axis for the analysis. In a typical case the measurement is conducted with the patient's hands kept horizontally and only the sensor axis that is approximately vertical is processed (Foerster and Smeja 1999, Louis and Pullman 2001, Morrison et al. 2005). In addition, the hand motion can be restricted as in (Elble 2003). This case is analyzed with the use of a simplified model of a hand by (Elble 2005). Nevertheless, analysis of just one sensor axis obscures the other movement components and the choice of the vertical axis is not always appropriate, especially if some movement task is to be accomplished, like in tests for intention tremor.

A different approach to cope with the gravitational artifact may be the use of the magnitude of the 3D output of a triaxial accelerometer. The main idea is that the magnitude is steady and equals gravity if no linear acceleration is applied to the sensor, even if the sensor changes its orientation in time (Veltink et al. 1995, van Someren et al. 1996). Besides sacrificing the possibility to estimate the direction of the movement when using only the magnitude of the signal, the measured magnitude minus gravity does not exactly correspond to the amplitude of the acceleration caused by linear motion because it depends also on the direction of the movement with respect to gravity. Moreover, a movement with rotational character may produce some additional DC component in the magnitude while the alternating component may be quite low. Therefore in this case, the amplitude of tremor motion may be underestimated when using the AC component of the magnitude. Nevertheless, the magnitude-based approach was used in several studies to roughly quantify a movement (Frost 1978) or tremor (Kuncel et al. 2007).

Alternative sensors have also their own disadvantages: MEMS gyroscopes (Burkhard et al. 2002, Rocon de Lima et al. 2006, Salarian et al. 2007b, Giuffrida et al. 2009) may be a good choice especially for the cases where the movement is limited to a particular joint near to the site of measurement, or if sensors are placed at several segments of the arm (Rocon de Lima et al. 2006), but they also obscure some more complex movements. Displacement sensors like mechanical devices (Matsumoto et al. 1999), camera kinematic systems (Deuschl et al. 2000), and magnetic systems (Spyers-Ashby et al. 1999) are usually bulky and expensive. Moreover, the limited resolution of common camera systems makes the analysis of a very mild tremor infeasible.

Attitude estimation using measured data from both accelerometers and gyroscopes is a way to decompose the measured acceleration into the gravitational and motional components, hence it makes short-time estimates of displacement by double integration feasible. The bulky size of an inertial measurement unit (IMU) used to be the limiting factor, but with the advances in MEMS based devices, this is no longer a major issue. Nowadays, even devices containing accelerometers and gyroscopes suitable for fixing to a human finger are available – Kinesia^{TM} by CleveMed (Giuffrida et al. 2009). However, in the present work, slightly larger units were used.

The task of tremor measurement by a set of inertial sensors that allow decoupling from the gravitational artifact was already dealt with in several works: Ang et al. (2003) proposed a pure-accelerometer system for tremor sensing and active compensation of surgeon's tremor in a microsurgical instrument with accelerometer units fixed 10 cm apart from each other. The size of one of the units was reduced by Latt et al. (2009), but the need of the two distant sites on a rigid body remains. By Hyde et al. (2008) a system was designed for estimation of an upper limb orientation from inertial sensors placed at several sites on the arm. Sensitivity analysis with the use of simulations demonstrated its proficiency at frequencies of tremor. The proficiency was also demonstrated by means of comparison with the measurement by a mechanical device. The angle of an elbow joint manifesting tremor was the observed quantity. However, in this approach a mathematical model of the arm and a set of several sensor units are needed. By Giuffrida et al. (2009) gravity was not explicitly decoupled from accelerometer measurement, although sensors potentially allowed it. Rather, clinical scores were regressed by linear models with several features of the measured signals acting as inputs.

The goal of our study was to demonstrate the feasibility of quantifying tremor using the decomposition of the signal registered with accelerometers into the gravitational and movement components by inertial estimation of orientation (attitude). This is to make the tremor quantification as independent as possible from the orientation and the direction of movement of the observed body segment relative to gravity. Frequency spectrum-based features of the measured signals and of the outputs of the decomposition were extracted and their performance was compared in two tasks, to classify a single measurement from one hand or both hands to come from a patient or a healthy control, provided only the information that the measurement is from a test for postural hand tremor, without the knowledge of the particular task, to predict a visual assessment of tremor amplitude by clinicians, without the knowledge of the type of tremor (rest/postural) and particular task. The performance of the regression was compared to results of other works.

A regression of a visual tremor assessment by quantities from an instrumented assessment was already done in a number of studies. Part of them deal with long-term ambulatory monitoring of tremor (eg. (van Someren et al. 1993, 1998, van Someren et al. 2006, Salarian et al. 2007b)), other with short measurements in defined hand positions (eg. (Matsumoto et al. 1999, Elble et al. 2006, Giuffrida et al. 2009, Mostile et al. 2010)).

5.2 Methods

5.2.1 Subjects

The algorithm was used to quantify tremor on a sample of 59 subjects: 30 patients with essential tremor diagnosed according to the clinical criteria (Deuschl et al. 1998), age (mean $\pm$ standard deviation) 55.8 $\pm$ 18.1 years (range 19–81), disease duration 24.8 $\pm$ 16.5, Fahn-Tolosa-Marín Tremor Rating Scale score (Fahn et al. 1993) 27.0 $\pm$ 13.4 (range 9–67), 8 females, and 29 healthy individuals without any tremor-inducing disorder, age 53.8 $\pm$ 17.4 years (range 19–81), 8 females.

5.2.2 Experimental setup and data acquisition

Hand tremor was measured in several conditions, all with the subjects sitting in an armchair (see figure 5.1),

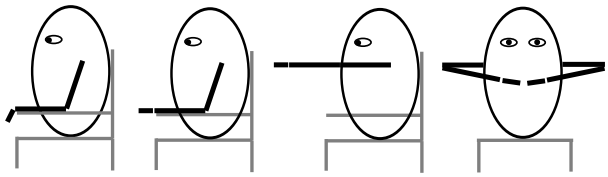

Figure 5.1: Sketch of tasks conducted to test rest and postural tremor

- forearms leaned on the armrests and hands hanging freely down,
- forearms leaned on the armrests and hands extended forward horizontally,
- arms held forward horizontally towards a horizontal target placed in front of the subject at the height of shoulders, hands pronated,
- "wing" position.

The first task is intended for the assessment of the rest tremor. The other tasks are intended for the assessment of the postural tremor. Tests lasted 20 seconds and were conducted twice (except for two subjects). Totally, 464 recordings of tasks to test the rest and postural tremor were acquired with sensors placed on both hands, that means 928 recordings from a hand in a test were obtained. Whole trials were 8 to 15 minutes long and included also tests for the intention tremor.

Integrated inertial measurement units MTx® by Xsens® were placed on subjects' hand dorsa over third and fourth metacarpal bones using neoprene bands with hook-and-loop fasteners. The units measure acceleration, angular rate, and local magnetic field in three axes. Internally computed estimates of the orientation may be acquired too. The measured quantities were transmitted with the sampling frequency of 100 Hz by cables to a personal computer and acquired using our own software. The software served also to identify starts of the tests by pressing keys on the PC keyboard by one of investigators. The internal orientation estimates provided by the unit were not acquired because in our original clinical study we were only interested in the acceleration. Moreover, technical problems with the software at the beginning of the study hindered the acquisition of orientation estimates.

5.2.3 Preprocessing and inertial estimation

Time-varying gyroscope biases may produce large errors in the estimation of orientation. To reduce them, they were calibrated out in each measurement trial using the following scheme. The intensity of movement was quantified by means of variation of the gyroscope signal ω and the filtered accelerometer signal a (low-pass, 8 Hz) in 0.3 s segments. Segments with RMS of standard deviations over the 3 axes (σ_a, σ_ω) lying below the predefined threshold (0.1 $\mathrm{m\,s^{-2}}$ and 0.05 $\mathrm{rad\,s^{-1}}$ for accelerometer and gyroscope, respectively) were marked as quasistatic. Each segment was characterized by its mean measured angular rate, σ_a, and σ_ω. Consecutive segments with similar properties were joined. Gyroscope bias was then estimated as the mean angular rate in the quasistatic segments. Similar approach was used for the calibration of accelerometers in several calibration sessions. The sensor was rotated into 6 different inclinations and the measurements were segmented as described above. The biases and gains of the accelerometers were obtained using the quasistatic state approach

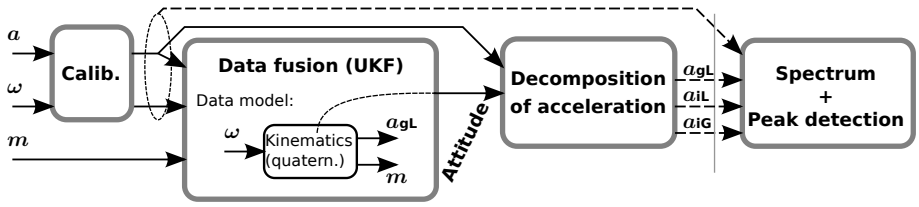

Figure 5.2: Block scheme of estimation and quantification

(Lötters et al. 1998) with the use of a different optimization procedure (Grammalidis and Strintzis 1998) and $1/\sigma_a^2$ as weights in the optimization criterion.

The orientation estimate provided by IMU was not acquired in real-time during measurement, instead, we applied own estimation of orientation with the use of calibrated data off-line. The unscented Kalman filter (UKF) (Julier and Uhlmann 1997, Wan and van der Merwe 2001) was used to fuse the information from IMU data (linear acceleration in 3 axes, angular rate around 3 axes and 3 components of local Earth magnetic field). The UKF was chosen as the tool because the unscented transform can propagate covariances better through a nonlinear system than the more commonly used Extended Kalman filter (EKF) using linearization of the system equations. Better accuracy of UKF compared to EKF was demonstrated in a navigation application involving a nonlinear equation of quaternion update by van der Merwe and Wan (2004). Quaternion update is a fundamental part of our model too. The filter forms the UKF block in fig. 5.2.

First three blocks represent preprocessing and inertial estimation, the last block represents amplitude and frequency extraction. Values a, ω, m are the acceleration, angular rate and local magnetic field, respectively, measured in the coordinate system of the measurement unit. Decomposition outputs are a_{gL} (gravitational artifact), a_{iL} (acceleration due to movement observed in the sensor frame), and a_{iG} (the same quantity transformed into the Earth-fixed frame).

The data fusion filter is based on quaternion representation of kinematics. Quaternions and their algebra provide an efficient tool for representing rotations in 3D lacking the gimbal lock of 3-angle systems (e. g. Euler angles) and using only four numbers ($q = [q_0\ q_1\ q_2\ q_3]^{\mathrm{T}}$) instead of nine in 3×3 rotation matrices, see for example Stevens and Lewis (2003). The rotation from an Earth-fixed reference frame to the reference frame of the sensor was used to represent the orientation of the sensor. The rotation matrix R corresponding to a known quaternion with unit size may be expressed for example by

$$R = \begin{bmatrix} q_0^2 + q_1^2 - q_2^2 - q_3^2 & 2(q_1 q_2 + q_0 q_3) & 2(q_1 q_3 - q_0 q_2) \\ 2(q_1 q_2 - q_0 q_3) & q_0^2 - q_1^2 + q_2^2 - q_3^2 & 2(q_2 q_3 + q_0 q_1) \\ 2(q_1 q_3 + q_0 q_2) & 2(q_2 q_3 - q_0 q_1) & q_0^2 - q_1^2 - q_2^2 + q_3^2 \end{bmatrix} \tag{5.1}$$

The quaternion representation of the orientation forms the state vector of the data fusion filter. The angular velocity acts as an input. The projection of gravity and the projection of the local Earth magnetic field to the sensor coordinate frame are model outputs. The continuous quaternion update equation and output equations are

$$\begin{aligned} \dot{q}(t) &= \tfrac{1}{2}[\Omega(t)\times]\, q(t), \\ a_{\mathrm{gL}}(t) &= R(q(t))\,[0 \;\; 0 \;\; \mathrm{g}]^{\mathrm{T}}, \\ m(t) &= R(q(t))\, m_0, \qquad m_0 = [\cos\phi_{\mathrm{m}} \;\; 0 \;\; -\sin\phi_{\mathrm{m}}]^{\mathrm{T}}, \end{aligned}$$

where q is the quaternion of the rotation from the global reference frame to the local frame of sensor, $R(q)$ is the corresponding rotation matrix, a_{gL} is the projection of gravity to the local reference frame, g is the size of gravitational acceleration, m is the estimated direction of the magnetic measurement, ϕ_{m} is the local magnetic inclination, and $[\Omega(t)\times]$ is the matrix derived from the instantaneous angular rate ω as defined in equation 2.3.

Approximate Euler discretization of the quaternion update was used as the state update equation in the model,

$$q(t_{k+1}) = f(q(t_k), \omega(t_k)) = q(t_k) + \frac{1}{2}[\Omega(t_k)\times]\, q(t_k)\, \mathrm{T_s}, \tag{5.2}$$

where $\mathrm{T_s}$ denotes the sampling period (0.01 s in our case). To ensure numerical stability of the quaternion estimate, it was divided by its amplitude between samples. Hence, the norm of the quaternion was forced to equal one. The (calibrated) measured angular rate ω was used as the input. The output measurements were measured acceleration a as a measure of the projection of gravity (that is a good measure under static conditions), measured vector of magnetic field – the sensors used were calibrated to give vectors of amplitude approximately 1 in non-corrupted Earth magnetic field.

In a standard setting, Kalman filter assumes exactly known inputs. That is not our case because of the noisy measurement of the angular velocity. The noise was taken into account using a covariance added to the process noise covariance in the model as shown for linear systems by Markovsky and De Moor (2005). The instant linearization of discretized quaternion update equation (5.2) at the estimated quaternion was used as the input matrix, (time argument omitted)

$$B = \frac{\partial f(q,\omega)}{\partial \omega} = \frac{1}{2}\mathrm{T_s}\begin{bmatrix} -q_1 & -q_2 & -q_3 \\ q_0 & -q_3 & q_2 \\ q_3 & q_0 & -q_1 \\ -q_2 & q_1 & q_0 \end{bmatrix}.$$

Then the process noise covariance used was

$$Q(t_k) = B(t_k) V_\omega B^{\mathrm{T}}(t_k) + \epsilon_{\mathrm{p}} \mathcal{I}_4,$$

where V_ω is the covariance of the gyroscope measurement noise, ϵ_{p} is a small constant (10^{-12} was used), and $\mathcal{I}_4$ is diagonal matrix. The small diagonal term was used as imaginary process noise to cope with errors caused by the discretization and to ensure positive definiteness of Q.

Simple rules modifying the observation covariance matrix were incorporated to reduce influence of magnetic disturbances and influence of movement to the accelerometer as a sensor of gravity. The rules are based on differences between the magnitudes of the measured acceleration and magnetic field vectors and the expected sizes.

$$R_a(t_k) = V_a + k_a N_a^2(t_k)\, \mathcal{I}_3; \quad R_m(t_k) = V_m + k_m N_m^2(t_k)\, \mathcal{I}_3,$$

where V_a and V_m are covariances of accelerometer and magnetometer noise, respectively. Local relative discrepancies between found and expected amplitudes of measured signals as measures of the model outputs are defined

$$\begin{aligned} N_a(t_k) &= \mathrm{WA}\left(\tfrac{|\|a(\tau)\|_2 - \mathrm{g}|}{\mathrm{g}}\right); \quad t_k - n \le \tau \le t_k + n, \\ N_m(t_k) &= \mathrm{WA}\left(|\|m(\tau)\|_2 - 1|\right); \quad t_k - n \le \tau \le t_k + n, \end{aligned}$$

where operation WA stands for a weighted average. The averaging is a filtering by a non-causal FIR filter with length $2n + 1$. The length used was 3 ($n = 1$) and weights [0.25 0.5 0.25]. Constants $k_a = 200$ and $k_m = 2$ were found experimentally by iterating on their values and comparing a known displacement with the displacement estimated by double numerical integration of the movement acceleration estimated via the orientation estimation procedure – sensor was moved several times by hand from one place and put back or to another place at known distance.

The Unscented Kalman filter was implemented using ReBEL Toolkit (OGI School of Science & Engineering 2008) in Matlab® without particular focus on computational efficiency. Having obtained the estimates of orientation, gravity was projected to the sensor reference frame and subtracted from the measured acceleration. Finally, we analyzed five 3D signals,

- a measured acceleration, calibrated,
- a_{gL} estimated projection of gravity to the local frame, called also gravitational artifact or component in the text, $a_{\mathrm{gL}}(t_k) = R(t_k) \cdot [0 \;\; 0 \;\; \mathrm{g}]^{\mathrm{T}}$, where $R(t_k)$ is the rotation matrix determined by the estimated quaternion,
- a_{iL} estimated acceleration due to movement in an Earth-fixed reference frame, observed in the local (sensor) frame, called also motion acceleration or component in the text, $a_{\mathrm{iL}}(t_k) = a(t_k) - a_{\mathrm{gL}}(t_k)$,
- a_{iG} motion acceleration observed in the global Earth-fixed reference frame, $a_{\mathrm{iG}}(t_k) = R^{\mathrm{T}}(t_k)\, a_{\mathrm{iL}}(t_k)$,
- ω measured angular velocity, with estimated bias removed.

See figure 5.3 for examples of the acceleration decomposition. The obtained motion acceleration can be transformed to the global reference frame and potentially used for an estimation of position by double integration (figure 5.4).

The signals were measured with the same patient: (a) and (c) are from the first test on postural tremor, (b) is from the test on rest tremor. Approximate hand positions and the used axes are displayed. Means were subtracted from a and a_{gL} signals to get plots ranging around zero.

Sensors are subject to errors, especially biases that deteriorate the quality of orientation estimate and consequently our tremor detection scheme. We did some calibration as noted above. But even if the initial calibration had been perfect, errors could arise from the drift of biases. Therefore, check was made for additional errors in measured quantities. Namely, biases of 0.02 $\mathrm{m\,s^{-2}}$ and 0.01 $\mathrm{rad\,s^{-1}}$ were added to Y axes of accelerometers and gyroscopes, respectively. The errors are approximately of the size of the biases found in single axes of the sensors used: Biases of the two accelerometers found in one of the calibration sessions were [-0.019 0.027 -0.017] and [0.021 -0.054 -0.043] $\mathrm{m\,s^{-2}}$. Gyroscope biases found

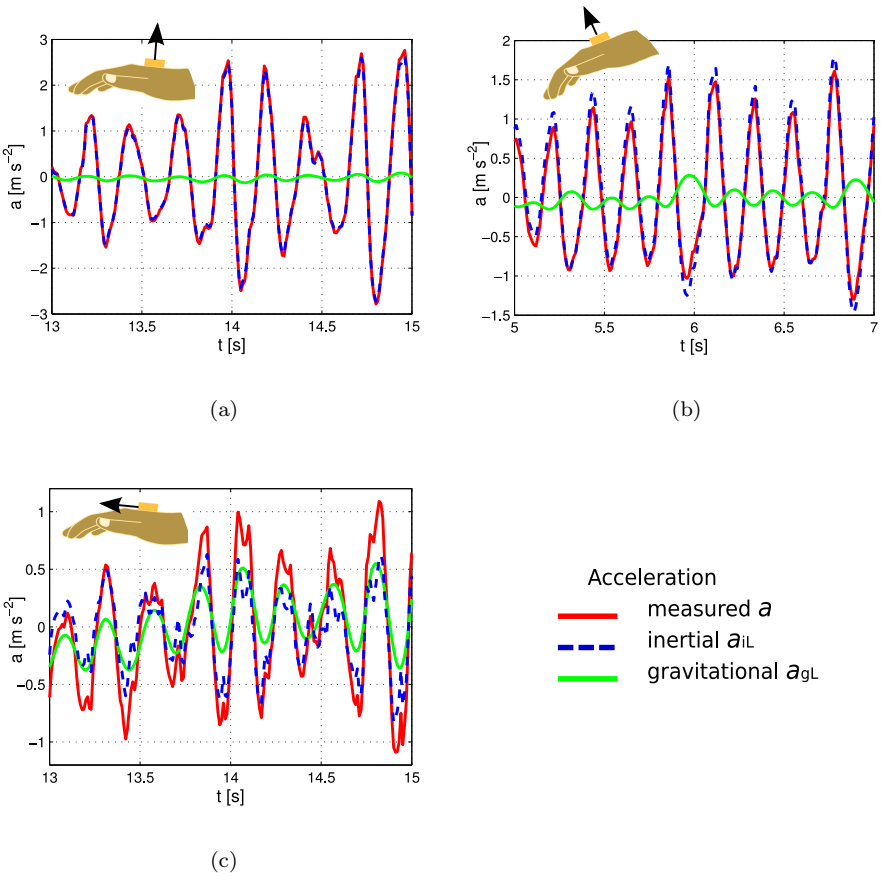

Figure 5.3: Examples of decomposition

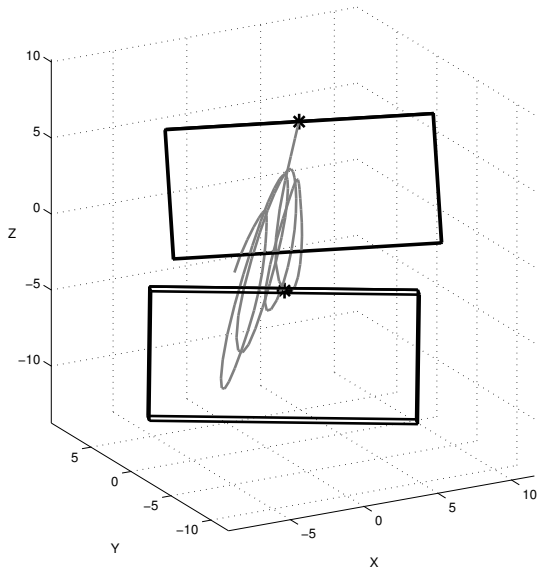

Figure 5.4: Example of tremor movement reconstructed by inertial estimation. The displacement estimate (mm) in a one-second interval of a measurement of relatively strong tremor is displayed (gray). The double integration of a_{iG} was combined with high pass filtering to eliminate drift caused by the integration of errors in a_{iG}. The estimated orientation of the sensor is visualized at two instants (stars), 0.1 s apart, using black line boxes ($16 \times 12 \times 8$ mm).

in the 59 measurement sessions were (mean ± standard deviation) [0.001 ± 0.004, 0.004 ± 0.002, 0.017 ± 0.002] rad s^{-1} for one gyro and [-0.030 ± 0.005, 0.015 ± 0.002, 0.022 ± 0.003] rad s^{-1} for the second one.

The acceleration was decomposed twice in addition to the original decomposition – using a corrupted by the constant bias and using ω corrupted by the constant bias. The resulting acceleration components were fed to the spectral peak quantification scheme. Obtained amplitudes were compared to the amplitudes of the components derived using the original, calibrated, measurements.

5.2.4 Amplitude and frequency extraction

Fast Fourier transform was used to quantify tremor frequency and amplitude as it is widely used technique in the field (Foerster and Smeja 1999, Matsumoto et al. 1999, Louis and Pullman 2001, Burkhard et al. 2002, Elble 2003, Morrison et al. 2005, Giuffrida et al. 2009) and provides a straightforward representation of frequency distribution of the signal amplitude. As alternatives, time-domain algorithms based on thresholds (van Someren et al. 1993), parametric identification methods (Salarian et al. 2007b, Spyers-Ashby et al. 1998), and techniques based on empirical mode decomposition (EMD) (Rocon de Lima et al. 2006) have been proposed in the literature.

First, means were removed from signals. Then, power spectral density (PSD) was computed for every component of a 3D signal via a filtered periodogram. The periodogram was smoothed by a weighted moving average with the window of width approximately 1 Hz and triangular weights b defined by

$$b(k) = \frac{hl - |k|}{\sum_{m=-hl+1}^{m=hl-1} hl - |m|}; \quad -hl < k < hl; \quad hl = \mathrm{round}(0.5\,\Delta f); \quad \Delta f = \frac{\mathrm{f_s}}{dl},$$

where $\mathrm{f_s}$ is the sampling frequency (Hz), Δf frequency step in the periodogram (Hz), dl data length (samples), hl length of a half of the averaging window (number of frequency steps), and b is the vector of filter coefficients. This method gives a high frequency resolution compared to averaged periodogram. The length was chosen based on the heuristic idea not to over-smooth the periodogram and on our visual observations (see figure 5.5 for examples). The length of 1 Hz coincides with the choice by Timmer et al. (1996), where it was used to get an initial estimate of PSD to start a more complex adaptive scheme. Frequency distribution of power of the 3D signal was computed as the sum of the three PSD.

Peaks were detected in the composite PSD by the following algorithm.

1. In the interval 1–15 Hz find all local minima and maxima between them,
2. reduce the number of maxima to get the set of highest maxima separated from each other by minima deep at least 3 dB (with the value half the lower of the resting neighbor maxima),
3. take the position of the highest resting maximum between 3.5 and 12 Hz as tremor frequency f_α , where α stands for the name of the signal used (a, a_{iL}, a_{iG}, a_{gL}, or ω).

Usually, this algorithm gives the same frequency as a simple position of the maximum of PSD in the interval 3.5–12 Hz. The difference was especially in the cases where a non-tremor movement produces a low frequency artifact with amplitude higher than the tremor peak and with falling slope of PSD crossing the lower boundary of the frequency range of

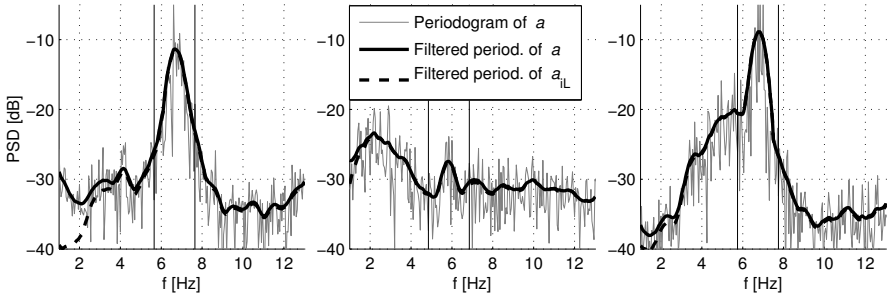

Figure 5.5: Examples of PSD estimate

tremor (figure 5.5, in the middle), and in the cases where no marked peak appeared (no peak separated from the rest of PSD by sufficiently deep minima). The first situation may arise especially in measurements where a combination of marked voluntary movement and tremor occurs. As alternatives to find the tremor frequency in presence of other motion, there may be used parametric methods of PSD estimation, EMD (Rocon de Lima et al. 2006, Slack and Ma 2007), or EKF with a harmonic model of the tremor and low frequency random noise model of the other motion (Bó et al. 2009).

For each signal α (α standing for a, a_{iL}, a_{iG}, a_{gL}, or ω), its amplitude A_α, called also tremor amplitude in the text, was determined. The amplitude (effective value) was computed as the square root of the numerical integral of PSD in the ± 1 Hz neighborhood of the detected frequency f_α. The width of 2 Hz was found enough to cover the width of typical peaks, although in some cases parts of sidelobes were missing (figure 5.5). When no peak was detected, the amplitude was set to zero.

Composite PSD estimates of 3D accelerometer signals from three measurements. Thin line corresponds to the periodogram method; thick line corresponds to the method of filtered periodogram. Dashed line corresponds to the PSD estimate of the motion component of acceleration. Two vertical lines mark ± 1 Hz neighborhood of the peak frequency.

5.2.5 Correlations of amplitudes and frequencies detected for different signals

The signals (a, a_{iL}, a_{iG}, a_{gL}, ω) were compared in terms of Pearson's linear correlation coefficients between the amplitudes (A) and between the frequencies (f) derived from the peaks detected in their spectra. The cases where no peaks were detected in some of the signals were removed from this analysis.

Amplitudes may range over several decades, and then linear correlation coefficients between raw amplitudes may be dominantly determined by several highest amplitudes. Logarithms of amplitudes reduce the influence of highest values to correlation coefficients. They were also found to be linearly related to tremor severity as rated by clinicians (Elble et al. 2006). Therefore, correlations of amplitude logarithms were computed too.

5.2.6 Alignment with hand axes

Part of the measurements was also treated in more detail via the calculation of amplitudes in individual axes. Estimated axes of hands were used instead of axes of sensors. The relative

orientation of hand and sensor axes was determined from the task with arms held forward towards a horizontal target. Rotation matrices were computed using following rules. Axes Z of hands are considered to be vertically heading up during the test. Axes X are considered to be parallel to the average of projections of sensor's axes X (aligned approximately to proximodistal axes of hands) to horizontal plane. Axes Y then head horizontally to the left from the view of the subject. Amplitudes obtained for the motion and gravitational components in the estimated axes were compared.

5.2.7 Differences between groups

The group of patients with essential tremor and the group of healthy subjects were compared in averages and variances of amplitude logarithms. The amplitude of the acceleration a_Z measured in the direction perpendicular to the hand was analyzed beside the amplitudes of the 3D signals.

In cases where no peak was detected the amplitude was set to a small value to get a finite logarithm. The value chosen was 0.0025 for A_{aZ}, 0.01 for A_a, $A_{a\mathrm{iL}}$, and $A_{a\mathrm{iG}}$, 0.001 for $A_{a\mathrm{gL}}$ and 0.005 for A_ω, that is near to the least nonzero amplitude (0.0025, 0.0114, 0.0107, 0.0012, 0.0052 for A_{aZ}, A_a, $A_{a\mathrm{iL}}$, $A_{a\mathrm{gL}}$, A_ω, respectively). The limited logarithm calculated in this way from amplitude A_α is denoted L_α.

Two-sample t-test was accomplished to trace differences between the groups. It was applied to amplitude logarithms from

- the test for rest tremor,
- all the tests for postural tremor taken together.

Two parameters of receiver operating characteristic (ROC) curves were extracted for the amplitudes from all the tests for postural tremor taken together,

- the area under the ROC curve (AUC),
- potential percentage of correct classification of the signal to come from the group of patients or controls based on its amplitude.

First, all the parameters were obtained for the scenario that the amplitude derived from the signal only in one hand in one test was used to classify the subject as a patient or as a control. In the second scenario, the greater of the amplitudes from the left and right hand in one test was used. Note that in the first scenario the number of samples was twice the number of samples in the second scenario because the amplitudes from the left hand and from the right hand were taken separately.

5.2.8 Regression of visual assessment

In part of the measurements (177 tests with 21 patients and two controls), a video of hands and arms of subjects was recorded simultaneously with the acquisition of inertial data. Tremor amplitude in both hands was assessed from the video recordings by two trained clinicians according to the amplitude assessment in the Fahn-Tolosa-Marín Tremor Rating Scale (0, 1, 2, 3, 4). When scores assessed by the two clinicians differed, the average was used for statistical analysis. Totally, 354 scores of a hand tremor were obtained (177 tests, 2 hands).

	Rest tremor					Postural tremor				
	Amp [$\mathrm{m\,s^{-2}}$, $\mathrm{rad\,s^{-1}}$]			Freq [Hz]		Amp [$\mathrm{m\,s^{-2}}$, $\mathrm{rad\,s^{-1}}$]			Freq [Hz]	
	median	IQR	max	median	IQR	median	IQR	max	median	IQR
Patients										
a	0.05	0.07	7.08	5.95	3.10	0.16	0.23	13.46	6.30	2.11
a_{iL}	0.05	0.07	6.64	5.93	3.00	0.15	0.22	13.12	6.28	2.05
a_{gL}	0.005	0.009	1.13	5.78	2.25	0.009	0.020	1.09	6.30	1.85
ω	0.018	0.036	3.66	6.53	2.75	0.040	0.059	3.48	6.60	2.15
Norms										
a	0.03	0.02	0.15	7.65	2.60	0.07	0.04	0.36	6.95	2.80
a_{iL}	0.03	0.02	0.14	7.60	2.53	0.07	0.04	0.35	6.95	2.78
a_{gL}	0.002	0.004	0.015	7.85	2.48	0	0	0.03	8.05	3.15
ω	0.011	0.010	0.084	8.10	2.30	0.015	0.009	0.14	8.15	3.25

Table 5.1: Median and inter-quartile ranges (IQR) for the amplitudes and tremor frequencies in rest and postural tremor in essential tremor patients and healthy subjects. For amplitudes, also maximum found values are shown.

The score was regressed using the linear least squares method. The regression functions were polynomials with the logarithms (limited, see the previous section) of the obtained amplitudes as variables. Polynomials in a single amplitude logarithm were used with the degree up to 15. 2D polynomials were used with total degree up to 15. 3D polynomials were used with total degree up to 13. For example, the total degree of 2D polynomial in L_a, and L_ω, $b_{00} + b_{10}L_a + b_{01}L_\omega + b_{11}L_aL_\omega + b_{02}L_\omega^2 + b_{12}L_aL_\omega^2$, is considered to be 3 (1 in L_a and 2 in L_ω).

The leave-one-out method was used to verify the ability of the different polynomial structures of the regression function to predict the visual assessment. One visual score and the corresponding set of amplitudes were left out each time. The root mean squares error (RMSE), mean absolute error (MAE), coefficient of determination (r^2), and percentage of predictions with error lower than 1 (%E<1) were computed as the measures of regression accuracy.

5.3 Results

5.3.1 Amplitudes and frequencies

Medians and inter-quartile ranges (IQR) of the amplitudes and frequencies provide a description of the values found in the patients and healthy subjects in our sample. See table 5.1 for the results. Medians and IQR were used instead of means and standard deviations due to skewed spread of the values, especially of the amplitudes. In the text below, logarithms of the amplitudes are often used instead of the amplitudes themselves, reducing the skewness.

Amplitudes are calculated from powers, so they correspond to RMS instead of peak-to-peak. Frequencies are taken only from the cases, when a peak in spectrum was detected. Amplitudes are taken also from the cases when no peak was detected – then the amplitude was assumed zero.

In clinical evaluations, most of the patients included in the study exhibitted only mild to moderate tremor.[2]

[2]M. Hoskovcová, O. Ulmanová, O. Šprdlík, T. Sieger, J. Nováková, R. Jech, E. Růžička: Disorders of balance and gait in essential tremor are associated with midline tremor and age. 2012. Submitted.

	Correlation		Mean difference (%)	
	Bias in a	Bias in ω	Bias in a	Bias in ω
$A_{a\mathrm{iL}}$	0.99999999	0.999991	0.08	0.2
$A_{a\mathrm{iG}}$	0.99999999	0.999998	0.08	0.2
$A_{a\mathrm{gL}}$	0.99998	0.9999	2.8	5.6

Table 5.2: Influence of calibration accuracy **Left:** Pearson's correlation coefficients between amplitudes of 3D signals calculated from the calibrated sensors data and amplitudes calculated from the data corrupted by additional errors in acceleration (a) and angular rate (ω). The amplitudes were calculated from peaks in PSD of the signals. **Right:** Mean relative differences between the original amplitudes and amplitudes from corrupted signals. Mean relative difference was defined as the mean of absolute values of the differences between the two values divided by the maxima of the two values, e. g. for the amplitude of motion component $A_{a\mathrm{iL}}$ obtained from one measurement with the use of the calibrated data and the amplitude obtained with the acceleration corrupted by additional bias ($A_{a\mathrm{iL,\,corrupted}\,a}$) the relative difference was $|A_{a\mathrm{iL}} - A_{a\mathrm{iL,\,corrupted}\,a}| / \max(A_{a\mathrm{iL}}, A_{a\mathrm{iL,\,corrupted}\,a})$. Where both amplitudes were zero, the relative difference was also considered zero.

5.3.2 Influence of sensor biases

The amplitudes of acceleration components obtained using the acceleration measurement corrupted by the additional bias and using the angular rate measurement corrupted by the additional bias were compared to the amplitudes of acceleration components obtained using the calibrated data, see table 5.2. The differences between amplitudes were relatively low, especially for the motion component. The most apparent mean differences were contributed by several occurrences of the situation, when in calibrated or impaired data a peak was found fulfilling the criteria stated in section 5.2.4 and in the other not. The relative difference was 100 % in such situation. Note that amplitudes $A_{a\mathrm{gL}}$ were much lower than amplitudes of the motion component (see tables 5.1 and 5.5 and figure 5.6).

5.3.3 Relationships between amplitudes and frequencies detected for different signals

The amplitudes and frequencies were compared in terms of correlation coefficients according to section 5.2.5. The cases where no peaks were detected in some of the signals were removed from this analysis. A peak was detected in PSD of a in 891 from 928 tests, in 895 cases for a_{iL}, 894 for a_{iG}, in 455 for a_{gL}, and in 878 for ω. Totally, 449 tests remained with peaks detected in all the signals.

Correlation coefficient for both raw amplitudes and their logarithms to base 10 are listed in table 5.3. The most correlated amplitudes were $A_{a\mathrm{iL}}$ and $A_{a\mathrm{iG}}$. They also correlate well with the amplitude of the measured acceleration (A_a). Amplitude of the gravitational component ($A_{a\mathrm{gL}}$) correlate better with the amplitude of angular rate (A_ω) than do these two amplitudes with amplitudes of other accelerations (A_a, $A_{a\mathrm{iL}}$, $A_{a\mathrm{iG}}$). The same holds for the logarithms of amplitudes. Correlation coefficients between peak frequencies of different signals are listed in table 5.4. The highest correlations are again for a, a_{iL}, and a_{iG} mutually. Frequency of a_{gL} correlates the most with the frequency of ω. The amplitudes of the gravitational component of acceleration were lower than the amplitudes of motion acceleration (about one tenth, see tables 5.1 and 5.5 and figure 5.6).

	Corr. of amplitudes			Corr. of logarithms		
	$A_{a\mathrm{iL}}$	$A_{a\mathrm{gL}}$	A_{ω}	$A_{a\mathrm{iL}}$	$A_{a\mathrm{gL}}$	A_{ω}
A_a	0.999	0.92	0.93	0.9995	0.94	0.95
$A_{a\mathrm{iL}}$		0.90	0.91		0.94	0.95
$A_{a\mathrm{gL}}$			0.996			0.97

Table 5.3: Correlation coefficients between amplitudes derived from spectral peaks of different signals **Left:** Correlations of amplitudes. **Right:** Correlations of amplitude logarithms. Correlations of $A_{a\mathrm{iG}}$ and its logarithms (not included in the table) with $A_{a\mathrm{iL}}$ and its logarithms were greater than 0.9998. Differences between their correlations with other quantities were lower than 0.0005.

	Correlations of frequencies		
	$f_{a\mathrm{iL}}$	$f_{a\mathrm{gL}}$	f_{ω}
f_a	0.96	0.71	0.68
$f_{a\mathrm{iL}}$		0.67	0.65
$f_{a\mathrm{gL}}$			0.79

Table 5.4: Correlation coefficients between tremor frequencies derived from different signals Differences between correlations of $f_{a\mathrm{iG}}$ (not included in the table) and $f_{a\mathrm{iL}}$ with others were lower than 0.0005.

Usually, the frequency of the detected peak was (at least approximately) the same from all signals where a peak was detected in the same test. In some cases the frequency differed notably (e. g. f_a and $f_{a\mathrm{gL}}$). In 238 tests from 928 the maximum difference between detected peaks was greater than 1 Hz. Most of these cases occurred in tests with signals of relatively low amplitudes. Part of the cases involved such peaks that the frequency of one of them was approximately double of the frequency of another one. That may stem from the nonlinear properties of periodic movement with rotational character mentioned in the introduction.

5.3.4 Analysis in individual axes

More detailed analysis was done for the test on postural tremor with hands extended horizontally and for the test on rest tremor with hands hanging freely down from arm support. Amplitudes were computed not only from composite PSD of 3-component signals but also for all signal components separately. Hand axes were used instead of sensor axes. Ratios between amplitudes of gravitational artifact and motion acceleration were studied.

See table 5.5 for ratios of gravitational and motion acceleration amplitudes. In the test on postural tremor the ratio is notably lowest in the Z axis. That agrees with the results of the analysis realized by Elble (2005). In the test on the rest tremor the difference between the mean ratios in individual axes is not so high – Z axis is more inclined from the vertical due to the hanging position of the hand and its sensitivity to changes of the gravitational component due to rotations is greater.

	X	Y	Z	All
Postural				
max	0.50	0.42	0.09	0.17
average	0.18	0.11	0.02	0.07
min	0.05	0.02	0.001	0.03
Rest				
max	0.56	1.11	0.51	0.49
average	0.09	0.14	0.10	0.12
min	0.02	0.03	0.02	0.04

Table 5.5: Ratios of amplitudes of gravitational and motion components. That is, mean and extremal ratios found between the amplitudes of gravitational artifact and motion acceleration ($A_{a\mathrm{gL}}/A_{a\mathrm{iL}}$) in tests for postural and rest tremor. The ratio is listed for different sensor axes as well as for the overall amplitudes of three-component signals. Cases where some of the two amplitudes was zero were not included in the averaging.

5.3.5 Differences between groups

Means and standard deviations of limited amplitude logarithms were computed. For the visualization they were transformed back to absolute values and shown in figure 5.6 in logarithmic coordinates.

In all signals both groups were far from having same mean amplitude logarithm ($P < 10^{-8}$). Not surprisingly, in tests for postural tremor the groups were distinguished better (see figure 5.6). The tests are known to be more suitable to distinguish the groups as postural tremor is more typical in essential tremor patients than rest tremor. The parameters of ROC curves were also extracted for amplitudes of each signal in all the tests for postural tremor taken together.

See table 5.6 for the results. In most of separability measures, amplitudes of motion acceleration ($A_{a\mathrm{iL}}$ and $A_{a\mathrm{iG}}$) and the amplitude of measured acceleration (A_a) distinguished the groups best. The exception is the P-Value in the first scenario that is lower for the amplitude of angular rate (A_ω). ROC parameters of A_ω are comparable to the parameters of A_a, $A_{a\mathrm{iL}}$, and $A_{a\mathrm{iG}}$ in the first scenario.

In some parameters (P-value in both scenarios and potential classification accuracy in the first scenario), amplitudes of motion components performed a little better than the amplitude of the measured acceleration. The amplitude derived from the acceleration measured in the approximately vertical axis (A_{aZ}) performed worse in all the parameters than A_a, $A_{a\mathrm{iL}}$, and $A_{a\mathrm{iG}}$ and in most of the parameters worse than A_ω.

5.3.6 Regression of the visual assessment

The visual assessment of tremor severity by clinicians was interpolated by polynomials of different degrees and in different number of variables. Limited logarithms of amplitudes were used as the variables. See section 5.2.8 for more details and figure 5.7 for an example. The proficiency of different regression function structures was quantified by root mean square error (RMSE) and by the percentage of predicted tremor scores that differed from the values assessed by clinicians by less than 1 with the use of the leave-one-out methodology. See table 5.7 for an excerpt of results. For the sake of brevity, only several combinations of 2 and 3 amplitudes are shown, that reached the best RMSE. Only results for the two best polynomial

	First scenario: A_α			Second scenario: max(A_α left, A_α right)		
	P-Value	AUC	Pot. accuracy (%)	P-Value	AUC	Pot. accuracy (%)
A_{aZ}	$2.1\ 10^{-35}$	0.783	74.4	$9.3\ 10^{-24}$	0.807	78.7
A_a	$3.8\ 10^{-43}$	**0.809**	**76.7**	$7.2\ 10^{-26}$	**0.834**	**79.9**
$A_{a\mathrm{iL}}$	$2.2\ 10^{-43}$	**0.808**	**76.9**	$\mathbf{1.5\ 10^{-26}}$	**0.833**	**79.9**
$A_{a\mathrm{iG}}$	$1.1\ 10^{-43}$	**0.809**	**76.9**	$\mathbf{1.5\ 10^{-26}}$	**0.833**	**79.9**
$A_{a\mathrm{gL}}$	$3.7\ 10^{-40}$	0.747	73.6	$2.4\ 10^{-25}$	0.793	77.9
A_ω	$\mathbf{1.3\ 10^{-44}}$	**0.808**	76.1	$1.5\ 10^{-25}$	0.821	77.3

Table 5.6: Measures of the separability of the groups of patients and controls in terms of tremor amplitude of postural tremor. Best values (with some tolerance) are highlighted in bold. **Top:** Tremor amplitude taken from a hand in one test. **Bottom:** Greater of the amplitudes from the left and right hand in one test. ***P*-Value:** P-Values of two-sample t-tests applied to amplitudes of postural tremor of the group of patients and the group of controls. Note that in the second scenario, the number of samples is half of the number in the first scenario. **AUC:** The area under the ROC curve. **Potential accuracy:** Percentage of correct group classifications with the amplitude thresholds set up optimally in terms of this criterion.

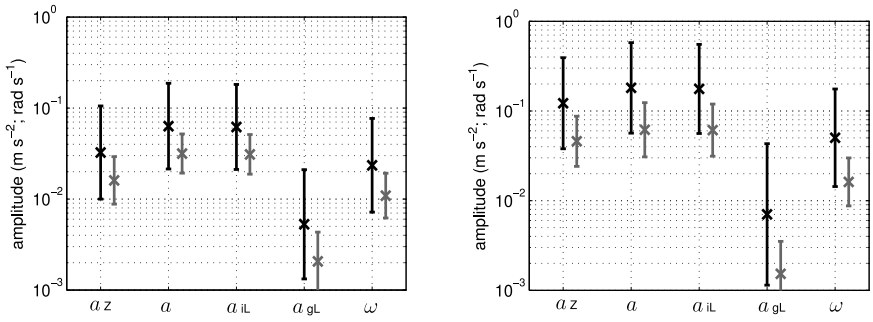

(a) (b)

Figure 5.6: Means and standard deviations of the amplitudes obtained from peaks in spectra of the measured acceleration in axis perpendicular to the hand a_Z, measured 3D acceleration a, movement acceleration in local coordinates a_{iL}, projection of gravity a_{gL}, and measured angular velocity ω. (a) Amplitudes from the test for rest tremor. (b) Amplitudes from all the tests for postural tremor. Means and standard deviations were computed in logarithmic coordinates. Left (black) bars correspond to the group of patients; right (gray) bars correspond to the group of healthy subjects.

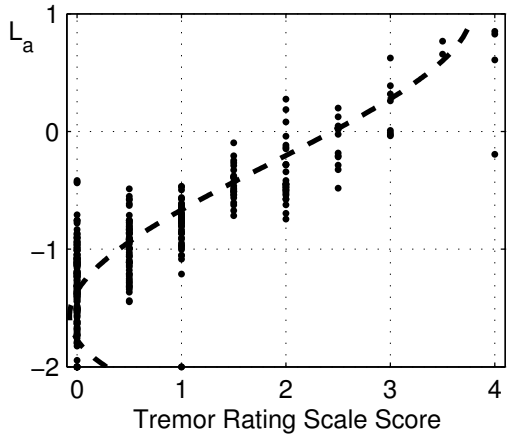

Figure 5.7: Mean visual scores and corresponding limited logarithms of the amplitudes derived for the measured acceleration (L_a). Scores were regressed by a polynomial in L_a, degree = 3, dashed line.

degrees are presented for each amplitude combination shown, plus the results of the first degree polynomials with one variable (linear regression).

From the first degree polynomials, the regression function using the angular rate amplitude had the lowest RMSE. However, when using the optimal degree, regression functions using amplitudes derived from measured and motion acceleration performed better.

Using more than one amplitude in the regression function usually improved the proficiency. All the presented regression functions using two and three amplitudes performed better in RMSE than any regression function using only one amplitude. All the regression functions using two variables presented in the table 5.7 also performed better or equally in the %E<1 parameter.

The optimal regression function structure, according to RMSE in the leave-one-out setting, was a polynomial of total degree 5 in logarithms of the three amplitudes derived from the angular rate, the motion acceleration in the global reference frame and the motion acceleration in the sensor frame. The error was 0.377 on the tremor rating scale. For most amplitude combinations presented, the proportion of predictions with error lower than 1 was about 98 %. The exceptions are 1D regression functions using $A_{a\mathrm{gL}}$ and A_ω.

Coefficients of determination (r^2) and mean absolute errors (MAE) were also computed in the leave-one-out setting for the regression function structures presented in table 5.7. From the linear functions, the one using A_ω was the best according to both criteria: r^2=0.72, MAE=0.375. From the other regression functions, the one using $A_{a\mathrm{iL}}$, $A_{a\mathrm{iG}}$, and A_ω, degree [1 2 2], was the best according to r^2 (0.83) and the one using $A_{a\mathrm{iL}}$ and A_ω, degree [5 2], was the best according to MAE (0.273). The coefficients of determination were greater than 0.8 and MAE lower than 0.3 for all the 2D and 3D regression function structures listed in the table and for all the 1D polynomials of optimal degrees listed that use A_a or $A_{a\mathrm{iL}}$.

	Best degree			Degree=1	
Amplitudes used	Degree	RMSE	%E<1	RMSE	%E<1
A_a	7	0.402	98.0	0.502	96.9
$A_{ai\mathrm{L}}$ ($A_{ai\mathrm{G}}$)	7	0.403	98.0	0.498	96.9
$A_{ag\mathrm{L}}$	7	0.516	94.1	0.655	89.5
A_ω	5	0.453	95.5	0.481	95.5
$A_{ai\mathrm{L}}$, A_ω ($A_{ai\mathrm{G}}$, A_ω)	10 1	0.380	98.0		
A_a, A_ω	5 2	0.384	98.0		
$A_{ai\mathrm{L}}$, $A_{ag\mathrm{L}}$ ($A_{ai\mathrm{G}}$, $A_{ag\mathrm{L}}$)	3 2	0.389	98.3		
$A_{ai\mathrm{L}}$, $A_{ai\mathrm{G}}$, A_ω	1 2 2	0.377	98.0		
$A_{ai\mathrm{L}}$, $A_{ag\mathrm{L}}$, A_ω ($A_{ai\mathrm{G}}$, $A_{ag\mathrm{L}}$, A_ω)	3 1 1	0.384	97.7		
$A_{ai\mathrm{L}}$, $A_{ai\mathrm{G}}$, $A_{ag\mathrm{L}}$	1 1 3	0.387	98.3		
A_a, $A_{ag\mathrm{L}}$, A_ω	3 1 1	0.387	97.5		

Table 5.7: Results of the regression of the visual assessment. The proficiency of regression functions was presented for the polynomial degrees that were the best according to the root mean square error (RMSE) with the leave-one-out method used. Limited logarithms of the listed amplitudes were the variables of the polynomials. For the polynomials of 2 and 3 variables, the numbers in the Degree columns correspond to degrees in the amplitude logarithms in the order as listed. Columns %E<1 contain the percentage of predicted tremor scores that differed from the values assessed by clinicians by less than 1. For the combinations of amplitudes listed in round brackets, %E<1 was the same as listed in the table, RMSE differed by less than 0.002. The proficiency of linear regression functions (polynomial degree = 1) with one variable is presented too.

5.4 Discussion

5.4.1 Relations of amplitudes

Findings about the ratio between the amplitudes of the estimates of the gravitational artifact and the motion acceleration agree with the analytic findings about the component of gravitational artifact by Elble (2005): The AC component of the gravitational artifact is relatively lowest in the (approximately) vertical axis and it is much greater in the other axes. The ratio implies that in other axes an error of up to tens of percent may occur if the measured acceleration is directly used to estimate the amplitude of spatial displacement by double integration.

Following the simplified model in (Elble 2005), the ratio in the proximodistal hand axis in the first test for postural tremor should be notably higher than that in table 5.5 and observed in the example in figure 5.3(c). The difference can be explained by differences between the measurement setup and the simplified model:

- The sensors were placed notably above the hand axis.
- Sensor/hand alignment and the orientation itself might be estimated inaccurately.
- Although the flexion-dorsiflexion movement of hands implying the high ratio in the model was typical in the used test for postural tremor, other movements also occurred.

Amplitudes and frequencies derived from the estimated 3D gravitational artifact correlate more with amplitudes and frequencies of the angular rate than do amplitudes and

frequencies of the estimated motion acceleration. That agrees with the fact that any changes in the gravitational component are only caused by rotations.

5.4.2 Relations to disease and visually assessed severity

Several measures were used to quantify the performance of amplitudes of different signals to distinguish the group of patients from healthy subjects: parameters of the ROC curve and the two-sample t-test applied to amplitude logarithms. The amplitudes of the 3D measured and motion acceleration (A_a, $A_{ai\mathrm{L}}$, $A_{ai\mathrm{G}}$) and the amplitude of angular rate (A_ω) distinguished the groups best according to different criteria. All these amplitudes performed better in most of the measures than the single accelerometer axis perpendicular to the hand that is used widely in the literature. In some separability measures, the amplitudes of the motion component performed better than the amplitude of the measured acceleration. However, the differences were low.

Polynomial regression functions with suitable inputs and polynomial degrees were able to predict the visual assessment of tremor intensity with the root mean square error under 0.4. In about 98 % of the measurements they predicted the score with the error lower than 1. The performance was very good with respect to the fact that the resolution of the visual assessment was 1 (0.5 when averaging two raters with different rates). The regression functions using several amplitudes including the amplitude of motion component performed a little better than if using the measured acceleration instead of the motion component.

5.4.3 Comparison of visual assessment regression to other works

A number of other works deal with the regression or correlation of a visual rating with quantities from an instrumented assessment. Part of them deal with a long-term ambulatory monitoring of tremor (Salarian et al. 2007b, van Someren et al. 1998, van Someren et al. 2006), other part use short measurements in defined hand positions (Matsumoto et al. 1999, Elble et al. 2006, Giuffrida et al. 2009, Mostile et al. 2010). The first approach differs from this study as the data were captured and averaged in long time intervals on one hand, but the setup was more relaxed on the other hand – even measurements from free movement of persons were included. In the second approach, the setup was tighter than our: The regression was done for a particular task and well defined hand position each time. Moreover, various clinical scales were used in the studies as the quantities to regress (or to use as regressors of measured amplitudes). Due to these facts, it cannot be judged which regression was of the best quality directly by comparing the coefficients of determination, residual errors, etc.

A specialized time-domain algorithm using data from accelerometers placed on forearms was presented by van Someren et al. (1993) to assess in daily life the tremor amplitude and the proportion of time with tremor present. Other movements were also quantified beside tremor. The algorithm was further refined, ported to different hardware, and validated by van Someren et al. (1998) and van Someren et al. (2006). Relatively long-term measurement and simultaneous minute-by-minute UPDRS rating of tremor amplitude were done. Tremor detection accuracy was good. High correlations were found between the obtained quantities and UPDRS when averaging over long time periods. The correlation of the estimated mean tremor duration with the mean clinical score was as high as $r = 0.96$ (r^2 about 0.92) in (van Someren et al. 1998). However, without averaging, the correlations of minute-by-minute quantities were published only within subjects, causing them relatively

low due to a limited variation of tremor amplitude and occurrence in a single subject: Mean correlation coefficient was 0.71 (corresponding to r^2 about 0.5) in (van Someren et al. 1998).

By Salarian et al. (2007b) another method was proposed to quantify tremor in daily life using gyroscopes placed on forearms instead of accelerometers. The algorithm was tested on a sample of 10 patients with Parkinson's disease (PD) and 10 control subjects. Very high sensitivity and specificity was found when detecting tremor in periods of 3 seconds in a long protocol when compared to the visual assessment from a video recording. Correlations up to $r = 0.87$ (r^2 about 0.76) were found between an UPDRS tremor subscore (items 20+21, rest and action tremor) and mean logarithm of amplitudes computed from measurement in a 45 minutes long fixed protocol. The protocol was performed immediately after the UPDRS rating. Similar correlation was found in a free-move setting when averaging amplitude logarithms in periods of 30 or 45 minutes preceding the UPDRS evaluations.

A wide range of clinical scales and instrumented assessments at several institutions was studied by Elble et al. (2006). Two regressions respecting approximately logarithmic relations of amplitudes and clinical scores were done, one of them being linear regression with the use of the amplitude logarithm as the independent variable. The instrumented assessment was based on short-time measurements, but the visual assessment was not done simultaneously. In some sub-studies, the assessment was done immediately before or after the measurement. In others, the time lag was up to several weeks. In one sub-study, scores assessing social handicap and amount of water spilled when pouring from one tube to another were used instead of a direct visual assessment of the tremor amplitude. Coefficients of determination were computed from the published correlation coefficients: The coefficients range from $r^2 = 0.17$ (for a 0-3 scale, spilled water) and 0.30 (for a 0-4 scale, visual amplitude) to 0.74 in sub-studies using accelerometers, from $r^2 = 0.65$ to 0.78 in sub-studies using digitizing tablets, and $r^2 = 0.89$ in a sub-study using the linkage device (Matsumoto et al. 1999). The latter result is very good. However, each regression function was trained to a particular arm position and the correlations were computed for all the data available, no leave-one-out or similar methodology was used by Matsumoto et al. (1999) and Elble et al. (2006). Instead, standard errors of the estimated slopes of regression lines were estimated, being about 10 % of the values, see (Elble et al. 2006), table 2. On the other hand, all their results may suffer from the fact that the acquisition of the amplitude and the visual rating by a clinician were not synchronized.

By Giuffrida et al. (2009), a visual score of the postural and rest tremor in PD patients was regressed using short-time accelerometer and gyroscope measurements. Measurements were done simultaneously with video recordings used for the visual assessment. The regression results for the rest/postural tremor were $r^2 = 0.89/0.90$ when using all the data, and $r^2 = 0.85/0.88$, RMSE $= 0.32/0.35$ when using the leave-one-out approach. The performance measures are better than ours. However, the resolution of the visual scale they used was more fine than the scale we used (see Giuffrida et al. (2009), figure 6), reducing the error caused by the discrete nature of clinical scales. Moreover, the regression function was trained to assess a concrete type of tremor in a concrete hand posture while we included several hand postures. In (Giuffrida et al. 2009), all amplitudes from separate sensor axes were used while we used only the overall amplitudes derived from the composite spectra of 3D signals. On the other hand, only linear functions of the amplitude logarithms were used as regression functions by Giuffrida et al. (2009), while we used more general polynomials besides the linear regression by one amplitude logarithm.

Mostile et al. (2010) extended the work by Giuffrida et al. (2009) by correlations with another visual scale used to quantify the postural and kinetic tremor in patients with

the essential tremor. A relatively small sample of tremor assessments was used in the study. The correlation between the score provided by the used system and the visual score in the postural tremor was $r = 0.738$ (r^2 about 0.54) and error MAE = 0.42. The found accuracy of the regression is lower than our results. The accuracy may suffer from the fact that they used much smaller sample of data from a similar number of subjects as we involved.

5.5 Conclusions

Estimates of the motion acceleration caused purely by a translational movement in an Earth-fixed reference frame and of the gravitational artifact were used for tremor quantification in addition to the actually measured acceleration and angular rate. The decomposition of the acceleration into the two components was performed with the use of an attitude estimation using the data provided by the inertial measurement unit.

The orientation estimation accuracy was not directly validated using any alternative methodology, but low sensitivity of the proposed detection scheme to corruption of the measured data with constant bias was demonstrated. It appears that high accelerations of a severe tremor may influence the orientation estimate. An analysis of this influence and its reduction are the subjects of the investigations in chapter 7.

The performance in separating the group of patients from healthy persons and in the regression of the visual tremor rating was good and comparable to the results presented in other publications. 3D accelerometry was more efficient in separating the groups than uniaxial accelerometry. The use of the decomposed acceleration further improved the performance in both tasks. However, the differences were low and further investigation may be needed to make a definite conclusion about the better suitability of the acceleration components for tremor detection and quantification when compared to raw measured signals.

Other motion variables like position or velocity are often used to quantify tremor as they are more related to visual observations by a human than acceleration. In the future work, they may be estimated from the acceleration and investigated beside the variables from the presented work in order to find reasonable representation of tremor intensity and frequency without dependence on particular hand position. More information about the movement may be also utilized for the regression or classification if amplitudes in separate axes are extracted instead of the single amplitude for the 3D signal. Then, separating the gravitational artifact may be more helpful, as the amplitude of its spectral peak manifests more in some particular axes than in the summed spectrum of 3D acceleration.

Chapter 6

Auxiliary Estimation Methods

This chapter contains a description of two important methods used in the next chapter about attitude estimation during tremulous rotational motion.

The first of the methods, described in section 6.1, deals with the estimation of the center of rotation from the data measured by an inertial measurement unit (IMU) containing 3D accelerometer and 3D rate gyroscope. A dynamical state observer is proposed to perform the estimation and is tested in a very simple example. The center of rotation estimated during human hand tremor is then used in chapter 7 to increase the accuracy of attitude estimation.

The second method, described in section 6.2, is dedicated to finding the mutual orientation of two technical measurement systems of attitude or pose. That means to find

- relative orientation of their reference coordinate frames and
- relative orientation of frames of the objects (parts of the measurement systems) whose attitudes are measured.

Relative orientation of IMU and Polhemus Isotrak magnetic system estimated by the method is used in chapter 7 to validate the accuracy of IMU-based attitude estimators.

6.1 Estimation of center of IMU rotation

6.1.1 Introduction

The purpose of this section is to describe the procedure which was used to estimate where lay the center of the rotation motion of palm during tremor. The obtained center estimate was used to get estimates of centripetal and tangential acceleration. The acceleration was then subtracted from the measured acceleration to increase the precision of the attitude estimation in chapter 7. However, the attitude estimation may be even fused with this method into one estimator – even in the presented form, the inclination is estimated as a side product of the center estimation.

The goal is to find the negative of the relative position of the center of rotation of IMU in the coordinates of IMU, i. e. to find the vector from the center of rotation to the sensor expressed in coordinates of the sensor. The rotation movement need not to be a uniform rotation motion, but may be for example an oscillating motion (back-and-forth)

of rotational character. The center of rotation is supposed to be fixed or to change slowly compared to the frequency of alternations or rotations. Accelerometer and rate gyroscope measurements are needed, although inclusion of other sensor readings (e. g. magnetometer) would be also possible.

An observer-based method with smoothing was used to estimate the vector. The Extended Kalman Filter (EKF) framework was used with some assumptions about the noises not fulfilled completely (whiteness, Gaussian distribution, knowledge of variances and covariances).

6.1.2 Model equations

The inclination of the sensor is stored as the projection to the sensor axes of vertical unit vector s heading up. Its time evolution in continuous time and a time discretized version of the equation are

$$\dot{s}(t) = -\omega(t) \times s(t)\,, \qquad s_{k+1} = e^{-[\omega_k \times]\,\mathrm{T_s}}\; s_k,$$

where ω is the angular rate of the sensor, in an idealized case measured by rate gyroscopes, $\mathrm{T_s}$ is the sampling period, and matrix $[\omega_k \times]$ is

$$[\omega_k \times] = \begin{bmatrix} 0 & -\omega_{k,3} & \omega_{k,2} \\ \omega_{k,3} & 0 & -\omega_{k,1} \\ -\omega_{k,2} & \omega_{k,1} & 0 \end{bmatrix}.$$

The vector r from center of rotation to the sensor is modeled as Brownian motion.

$$\dot{r}(t) = 0 + v_r(t)\,, \qquad r_{k+1} = r_k + v_{r,k},$$

where v_r is the random time derivative/difference of the vector.

To enhance the observer in the presence of nonzero gyro bias, the bias was also included in the observer and estimated. If the inclination of the sensor does not change enough, the bias about the vertical cannot be estimated well by the observer. In such a case, only part β of the bias b was estimated: $\beta = E\,b$, $\hat{b} = E^{\mathrm{T}}\,\beta$. Matrix E is an identity matrix if whole bias is estimated, otherwise it is a $p \times 3$ matrix, $p < 3$, its rows are unit and orthogonal.

$$\dot{\beta}(t) = 0 + v_\beta(t)\,, \qquad \beta_{k+1} = \beta_k + v_{\beta,k}$$

The output of the estimation filter is the expected measured acceleration under the condition that all the movement is described by the rotation,

$$a_k = \mathrm{g}\, s_k \;+\; \epsilon_k \times r_k \;+\; \omega_k \times (\omega_k \times r_k),$$

where ϵ is angular acceleration, i. e. time derivative of angular rate. Various methods exist for estimating the derivative of a signal. We used five-point stencil method to estimate angular acceleration from the measured angular rate off-line and used the estimate as another input to the system. The fact that the angular rate and angular acceleration as well as their errors are dependent is neglected in the design of the observer.

The state x, input u, and output y of the system at sample k are

$$\begin{aligned} x_k &= [s_k^{\mathrm{T}} \quad r_k^{\mathrm{T}} \quad \beta_k^{\mathrm{T}}]^{\mathrm{T}} \\ u_k &= \left[(\omega_{\mathrm{b},k} + w_{\omega,k})^{\mathrm{T}} \quad (\epsilon_k + w_{\epsilon,k})^{\mathrm{T}}\right]^{\mathrm{T}} \\ y_k &= a_k + w_{a,k} \\ w_{\mathrm{u},k} &= \left[w_{\omega,k}^{\mathrm{T}} \quad w_{\epsilon,k}^{\mathrm{T}}\right]^{\mathrm{T}} \end{aligned}$$

where $\omega_{\mathrm{b},k}$ is the angular rate plus gyroscope bias ($\omega_k = \omega_{\mathrm{b},k} - b_k$), w_{u} is the measurement noise of input, and $w_{a,k}$, $w_{\omega,k}$, and $w_{\epsilon,k}$ are measurement noises of acceleration and angular rate and estimation error of angular acceleration, respectively.

6.1.3 Linearization

In an extended Kalman filter, for the output update part of a step of the filter, the system matrices of a linear system are replaced by appropriate Jacobians of the nonlinear state and output equations. In fact, for that operation, the system is substituted by an affine system

$$\begin{array}{rcl} x_{k+1} & \simeq & x_{\mathrm{OP},k} + A_k\,(x_k - x_{\mathrm{OP},k}) + B_k\,(u_k - u_{\mathrm{OP},k}) \\ y_k & \simeq & y_{\mathrm{OP},k} + C_k\,(x_k - x_{\mathrm{OP},k}) + D_k\,(u_k - u_{\mathrm{OP},k}) \end{array}, \tag{6.1}$$

where

$$y_{\mathrm{OP},k} = h(x_{\mathrm{OP},k}, u_{\mathrm{OP},k}),$$

h is the (nonlinear) output equation, $x_{\mathrm{OP},k}$ and $u_{\mathrm{OP},k}$ are the state and input defining the operating point. In a regular extended Kalman filter, $x_{\mathrm{OP},k}$ is the nonlinear prediction from the previous step.

In our case, the matrices of the linearized state update equation are

$$A_k = \begin{bmatrix} e^{-[\omega_k\times]\,\mathrm{T_s}} & . & -\frac{\partial s_{k+1}}{\partial \omega_k}\,E^{\mathrm{T}} \\ . & \mathcal{I}_3 & . \\ . & . & \mathcal{I}_p \end{bmatrix} \quad B_k = \begin{bmatrix} \frac{\partial s_{k+1}}{\partial \omega_k} & . \\ . & . \\ . & . \end{bmatrix}$$

where dots represent zero matrices of appropriate sizes, $\mathcal{I}_n$ denotes identity matrix of size n, and the partial derivative of s_{k+1} may be get for example by expansion using the Haddamad lemma:

$$\frac{\partial s_{k+1}}{\partial \omega_{k,i}} \simeq \left(dX_{k,i} + \frac{1}{2}\mathrm{L}(X_k, dX_{k,i}) + \frac{1}{6}\mathrm{L}\left(X_k, \mathrm{L}(X_k, dX_{k,i})\right) + \dots \right) e^{X_k} s_k$$

where

$$X_k = -[\omega_k\times]\,\mathrm{T_s}; \qquad dX_{k,1} = \frac{d}{d\omega_{k,1}} X_k = -\left[[\mathrm{T_s}\ 0\ 0]^{\mathrm{T}}\times\right]; \quad \dots$$

$$\mathrm{L}(a,b) = ab - ba$$

We used the three members of the expansion.

The matrices of linearized output equation are

$$C_k = \begin{bmatrix} \mathrm{g}\,\mathcal{I}_3, & ([\epsilon_k\times] + [\omega_k\times][\omega_k\times]), & -\frac{\partial a_k}{\partial \omega_k}\,E^{\mathrm{T}} \end{bmatrix}$$

$$D_k = \begin{bmatrix} \frac{\partial a_k}{\partial \omega_k}, & -[r_k\times] \end{bmatrix}$$

where (time indices k omitted)

$$\frac{\partial a}{\partial \omega} = \frac{d(\omega \times (\omega \times r))}{d\omega} = \begin{bmatrix} \omega_2 r_2 + \omega_3 r_3 & 2\omega_2 r_1 + \omega_1 r_2 & -2\omega_3 r_1 + \omega_1 r_3 \\ -2\omega_1 r_2 + \omega_2 r_1 & \omega_1 r_1 + \omega_3 r_3 & -2\omega_3 r_2 + \omega_2 r_3 \\ -2\omega_1 r_3 + \omega_3 r_1 & -2\omega_2 r_3 + \omega_3 r_2 & \omega_1 r_1 + \omega_2 r_2 \end{bmatrix}$$

6.1.4 Estimation algorithm

As the data are processed off-line, a smoothing filter may be used to estimate the state of the system described above.

Several approaches were proposed to smooth the state observation of nonlinear systems. An iterated Kalman smoother was proposed by Bell (1994). The smoother uses affine Kalman smoother at each iteration. The approach was further extended by Johnston and Krishnamurthy (2001) and Bell et al. (2009) to handle different smoothing tasks and additional inequality constraint. There are also methods based on particle filters and on the unscented Kalman filter (Šimandl and Duník 2009).

The iterated Kalman smoother (IKS) was used. According to Bell (1994), a smoother for a nonlinear system may be constructed as follows:

1. Linearize the system at all the samples at an (operating) trajectory $\{x_{\mathrm{OP}}, u_{\mathrm{OP}}\}$.

2. For the obtained affine system (6.1) make a state estimate by affine Kalman smoother at all the samples.

3. Go to 1 and use the estimate from step 2 as the operating trajectory, or stop.

The trajectory estimated by a regular extended Kalman filter (EKF) was used as the operating trajectory for the first iteration. The iterations converged fast to an estimate. We did three iterations. The EKF was run twice before the IKS: First, full bias was estimated ($\beta = b$). Then, the covariance of estimate of b at the last sample was subject to eigenvalue decomposition to detect the direction, in which the variance of the estimate was the highest. The standard deviation in that direction was in our cases of alternating motions described in section 6.1.6 and chapter 7 typically between 0.001–0.2 $\mathrm{rad\,s^{-1}}$, that was approximately in the size of the bias, or greater. Therefore, the estimation of bias in this direction did not make sense. Standard deviations in other directions were typically 10–100 times lower. In the second run of EKF and by IKS, the bias was estimated only in the two other directions. The estimate by the second run of EKF was used as the operating trajectory for the first iteration of IKS as described above.

In a standard setting, Kalman filter assumes exactly known inputs. That is not our case because of the noisy measurement of the angular velocity and estimate of the angular acceleration. The noise was taken into account using the covariance of the input measurement noise R_u added to the process noise and output measurement noise covariances in the model as shown for linear systems by Markovsky and De Moor (2005):

$$Q_k = B_k R_u B_k^{\mathrm{T}} + Q_{\mathrm{orig},k} \tag{6.2}$$

$$R_k = D_k R_u D_k^{\mathrm{T}} + R_{\mathrm{orig},k} \tag{6.3}$$

$$S_k = B_k R_u D_k^{\mathrm{T}} + S_{\mathrm{orig},k} \tag{6.4}$$

where Q_k, S_k, and R_k are the assumed variances of process noise, output measurement noise, and their covariance, respectively, B_k and D_k are the input matrices the system (partial derivatives of the discrete-time state equation and the output equation), R_u is the covariance of measurement noise of the input, and matrices with orig subscript are the original covariances of process noise.

6.1.5 Settings

This section gives a description of the settings of covariances and other parameters used in the filter when estimating center of rotation of IMU held by hands simulating tremor in chapter 7.

Needed and generally time-dependent covariance matrices are

$$\begin{aligned} R_u &= \text{blkdiag}(R_\omega, R_\epsilon) \\ R_{\text{orig}} &= R_a \\ Q_{\text{orig}} &= \text{blkdiag}(Q_s, Q_r, Q_\beta) \\ S_{\text{orig}} &= \mathbf{0}; \end{aligned}$$

where sample indices are omitted, blkdiag means block diagonal concatenation of matrices, and $\mathbf{0}$ is a zero matrix of appropriate size.

For the sake of simplicity of the filter and computational burden, the noises of angular rate ω and angular acceleration ϵ are assumed to be white and independent, although in fact, neither is true.

$\mathbf{R}_\omega$ is the covariance of measurement error w_ω of the gyroscope in the frequency range used.

$\mathbf{R}_\epsilon$ $= 1/3\,(2\pi f_f)^2\, R_\omega$, where f_f is the filtration frequency (20 Hz), is the estimate of the covariance of the limited violet noise of filtered angular acceleration. The errors caused by the discrete numeric differentiation were neglected in the provided example and tremor measurements.

$\mathbf{R_a}$ is the covariance of measurement error w_a of acceleration a. The error contains not only the measurement noise, but also the accelerations that are not described by a rotation movement about a slowly changing center of rotation and that are generally not white. The variance was estimated from the second run of the EKF as the variance of output prediction error in ± 1 s neighborhood of each sample. Although the estimate is biased (Odelson et al. 2006) – overestimates the covariance, it is always positive definite and represents a careful, data-based approach to finding the unknown covariance. In the initial EKFs, variance of the accelerometer signal was used as highly overestimated variance of the measurement error.

$\mathbf{Q_s}$ is the covariance of a small virtual noise of the inclination added to the covariance of the error from the gyroscopes. This added covariance was used to ensure positive definiteness of Q and to left a space to cope with errors from the discretization. Constant $10^{-6}\,\mathrm{T_s}\,\mathcal{I}_3$ was used.

$\mathbf{Q_r}$ is the covariance of the noise of the Brownian motion model of the center of rotation. With the sampling frequency of 120 Hz, covariances about 10^{-7} were found to give usually smooth estimates of the center of rotation while enabling some degree of its adaptation to changes in tremor. Higher the covariance, faster was the adaptation to changes, but also higher were unwanted periodic changes of the estimate during the tremor oscillations. Therefore, an adaptive scheme was used: The covariance was estimated by covariance matching (Myers and Tapley 1976) from the second run of EKF, again with the use of moving average in ± 1 s neighborhood of each sample. Only the diagonal of the result was taken and the terms were limited to lie between $10^{-4}\,\mathrm{T_s}$ and $10^{-6}\,\mathrm{T_s}$. Fixed covariance $10^{-4}\,\mathrm{T_s}\,\mathcal{I}_3$ was used in the initial EKFs.

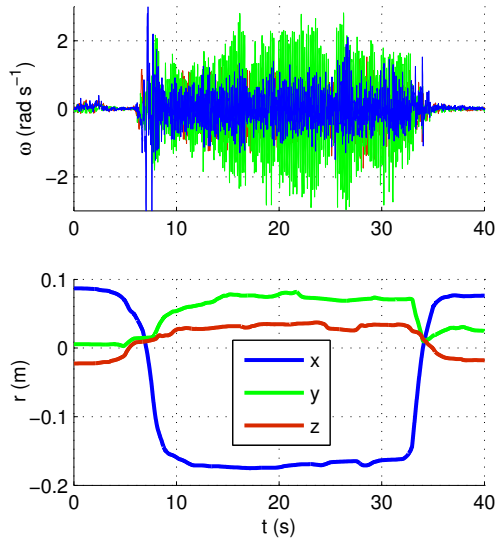

Figure 6.1: Estimated vector from the center of rotation to the sensor (r) during simulated tremor. Measured angular rate ω is shown above. The IMU was held by fingers, the X axis headed approximately in the medial direction (to the wrist), the tremor was dominantly about the wrist joint.

$\mathbf{Q}_\beta$ is the covariance of the noise of the Brownian motion model of the gyroscope bias. The bias is supposed not to change a lot during the short measurements. A constant $10^{-12}\,\mathcal{I}_m$ was used, where m is the size of the part of the bias estimated.

See figure 6.1 for an example of the estimate with the described settings.

6.1.6 Testing on a toy example

6.1.6.1 Methods

An inertial measurement unit Xsens MTx was fixed to a link connected to a base by a 3 DoF (degrees of freedom) revolute joint. The simple device was build-up from Lego bricks. The measurement unit could be fixed to the link at two positions. See figure 6.2 for the sketch of the situation. The positions of the sensor (accelerometer) in coordinate systems with centers at the joint center and axes parallel to sensor axes were (218.5 10.75 17.5) mm at position 1 and (−123.5 1.25 17.5) mm at position 2 as located by a ruler and/or the knowledge of the location of the accelerometer in the inertial unit and sizes of Lego bricks with the assumption of perfect perpendicular alignment of the sensors to the link. The accuracy is ±1 mm not counting with misalignment errors. The misalignment errors could induce additional position error especially in Y and Z axes.

The data were measured during two measurement sessions. Accelerometer bias and gain and gyroscope bias were calibrated from at the beginning of each session. The sampling frequency was 100 Hz.

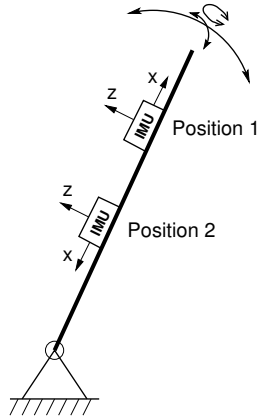

Figure 6.2: Schematic sketch of the link with the 3DoF joint. Two used positions of IMU on the link are shown.

	Position 1			Position 2		
	X	Y	Z	X	Y	Z
	218.5	10.75	17.5	-123.5	1.25	17.5
1	217.6	9.9	16.4	-122.5	0.7	16.4
2	217.4	9.7	16.4	-123.3	1.0	16.3
3	218.2	10.6	16.7	-121.6†	0.8†	15.9†
4	216.6	9.8	16.4			
5	217.0	9.8	16.2			
6	216.9*†	9.2*†	16.2*†			

Table 6.1: Results of the testing on the LEGO toy example. The numbers in the first row are the locations of accelerometer from the center of rotation measured with the help of a ruler. * Different session – misalignment error could differ † Limited range of motion: approximately ±3° about Y and Z axes, less than ±40° about X axis.

Data were measured repeatedly during time intervals of 12–30 s when the link was moved around by a hand whereas the base was fixed to a table.

For the estimation algorithm following settings were used:

- Covariance of the model of center changes $Q_r = 10^{-12}\mathcal{I}_3$: This small value was used instead of the adaptive estimation described above because contrary to tremor measurements, no changes of the center of rotation were expected.
- Filtration frequency $f_f = 20\,\mathrm{Hz}$

6.1.6.2 Results

See table 6.1 for the list of all the results. Mean coordinates estimated in position 1 of IMU at the link were (mean±standard deviation) $r_x = 217.3{\pm}0.6,\ r_y = 9.8{\pm}0.5,\ r_z = 16.4{\pm}0.2$ [mm]. In position 2 they were $r_x = -122.5{\pm}0.9,\ r_y = 0.8{\pm}0.2,\ r_z = 16.2{\pm}0.3$ [mm]. Root mean square distance of the center estimated from IMU and center measured with the help of a ruler was 1.96 mm.

6.1.7 Conclusions

An off-line procedure for the location of the center of rotation of an IMU was proposed with the help of iterated Kalman smoother. The procedure gave good estimates in the simple example, errors being typically about 1 mm in each axis.

The estimate obtained from an IMU fixed to a body part or a device may be used for subtraction of centripetal and tangential accelerations from the accelerometer measurements, that means, for the estimation of the acceleration at the center of rotation. That may be used e. g. for increasing the accuracy of attitude estimation of rotating objects or for estimating the motion of the center of rotation. The essential condition is that the center of rotation – expressed in the local coordinates of the sensor – do not change fast and that in the data used for the center estimation, the motion is about all 3 rotation axes. The results of the example suggest that the excitation need not to be high, see the marked results in table 6.1.

Possible applications are (not only):

- Calibration of the position of an IMU relative to a human joint. For example the ankle joint location in coordinates of an IMU placed at shank may be used for the estimation of the ankle acceleration. The obtained ankle acceleration then may be used e. g. for heel-off detection in walking or for step length estimation.

- Reduction of the movement artifact of the acceleration measured at a point on a hand which is subject to tremor around the wrist or other joint. The acceleration measurement modified in this way shall hypothetically increase the accuracy of attitude estimation, because part of the movement artifact of the acceleration is removed and therefore a bigger part of the rest belongs to the gravitational artifact which is desirable as the input of attitude estimation algorithms. Later in chapter 7, it is shown why especially the centripetal acceleration may corrupt the attitude estimate. In the used data set, the accuracy of the hand attitude estimation increased after the subtraction of the estimated centripetal and tangential accelerations from the measurement.

6.2 Estimation of relative orientation of two technical systems for attitude measurement

6.2.1 Introduction

The problem of alignment of two attitude measurement systems may arise in different tasks, one of them being their cross-validation. Such a task is performed later in chapter 7 where the estimate from inertial measurement unit is validated using Polhemus Isotrak magnetic measurement system.

The orientation matrix R_{A} of sensor A in reference frame of measurement system A expressed using the orientation measured by system B is

$$\begin{aligned} R_{\mathrm{A}} &= R_{\mathrm{sens}}\, R_{\mathrm{B}}\, R_{\mathrm{syst}}^{\mathrm{T}}, \\ &\text{or in quaternions} \\ q_{\mathrm{A}} &= \overline{q}_{\mathrm{syst}} \bullet q_{\mathrm{B}} \bullet q_{\mathrm{sens}} \\ &\text{or} \\ q_{\mathrm{A}} &= Q_{\mathrm{syst}}^{\mathrm{T}}\, Q_{\mathrm{B}}\, q_{\mathrm{sens}} \end{aligned} \tag{6.5}$$

where orientation matrices R_{A} and R_{B} represent the measurements. They are the rotation matrices transforming vectors by (left-) multiplication from the corresponding reference frames to the frames of the moving parts of the sensors (e. g. IMU in an Earth surface-fixed reference frame, or receiver coils in reference frame of magnetic field transmitter of magnetic system). Matrix of the relative orientation of the two reference frames R_{syst} is the rotation matrix transforming vectors from reference frame B to reference frame A. Matrix R_{sens} of the relative orientation of the two moving parts fixed to the same rigid body is the rotation matrix transforming vectors from local frame of the moving part B to moving part A. Unit quaternions (q) correspond to the rotation matrices with the same subscripts. Symbol $\overline{q}$ denotes the conjugate quaternion of q. Quaternion multiplication ($\bullet$) can be expressed using quaternion multiplication matrices (Q) that are constructed as follows. For the quaternion $q = [a \;\; b \;\; c \;\; d]^{\mathrm{T}}$ the multiplication matrix is

$$Q = \begin{bmatrix} a & -b & -c & -d \\ b & a & -d & c \\ c & d & a & -b \\ d & -c & b & a \end{bmatrix}$$

The problem of measurement systems alignment is to estimate relative orientation matrices R_{sens} and R_{syst} (or corresponding quaternions) from a set of measurements of orientation A and B.

From one measurement (6.5) we get more unknowns than is the number of equations. Moreover, the nonlinear participation of the parameters in the equations embarrasses the direct use of least squares method to an overdetermined system of equations from a number of measurements.

One possible solution of the problem is the usage of angular velocities which, as measured by ideal rate gyroscopes, fulfill

$$\omega_{\mathrm{A}} = R_{\mathrm{sens}}\, \omega_{\mathrm{B}} \tag{6.6}$$

Matrix R_{sens} could be estimated from a set of data using overdetermined set of equations (6.6) and provided that angular velocity is excited enough. Then, R_{syst} could be get using (6.5) from data from a set of static positions that provide for good measurements of R_{A} and R_{B}. Such an approach has a significant drawback: In (6.6) the measured angular rate ω suffers from (typically high) differentiation errors in case of its determination from measured orientations. If measured by rate gyroscopes, ω suffers from bias that may induce a significant violation in (6.6) especially if the angular rate is low.

Hence, a different original algorithm using only data from static positions and the relations (6.5) was applied. The algorithm uses pairs of measured static orientations to get a set of rotations from one orientation to another. In the equations for these rotations the matrices R_{sens} and R_{syst} are decoupled, contrary to (6.5). The matrices are then estimated by a least squares algorithm applied to the axis-of-rotation part of the rotation quaternions.

6.2.2 Derivation

In the following text, most of equations are written redundantly both in rotation matrices and quaternions. The calculation of rotational matrix from quaternion is possible e. g. by usage of (5.1), see for example Stevens and Lewis (2003).

Assume that we have two different orientations 1 and 2 and their measurements $R_{\mathrm{A}}^{\{1\}}$, $R_{\mathrm{B}}^{\{1\}}$ and $R_{\mathrm{A}}^{\{2\}}$, $R_{\mathrm{B}}^{\{2\}}$ which satisfy (6.5) with constant and unknown R_{sens} and R_{syst}.

The difference of the two orientations is

$$\begin{array}{rcl|rcl} q_{\mathrm{d,A}} & = & \overline{q}_{\mathrm{A}}^{\{1\}} \bullet q_{\mathrm{A}}^{\{2\}} & R_{\mathrm{d,A}} & = & R_{\mathrm{A}}^{\{2\}} R_{\mathrm{A}}^{\{1\}\mathrm{T}}, \\ q_{\mathrm{d,B}} & = & \overline{q}_{\mathrm{B}}^{\{1\}} \bullet q_{\mathrm{B}}^{\{2\}} & R_{\mathrm{d,B}} & = & R_{\mathrm{B}}^{\{2\}} R_{\mathrm{B}}^{\{1\}\mathrm{T}}, \end{array} \tag{6.7}$$

Such obtained quaternions and rotation matrices specify the rotation from orientation 1 to orientation 2 of the corresponding sensor in its appropriate reference frame.

In a similar way, let us define rotations using the quaternions as in (6.7) but with swapped conjugation:

$$\begin{array}{rcl|rcl} q_{\mathrm{d2,A}} & = & q_{\mathrm{A}}^{\{1\}} \bullet \overline{q}_{\mathrm{A}}^{\{2\}} & R_{\mathrm{d2,A}} & = & R_{\mathrm{A}}^{\{2\}\mathrm{T}} R_{\mathrm{A}}^{\{1\}} \\ q_{\mathrm{d2,B}} & = & q_{\mathrm{B}}^{\{1\}} \bullet \overline{q}_{\mathrm{B}}^{\{2\}} & R_{\mathrm{d2,B}} & = & R_{\mathrm{B}}^{\{2\}\mathrm{T}} R_{\mathrm{B}}^{\{1\}} \end{array} \tag{6.8}$$

Now, substituing (6.5) to (6.7) and (6.8) we get

$$\begin{array}{rcl|rcl} q_{\mathrm{d,A}} & = & \overline{q}_{\mathrm{sens}} \bullet q_{\mathrm{d,B}} \bullet q_{\mathrm{sens}} & R_{\mathrm{d,A}} & = & R_{\mathrm{sens}} R_{\mathrm{d,B}} R_{\mathrm{sens}}^{\mathrm{T}} \\ q_{\mathrm{d2,A}} & = & \overline{q}_{\mathrm{syst}} \bullet q_{\mathrm{d2,B}} \bullet q_{\mathrm{syst}} & R_{\mathrm{d2,A}} & = & R_{\mathrm{syst}} R_{\mathrm{d2,B}} R_{\mathrm{syst}}^{\mathrm{T}} \end{array} \tag{6.9}$$

Hence, for two measurements of orientation we get two equations, one for q_{sens} and and one for q_{syst}. The equality signs in the quaternion equations above mean equality of orientations or rotations, that means that negatives of the unit quaternions may be also used.

Rewriting (6.9) using quaternion elements and expression for rotation matrix by quaternion elements we get

$$q_{\mathrm{d,A}} = \begin{bmatrix} q_{\mathrm{d,A}}(0) \\ q_{\mathrm{d,A}}(1) \\ q_{\mathrm{d,A}}(2) \\ q_{\mathrm{d,A}}(3) \end{bmatrix} = \begin{bmatrix} q_{\mathrm{d,B}}(0) \\ R_{\mathrm{sens}} \begin{bmatrix} q_{\mathrm{d,B}}(1) \\ q_{\mathrm{d,B}}(2) \\ q_{\mathrm{d,B}}(3) \end{bmatrix} \end{bmatrix}$$

and

$$q_{\mathrm{d2,A}} = \begin{bmatrix} q_{\mathrm{d2,A}}(0) \\ q_{\mathrm{d2,A}}(1) \\ q_{\mathrm{d2,A}}(2) \\ q_{\mathrm{d2,A}}(3) \end{bmatrix} = \begin{bmatrix} q_{\mathrm{d2,B}}(0) \\ R_{\mathrm{syst}} \begin{bmatrix} q_{\mathrm{d2,B}}(1) \\ q_{\mathrm{d2,B}}(2) \\ q_{\mathrm{d2,B}}(3) \end{bmatrix} \end{bmatrix}$$

Note that the first element of a rotation quaternion corresponds to the amplitude of the rotation while the other elements define the axis of rotation.

Having a larger set of different data $q_{\mathrm{d,A}}$, $q_{\mathrm{d,B}}$, $q_{\mathrm{d2,A}}$, and $q_{\mathrm{d2,B}}$ the alignment matrices can be estimated by least squares algorithm applied to the axis-of-rotation part of the unit quaternions. It is the task of finding rotation transformation for matching two point patterns (Umeyama 1991), or Wahba problem (Wahba 1966). The problem may be solved with the use of singular value decomposition (Markley 1988).

6.2.3 Alignment procedure used for hand tremor measurement

The actual alignment procedure used in chapter 7 follows. In the above described general alignment procedure, as q_{A} is used q_{IMU} – the attitude measured by the inertial measurement unit, and as q_{B} is used q_{Iso} – the attitude measured by the Polhemus Isotrak device.

1. Place the board with Isotrak receiver and MTx to different static positions and orientations in approximately the same volume as the sensors will be later used for measurement. Have the data synchronized and accelerometers calibrated. Approximately known R_{sens} was used for transformation of angular rate ω_{Iso} for data synchronization (see section 7.4.1.1).

2. Split the data into equidistant intervals. Interval length of 0.5 s was used.

3. Remove the intervals which are not static. Standard deviation of all three accelerometer signals being lower than $0.1\,\text{m}\,\text{s}^{-2}$ was used as the criterion of staticity.

4. For each static interval k get $q_{\text{Iso}}^{\{k\}}$ as the quaternion of mean orientation retrieved from Isotrak in the interval. For orientation averaging the Euclidean sense (Moakher 2002) was used, i. e. the rotation matrix of the average rotation was get as the unique polar factor in the polar decomposition of the arithmetic mean of acquired rotation matrices.

5. For each static interval k get $R_{\text{IMU}}^{\{k\}}$ and $q_{\text{IMU}}^{\{k\}}$ from MTx data. The orientation of MTx was get by the following algorithm:

   (a) $\overline{a}$ is the mean acceleration measured in the interval, $\overline{m}$ is the mean magnetic field projection measured in the interval.

   (b) Get the third column Z of $R_{\text{IMU}}^{\{k\}}$ as $\overline{a}/\|\overline{a}\|_2$.

   (c) Get the second column Y of $R_{\text{IMU}}^{\{k\}}$ as $Z \times \overline{m}$ divided by its 2nd norm, $\times$ denotes cross product.

   (d) Get the first column of $R_{\text{IMU}}^{\{k\}}$ as $Y \times Z$.

6. Take all two-element combinations of static intervals. For each combination $\{i, j\}$, $i < j$, compute $q_{\text{d,IMU}}^{\{i,j\}} = \overline{q}_{\text{IMU}}^{\{i\}} \bullet q_{\text{IMU}}^{\{j\}}$. In the same manner compute $q_{\text{d,Iso}}^{\{i,j\}}$, $q_{\text{d2,IMU}}^{\{i,j\}}$, and $q_{\text{d2,Iso}}^{\{i,j\}}$ using (6.7) and (6.8).

7. Remove combinations with small differences between the two positions. They usually represent combinations of two 0.5 s static intervals measured in same position. A limit on the first element of the difference quaternion was used as the criterion: $|q_{\text{d,IMU}}^{\{i,j\}}(0)| > 0.99$. That corresponds to angular difference lower than approximately 16 deg.

8. Remove combinations with differences about 180 deg. The reason is that quaternions $[\alpha\ a\ b\ c]^{\text{T}}$ and $[-\beta\ a\ b\ c]^{\text{T}}$, α and β being very small positive numbers, represent almost same rotations but their axis parts after dividing by signs of angle parts ($\pm[a\ b\ c]^{\text{T}}$) are inverse. That would cause problems with the alignment algorithm used. A limit on the first element of the difference quaternion was used as the criterion for removal: $|q_{\text{d,IMU}}^{\{i,j\}}(0)| < 0.05$. That corresponds to angular difference greater than approximately 174 deg.

9. From this point on, two Wahba's problems are solved for axis-of-rotation parts of quaternions by the algorithm of Markley (1988).

   Construct $n \times 3$ matrix A_1 from n remaining quaternions $q_{\text{d,IMU}}$. The last three elements of each quaternion form one row of A_1. In a similar manner construct P_1

from quaternions $q_{\mathrm{d,Iso}}$ except that multiply each row by -1 if corresponding $q_{\mathrm{d,IMU}}(0)$ and $q_{\mathrm{d,Iso}}(0)$ have different polarity.

Construct A_2 and P_2 from quaternions $q_{\mathrm{d2,IMU}}$ and $q_{\mathrm{d2,Iso}}$ in the same manner as A_1 and P_1 from $q_{\mathrm{d,IMU}}$ and $q_{\mathrm{d,Iso}}$.

10. Perform singular value decompositions:

$$U_1\, D_1\, V_1^{\mathrm{T}} = A_1^{\mathrm{T}}\, P_1$$

$$U_2\, D_2\, V_2^{\mathrm{T}} = A_2^{\mathrm{T}}\, P_2$$

Define

$$S_i = \begin{bmatrix} 1 & 0 & 0 \\ 0 & 1 & 0 \\ 0 & 0 & \det(U_i\, V_i^{\mathrm{T}}) \end{bmatrix}, \quad i \in 1, 2, \quad \det(U_i\, V_i^{\mathrm{T}}) = \pm 1$$

11. The estimate of alignment matrices is

$$R_{\mathrm{sens}} = U_1\, S_1\, V_1^{\mathrm{T}}$$

$$R_{\mathrm{syst}} = U_2\, S_2\, V_2^{\mathrm{T}}$$

12. To transform orientation measurements from one measurement system to another, use (6.5) with the calculated R_{sens} and R_{syst} or with their inverses depending on the direction of transformation.

Chapter 7

Attitude Estimation during Tremulous Motion

This chapter deals with accuracy of inertial attitude estimation during tremulous movement inducing high accelerations. The acceleration deteriorates the measurement of projection of gravity into the sensor coordinate frame. The level of deterioration of attitude filter output depends on movement intensity, movement type, and estimation algorithm used. The influence of the structure of the attitude observation filter to the accuracy of the estimate is studied and several recommendations are proposed to improve the accuracy, some of them using assumptions about the movement being typical static tremor. The properties of algorithms are studied analytically in part and with the help of simulations: numerical simulation of static tremor around a single rotational joint and mimicking severe hand tremor by healthy humans. Besides the general outputs, this study provides some picture of what could be the accuracy of the attitude estimation during tremor in chapter 5.

7.1 Introduction

Inertial estimation of inclination, attitude (orientation), or position in space are sometimes used and still have a potential in the field of human motion analysis. A motion analysis is used especially in the motion disorders and many of them (e.g. Parkinson's disease) come with a tremor of extremities or other body parts. To our knowledge, nobody has studied the influence of the tremor to the accuracy of the inertial estimation. Related to the theme are the publications about the gravitational component in acceleration measurement of the tremor (van Someren et al. 1996, Elble 2005). The approach of Elble (2005) was used partially also in our study: to model a hand tremor as an oscillation about a fixed revolute joint. This is accompanied by a validation on measurements of a hand tremor simulated by healthy persons.

An inertial estimator of the above mentioned quantities suited to tremor may be helpful in the situations when

- just a good estimate of a quantity is desired, e.g. to study a voluntary motion, but a tremor is present and makes a distortion, or
- the tremor itself is the subject of the analysis and a more detailed description of it than

only by an amplitude and frequency of a measured signal is wanted, e.g. trajectory of the orientation or pose. An example of an attempt of a more detailed analysis is provided in chapter 5.

The basic idea of this study is that in all typical inertial estimation algorithms – independently if a Kalman filter approach is used, or a fixed-gains observer – a rate gyroscope is used to estimate the orientation at high frequencies and an accelerometer, sometimes accompanied by other sensors, is used to estimate the inclination or orientation at low frequencies. In the filters, the cut-off frequency where the influence of the gyroscope and accelerometer smoothly swaps is usually about or less than 1 Hz: See e.g. Xsens Technologies (2005) where it was recommended to use 1 Hz in the older version of MTx firmware or Mahony et al. (2008) where the cut-off frequency calculated from the used gains was about 0.32 Hz for an application in small flying vehicles instrumented with MEMS inertial sensors. That means, cut-off frequencies below the frequencies of human tremor are used: e. g., 4–12 Hz for essential tremor, 3–7 Hz (rarely more) for Parkinson's disease tremor, 3–5 Hz for cerebellar tremor, about 16 Hz for orthostatic tremor (Deuschl et al. 1996, 1998, Hallet 1998). Therefore during tremor, the intra-cycle change of the inclination or attitude estimate is given dominantly by the measured angular rate, while the absolute inclination is given by fusion of all the sensors. If the body part does not move much and the tremor is the only marked motion, the "mean" inclination is given dominantly by the accelerometer measurement which is used to provide an instantaneous measurement of inclination: its gravitational component.

The acceleration measurement comprises from the gravitational component and the movement component. Only the gravitational component is wanted as the measurement in inclination/attitude estimation algorithms where no detailed motion model is available. All other components form measurement distortions, especially the acceleration of the motion in an Earth-fixed reference frame. If the tremor induces high accelerations, also this distortion is high. Pathological tremor can induce high accelerations, see section 5.3.1 for the amplitudes in a study of essential tremor with the subjects having mild to moderate essential tremor. The essential thing for the inertial estimation algorithms during tremor is how to fuse the distorted accelerometer measurement of gravity to get the inclination estimate at low frequencies as accurate as possible.

It is obvious that the following phenomena have little influence to the accuracy if the low frequency component of the acceleration measurement is used as low frequency component of inclination:

- zero-mean noise
- high frequency periodical and symmetrical translational motion

because at low frequencies, the accelerometer measurements caused by them are near to zero.

A different situation is for a rotational motion. If a periodic rotational motion is present, the mean accelerometer measurement provides a biased estimate of inclination especially due to the centripetal acceleration. The situation is described in more detail in the next section and is of the essential interest of this study.

Discrete movements, usually of a voluntary origin, may be measured. The attitude estimation performance during them is more hard to describe and it also depends on the ratio of the movement speed and the accelerometer/gyroscope cut-off frequency. Dis-

crete movements are not in the focus of this study and rather a separated static tremor or superposed with only a slow motion is of the interest.

In the next section (7.2), the situation when a body part moves periodically about a fixed joint and the movement has a sinusoidal time course of the angle is studied. Different ways how to estimate the central inclination from accelerometer measurements are proposed and compared mainly with the use of numerical calculations. Section 7.3 describes various simple algorithms for attitude estimation including a method for estimation of the deteriorating centripetal acceleration. Two alternative approaches how to cope with deteriorating movement accelerations are also mentioned there: A greater set of measurement units and more complex model of arm using some anatomical properties and sensor placement known in advance (Hyde et al. 2008) and on the contrary, using motion modeled just as first-order dynamical system without any other parameters (Luinge and Veltink 2005). The described algorithms are then used in section 7.4 together with the auxiliary algorithms described above in chapter 6 to validate the different ways of the usage of accelerometer measurements in the attitude estimation in tremor simulations by healthy humans.

7.2 Mean inclination estimate during oscillation about a revolute joint

7.2.1 Introduction

This section provides an analysis of mean inclination estimate by an accelerometer during alternating rotational movements. The motion is rotational about a fixed center or axis of rotation and the angle of the joint is oscillating. Harmonic time course of angular rate is considered.

For the sake of simplicity, the IMU is considered to have one axis (longitudinal, X) aligned to the line between the center of rotation and position of the sensor, another sensor axis is horizontal in the central orientation, heads to the left (Y). The choice of axes does not affect generality. Two basic movements are studied:

- Oscillation about the horizontal axis. That is an idealized model of flexion/extension hand tremor. It is also called up-down tremor below.
- Oscillation about the axis parallel to the Z axis of the sensor. It is also called left-rigt tremor below.

See figure 7.1 for a sketch of the three types of movement. The dash-dot line symbolizes the central direction of the longitudinal axis of the sensor. Symbol φ_0 denotes angular amplitude of the movement. Symbol θ_0 denotes pitch (0 to π, 0 = down) of the central direction. The central direction is get by an averaging on sphere. Thanks to the symmetricity, the central direction may be also get by simple arithmetic averaging in time of vectors from the center of rotation to the position of the sensor. For the first type of motion, the inclination of the central direction may be get also by averaging in time of the projection of gravity to the axes of the sensor unit.

7.2.2 Mean inclination estimate from accelerometers

Terrestrial strap-down inertial navigation uses accelerometer measurements to represent inclination, i.e. the direction of the projection (a_{g}) of gravitational component of acceleration

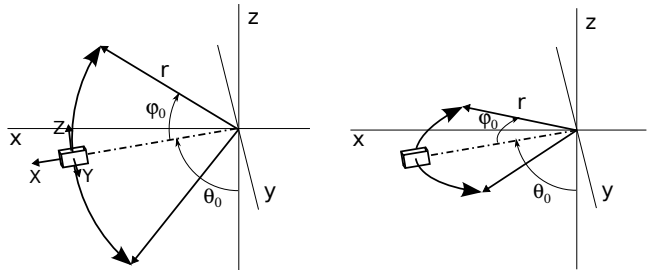

Figure 7.1: Sketch of the alternating rotation movements types considered. Sensor is shown in its central position as a box.

to the sensor axes. When considering situation that no other sensor like a magnetometer is used, the accelerometer is the only sensor that provides an information about IMU orientation at low frequencies. There are two ways how to approach the acceleration as a measurement of inclination. In both cases we assume that the orientation or inclination is estimated by a dynamical observer driven by angular rate measurement.

1. Take the estimated a_{g} as the output of the observer and use the actual accelerometer measurement as its measurement.

2. Take the direction of estimated a_{g} as the output of the observer and use the direction of actual accelerometer measurement as its measurement.

The second case is close also to the situation when the instantaneous acceleration measurement is used together with another sensor of a physical field (e.g. magnetometer) to estimate the instantaneous attitude and the attitude is then used as the output measurement of an observer which fuses it with the gyroscope measurement. The main difference of the two cases above is that the measurement of acceleration is used in the first case, while its direction in the second case. This seemingly small difference may have great influence when working with the measurement of an output of a dynamic attitude observer. Then at low frequencies, the inclination as estimated by the attitude filter tends to

- the direction of a low frequency component of acceleration in the first case,

- a low frequency component of the direction of acceleration in the second case.

These two values may markedly differ as will be shown later.

When estimating full orientation of the sensor, the orthogonality of the estimate must be ensured after the measurement update. That depends strongly on the orientation representation used and may be ensured by different ways: orthogonalization of generally nonorthogonal estimate after the measurement update, or including the criterion of orthogonality into the data model and measurement update. The second approach may be provided by using only the direction of actual accelerometer measurement (or an instantaneous attitude estimate from accelerometer and magnetometer) as the output measurement and operations restricted to SO(3) in the measurement update (Mahony et al. 2008).

Let us show an example of the mean inclination estimation by an accelerometer. See figure 7.2 for acceleration measurement and inclination estimates in the situation from

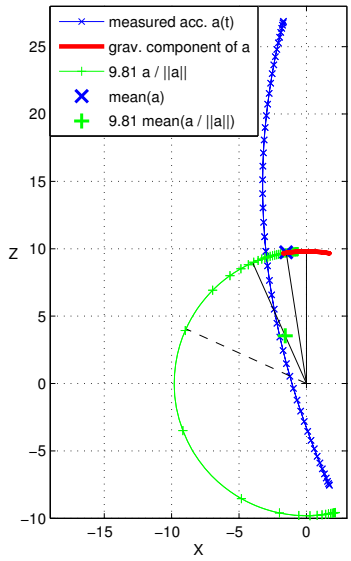

Figure 7.2: Measured acceleration ($\mathrm{m\,s^{-2}}$) and estimates of inclination and mean inclination. Black lines originating in 0 show mean inclination estimates by (from up to the left): mean of gravitational component of measured acceleration; mean measured acceleration; direction of acceleration averaged in the euclidean space; direction of acceleration averaged in the space of the angle (dashed). The estimation error is 0, 9, 24, and 66 deg, respectively.

figure 7.1a (up-down tremor). Mean inclination θ_0 is 90 deg, radius $r = 10$ cm, frequency of tremor 5 Hz, angular amplitude of tremor $\varphi_0 = 10$ deg.

The gravitational component of acceleration is not generally known. Therefore, only the other estimates of mean inclination are available. From them, in this particular example, the inclination of the mean measured acceleration is by far the best (9 deg). Its error comes from the centripetal acceleration that is the main source of the curvature of the time course of the measured acceleration. For the other estimates – averages of the acceleration measurement directions in the Euclidean and angle spaces – the errors are much higher. The increased errors come especially from the amplified direction change when the amplitude of acceleration reduces bellow |g|.

If one wants the mean acceleration to estimate the mean inclination but uses only the inclination or orientation in each sample estimated from accelerometer (and magnetometer) in the observer, there is a straightforward approach: Do not let the acceleration filtering only on the observer but prefilter the measured acceleration by a low pass filter with the cut-off frequency below the frequency of tremor before using it in observer.

7.2.3 Simulations of model tremor

See figures 7.3 and 7.4 for the estimation errors of the central inclination in regular, symmetrical, and sinusoidal movements as sketched on figure 7.1a and 7.1b, respectively. Three different central inclinations were used (columns of graphs) and three different distances from the center of rotation (rows of graphs). In each subfigure, the estimation errors are shown for three frequencies as functions of the angular amplitude φ_0 of the tremor.

The errors were get as the differences between the central directions and the mean inclinations estimated from the accelerometer measurements: Direction of the mean measured acceleration; direction of acceleration averaged in the Euclidean space; for the situation from figure 7.1a also average pitch angle that was estimated from acceleration in each single moment. The estimates were get numerically by averaging on a single period of movement. The period was discretized to 1000 samples. The acceleration at sample k was computed by

$$a_k = R_k \, [0 \; 0 \; |\mathrm{g}|]^{\mathrm{T}} \; + \; \epsilon_k \times r_k \; + \; \omega_k \times (\omega_k \times [r \; 0 \; 0]^{\mathrm{T}}), \tag{7.1}$$

where R_k is the orientation matrix specified by the actual angle of the tremor and by the central inclination. The angle, angular rate ω, and angular acceleration ϵ are harmonic. The computation of the mean acceleration was simplified using $\int_0^{2\pi} \mathrm{sc}(t)\, dt = 0$ and $\int_0^{2\pi} \sin(\alpha\, \mathrm{sc}(t))\, dt = 0$, where sc stands for sin or cos and α is a real constant.

The tremor simulations may represent some model types of tremor:

- The up-down tremor with central pitch $\theta_0 = 90$ deg and $r = 10$ cm represents a flexion-extension tremor of horizontally outstretched hand.
- The up-down tremor with $\theta_0 = 45$ deg and $r = 10$ cm represents a flexion-extension tremor of a hand hanged down from an armrest of a chair.
- The left-right tremor with $\theta_0 = 135$ deg and $r = 3$ cm represents a pronation-supination tremor of a hand hanged down from an armrest of a chair measured by a sensor fixed to the dorsum of the hand.
- The left-right tremor with $\theta_0 = 90$ deg and $r = 40$ cm represents a flexion-extension tremor of a forearm in wing position with arms outstretched and forearms flexed such that the fingers of the two hands come close in front of the chest.

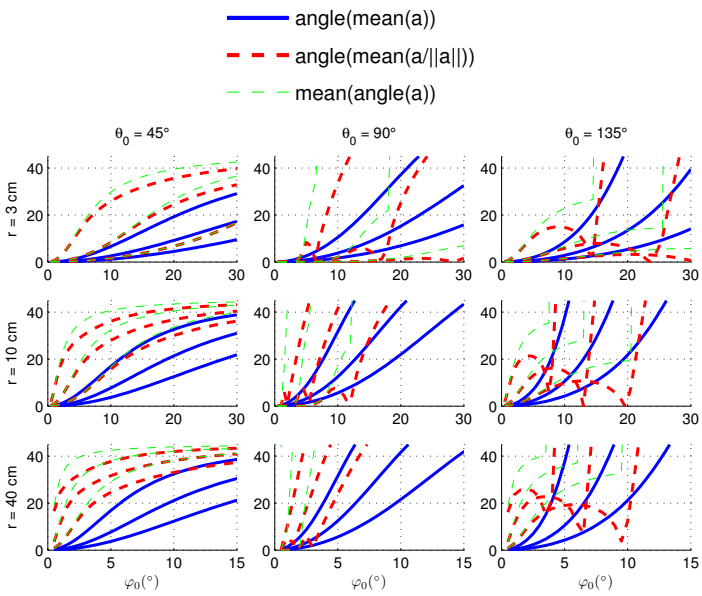

Figure 7.3: Errors of different estimates of inclination of the central sensor orientation (degrees). Rotation about horizontal axis (up-down tremor). Mean stands for averaging in an infinite interval or in a period of oscillation. Angle stands for pitch of the longitudinal axis of the sensor computed from an accelerometer measurement. Trios of curves correspond to three oscillations with frequencies of 4, 6, and 10 Hz from bottom up, respectively. Beware the different range of the horizontal axis of the graphs in the last row.

See figures 7.3 and 7.4 for the results. For the left-right oscillations (fig. 7.4), the error grows with growing angular amplitude of tremor (φ_0), growing distance r, and growing frequency of tremor. Usually, it also grows with growing central inclination θ_0. The errors by averaging the directions of accelerometer measurements are always greater than by averaging the raw measurements. The difference is not very big and grows with growing θ_0, r, and frequency. For small amplitudes φ_0 the difference also grows with growing φ_0.

For the up-down oscillations (fig. 7.3), the situation is more complicated. The error by averaging the raw measurements also grows similarly as described for the left-right tremor. But the errors by averaging the directions of accelerometer measurements often have non-monotone curves. For small θ_0 and for high amplitudes at high frequencies, the error is much higher than the error by averaging raw acceleration. On the other hand, for combinations of high θ_0 and low φ_0, especially also with low frequencies, the error by averaging directions of measured acceleration may be lower than by averaging the raw acceleration. See figure 7.3, $r = 3\,\text{cm}$, $\theta_0 = 90\,\text{deg}$ or $135\,\text{deg}$, $f = 4\,\text{Hz}$ for extreme cases, when averaging directions gives very low error. Averaging directions in the space of the angle gives always the error greater or equal to the error by averaging the direction vectors in the Euclidean space.

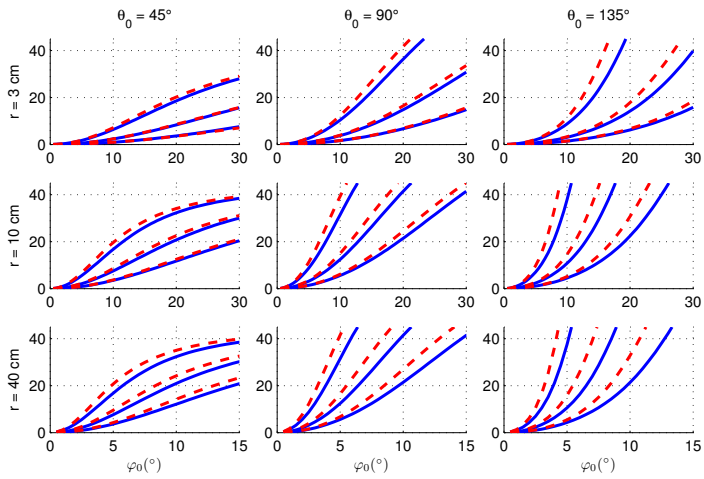

Figure 7.4: Errors of estimates of inclination of the central sensor orientation (degrees). Rotation about an axis parallel to Z (left-right tremor). Trios of curves correspond to three oscillations with frequencies of 4, 6, and 10 Hz from bottom up, respectively. See figure 7.3 for the legend. Beware the different range of the horizontal axis of the graphs in the last row.

7.3 Attitude estimation algorithms

This section provides the description of the simple estimation algorithms which were used to estimate the attitude if IMU from the data from tremor simulation by humans. They were not specially tuned to be numerically effective nor to provide optimal results. Rather, similar fixed settings were used for all the algorithms to demonstrate and compare the influence of the ways how the acceleration measurements were incorporated.

7.3.1 Common features of the used algorithms

The attitude is represented by a unit orientation quaternion $q = [q_0\ q_1\ q_2\ q_3]^{\mathrm{T}}$ that form the state of the estimation filter. The orientation quaternion is the quaternion of the rotation from the global reference frame (axis Z vertical, heading up) to the IMU reference frame. Its time evolution is described by differential equation

$$\dot{q}(t) = \frac{1}{2}\begin{bmatrix} -q_1(t) & -q_2(t) & -q_3(t) \\ q_0(t) & -q_3(t) & q_2(t) \\ q_3(t) & q_0(t) & -q_1(t) \\ -q_2(t) & q_1(t) & q_0(t) \end{bmatrix} \omega(t) = \frac{1}{2}\ DQ_\omega(t)\ q(t)\ , \tag{7.2}$$

where $\omega(t)$ is the actual angular rate of IMU in its local coordinate frame and

$$DQ_\omega(t) = \begin{bmatrix} 0 & -\omega_1(t) & -\omega_2(t) & -\omega_3(t) \\ \omega_1(t) & 0 & \omega_3(t) & -\omega_2(t) \\ \omega_2(t) & -\omega_3(t) & 0 & \omega_1(t) \\ \omega_3(t) & \omega_2(t) & -\omega_1(t) & 0 \end{bmatrix}$$

For the need of extended Kalman filter (EKF) used to estimate the quaternion, the equation was discretized by the Euler method. The use of the continuous-time equation for prediction would be also possible but its utility is limited by the discrete measurement of ω. The quaternion was divided by its norm in each step to force it to be a unit quaternion.

Angular rate is treated as an input to the system acting in the state equation – discretization of (7.2). In a standard setting, Kalman filter assumes exactly known inputs. That is not our case because of the noisy measurement of the angular velocity and estimate of the angular acceleration. The noise was taken into account using the covariance of the input measurement noise R_u added to the process noise and output measurement noise covariances in the model as shown for linear systems by Markovsky and De Moor (2005), see (6.2)–(6.4). Settings of the covariance matrices are listed in the section 7.4.1.3.

Two structures of model output were used: In the first algorithm, the estimate of gravitational component of acceleration was the output and an acceleration was used as its measurement. In the second algorithm, the estimate of orientation quaternion was the output and an estimate of orientation from acceleration and local Earth magnetic field was its measurement. A triaxial magnetometer, or electronic compass, was used in addition to accelerometer in the second algorithm.

7.3.2 Algorithm A: Output = gravitational component of acceleration

The output of the attitude estimation filter is the gravitational component a_{g} of acceleration as measured by an accelerometer (equals minus gravity in the coordinates of IMU).

$$a_{\mathrm{g}} = R \begin{bmatrix} 0 \\ 0 \\ \mathrm{g} \end{bmatrix} = \mathrm{g} \begin{bmatrix} 2\left(q_1 q_3 - q_0 q_2\right) \\ 2\left(q_2 q_3 + q_0 q_1\right) \\ q_0^2 - q_1^2 - q_2^2 + q_3^2 \end{bmatrix}$$

where time argument t of a_{g}, R, and q was omitted and rotation matrix $R(t)$ corresponds to the unit quaternion $q(t)$.

As the input measurement, the measured angular rate was used. In the case of measured data, an estimate of the bias was subtracted before.

As the output measurement, an estimate of a_{g} from measured acceleration a was used, see part 7.3.5.

7.3.3 Algorithm M1: Outputs = gravitational component of acceleration and projection of Earth magnetic field

In this algorithm, the state equation was the same as in the first algorithm as well as the treatment of the input.

Part of the input was the same: a_{g}, but in addition to it, also the projection of the Earth magnetic field to the sensor coordinates was used. The assumed unit of the magnetic field measurement was the intensity of the field at the Earth surface, making the actual projection a unit vector.

$$m = R \begin{bmatrix} \cos\phi_{\mathrm{m}} \\ 0 \\ -\sin\phi_{\mathrm{m}} \end{bmatrix}$$

where time argument t of m and R was omitted.

As the output measurement, an estimate of a_{g} and the measurement of m by IMU was used.

7.3.4 Algorithm M2: Output = orientation quaternion

In this algorithm, the state equation was the same as in the other algorithms as well as the treatment of the input.

The difference was in the output of the model: Orientation quaternion of IMU was used instead of gravitational component of measured acceleration. The output equation is linear in the case – output equals the state of the filter. As an output measurement, an orientation quaternion was estimated from

- direction of measured acceleration a, see part 7.3.5 for details about acceleration measurements used.

- direction measured projection of the Earth magnetic field into the coordinates of IMU.

The orientation matrix was estimated as the rotation matrix transforming the best in the LS sense the directions of quantities in the global reference frame with X axis heading to the magnetic north to the directions of the measurements of IMU. The directions in the global reference frame are $[0\ 0\ 1]^{\mathrm{T}}$ for direction of acceleration and $[\cos\phi_{\mathrm{m}}\ 0\ -\sin\phi_{\mathrm{m}}]^{\mathrm{T}}$ for magnetic field, ϕ_{m} is the local magnetic inclination. The rotation matrix was estimated as a solution of the least squares Wahba's problem (Wahba 1966). See section 6.2 for more details about the solution of Wahba's problem that appeared in another task.

7.3.5 Quantities used as the measurement of gravitational component of acceleration

In the previous paragraphs, attitude estimation algorithms were described. They use an an estimate of the gravitational component a_{g} of the acceleration as measured by an accelerometer. Here we describe more about the measurements.

The most straightforward is the use of the accelerometer measurement a as the measurement of a_{g}. In such a case, we get an exact measurement of a_{g} if the sensor is steady in an Earth-fixed coordinate frame. Any accelerations of the sensor cause errors of the measurement of a_{g}.

If the sensor is accelerated, usually the norm of the measured acceleration differs from the size of gravitational acceleration, g. In many cases, the difference between a and a_{g} may be reduced by normalizing the measurement, that means setting its norm to the expected value by multiplying it by a scalar value,

$$a_{\mathrm{n}} = a \cdot \mathrm{g}/\|a\|_2$$

See figure 7.2, the normalized acceleration measurement is usually more close to the gravitational component a_{g} than a, except the part where a is close to zero or has approximately opposite direction than a_{g}. The positive effect is marked especially if $\|a\| > \mathrm{g}$. Moreover, the direction of the accelerometer measurement is sometimes used in the attitude estimation algorithms. By using a_{n} we work in fact only with the direction and simulate in such a way the usage of the direction of the acceleration measurement as the input of the algorithm.

In the algorithm M2 – described in section 7.3.4 – there is no difference between the use of a and a_{n}, because only the direction (unit vector) is used.

Typical tremors are at least in part rotation motions and all our simplified simulations of tremor are rotations. The accelerations coming from the rotations, especially the centripetal acceleration, cause errors in the estimation of inclination by an accelerometer. An idea is to estimate these accelerations caused by the rotation and subtract them from the measured acceleration before application of the attitude estimation filter:

$$a_{\mathrm{red}} = a - \hat{a}_{\mathrm{rot}}, \qquad a_{\mathrm{red,n}} = a_{\mathrm{red}}\,\mathrm{g}/\|a_{\mathrm{red}}\|_2$$

The estimate of the acceleration produced by rotation motion is

$$\hat{a}_{\mathrm{rot},k} = \hat{\epsilon}_k \times \hat{r}_k \ + \ \omega_k \times (\omega_k \times \hat{r}_k),$$

where $\hat{r}_k$ is the vector from the estimated center of rotation to the sensor position, expressed in sensor coordinates, and $\hat{\epsilon}_k$ is an estimate of angular acceleration, i.e. time derivative of angular rate. Angular rate was measured by the gyroscopes. Angular acceleration was estimated from the rate by five-point stencil method. See section 6.1 for a procedure for the estimation of r.

To reduce the exacerbated noise of angular acceleration estimate due to the numerical derivation used, the angular rate was filtered by a noncausal low-pass filter first (20 Hz, Butterworth filter of 4^{th} order, run forwards and then backwards). The filtered angular rate was used to estimate r and then to estimate a_{rot}. Moreover, for the latter task, the gyroscope bias estimated as a side-product of estimation of r was subtracted from the filtered angular rate. See figure 6.1 for an example of the estimate of the center of rotation from data measured on a human simulating hand tremor.

As was demonstrated in section 7.2, when averaging over the time in a rotational motion, the normalized acceleration measurement often provides more biased estimate of the direction of gravity than provides the raw measured acceleration. We assume that it may also corrupt the performance of the attitude estimation algorithms. Therefore we propose, that for an algorithm where the direction of the acceleration measurement or the normalized acceleration is used, it may help to filter the acceleration measurement by a low-pass filter before passing it to the attitude estimation algorithm. In such a way, the average direction will be more close to the direction of the average acceleration measurement which usually provides a better estimate. That shall help when using a_{n} or $a_{\text{red,n}}$ and in the algorithm M2 where only the direction of the measurement is always used. The filtration time of the filter shall be longer than the period of the alternating movement.

Finally, we get the following quantities to be used as the estimates of the gravitational component of acceleration:

a acceleration measured by the accelerometer,

a_{n} normalized acceleration (a divided by its size and multiplied by the size of gravitational acceleration), equivalent to the use of instantaneous direction of the measured acceleration,

a_{red} reduced acceleration – measurement a with an estimate of rotation accelerations subtracted,

$a_{\text{red,n}}$ normalized a_{red}, equivalent to the use of instantaneous direction of the reduced acceleration

$a_{\text{F,n}}$ calculated same as a_{n}, but a first filtered by a low-pass filter

$a_{\text{red,F,n}}$ calculated same as $a_{\text{red,n}}$, but a_{red} first filtered by a low-pass filter

In algorithm M2, only the direction of acceleration is always used, therefore there is no difference between using the original and normalized values. In fact, using the direction is equal to always normalizing the measurement.

7.3.6 Alternative algorithms to deal with centripetal acceleration

In our algorithms described above there is no movement acceleration desired or only a movement acceleration which produces zero mean in the sensor coordinate frame (a_{iL}). Otherwise, e.g. in case of centripetal acceleration, a biased estimate of mean inclination may occur, see sections 7.2.2 and 7.2.3. This bias is dealt by us estimating the center of rotation with the presumption that it does not change much.

Our approach is close to the methods of Hyde et al. (2008) who used known distances of arm joints and known positions of the sensors placed on several arm segments to enhance the attitude estimation. However, in the paper, they presumed known distances and sensor

placement and did not deal with their assessment (called also calibration). On the contrary, we use just one sensor unit and estimate the needed parameters directly from the data measured at tremor, but we assume dominant rotation only about one joint, although they provide also possibility to count with rotation about several joints (e.g. wrist + elbow + shoulder) by using more sensor units.

An alternative to these approaches is a different construction of the attitude estimator: Luinge and Veltink (2005) proposed to include into the attitude estimator a model of the acceleration in an Earth-fixed reference frame. The acceleration is modeled by a first-order linear dynamical model. The prediction of the acceleration is then

$$a_{\mathrm{iG}}(k+1) = \mathrm{c_A} \cdot a_{\mathrm{iG}}(k); \quad \mathrm{c_A} < 1$$

The obtained estimate of the motion acceleration in global reference frame is incorporated into the observer to calculate the instantaneous acceleration in the sensor reference frame a_{iL} using the actual estimate of the attitude. In this way, rather the acceleration in the Earth-fixed reference frame a_{iG} is assumed to has zero mean than the motion acceleration expressed in the sensor reference frame a_{iL}. Therefore, the accelerations like the centripetal one which are connected to virtual accelerations do not produce such estimation bias. The performance would depend on the used constant $\mathrm{c_A}$ of the model and on the speed of the acceleration change in the Earth-fixed reference frame.

This algorithm was not deeply tested and compared to the other algorithms because its performance would likely not depend only on the covariances of the assumed measurement errors but also on the parameters of the dynamical model of the movement and on the relation of its time constant and the frequency of the tremor. But an algorithm with similar properties, as stated by the user manual (Xsens Technologies 2010), and likely with a similar basis was implemented in the Xsens inertial estimation algorithms. One of them – "Human, large acceleration" – was shortly tested besides our algorithms described above. This algorithm is not tuned specifically to the rotational motion as some of our algorithms, on the other hand it has a potential to better performance in other types of motion, e.g. irregular motion or fast changing center of rotation. Please, note that the settings of the algorithm (observer gains/covariances, initial state covariance) are not know to us and they may differ a lot from the settings of our algorithms.

7.4 Tremor mimicking by humans

In this section, the methods and the results of a set of measurements of human hand tremor voluntarily simulated by healthy humans are described. The measurements were done with the help of IMU and magnetic pose measurement system Polhemus Isotrak. The Isotrak system was used as the reference system to validate the performance of the different algorithms and ways how the acceleration measurement of IMU was incorporated into the attitude and inclination estimate as described in the previous section. Both the auxiliary methods described in chapter 6 are used here.

7.4.1 Methods

7.4.1.1 Subjects and measurement setup

Five healthy persons (all male) participated in the study in six measurement sessions (one subject participated at two different days). In each measurement session, 9 to 28 mea-

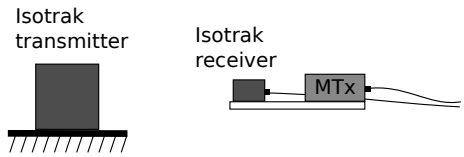

Figure 7.5: Sketch of the measurement setup.

surements were done. The subjects were simulating hand tremor while holding the below described measurement device in one hand. It was verified by the investigator, that part of the measurements was done with the other hand than the preferred one. Totally, 100 trials with hand tremor simulations were acquired with lengths from 12.2 to 92.8 sec, median 26.8 sec. In 50% to 100% of each trial, the tremor was present. In part of the measurements (26 trials), the subjects started to simulate tremor already before the recording of IMU data started. In the other 74 trials, there was only a physiological tremor and small movements present at the start of the measurement.

Hand tremor was measured by two mechanically coupled devices: inertial measurement unit Xsens MTx and magnetic system Polhemus Isotrak. MTx operated with sampling frequency of 120 Hz and transmitted data by a cable to Xbus unit connected to computer. A synchronization signal that switched its level at each sampling time was generated by Xbus unit and transmitted to the synchronization input of Isotrak. Therefore, Isotrak operated synchronously with MTx with half the frequency – 60 Hz, that is its maximum possible sampling frequency. As the used software did not allow for simultaneous start of generation of the synchronization signal and recording of the data, the following strategy was implemented to get synchronized data: Recording of inertial data was started before the start of data acquisition from Isotrak and stopped after the end of data acquisition from Isotrak. Then, the time lag between the two data sets was get by finding maximum correlation between the angular rate measured by gyroscopes and angular rate estimated from Isotrak. The angular rate was estimated by numerical derivation of Isotrak angular data and transformation to MTx reference frame using known relative orientation of the two sensors. See appendix A for more details.

The devices were fixed to a board with the distance of their mutual proximal sides being 30 mm. The apparatus was held by a hand of the subject in such a manner that the Isotrak receiver was about 10 to 20 centimeters away from the transmitter and the receiver was placed more close to the transmitter than IMU to reduce distortion of the Isotrak measurement by the magnetic field produced by MTx electronics.

7.4.1.2 Reference frames alignment

To relate the Isotrak and IMU measurements we have to know the relative orientation of reference frames of both the systems. Not only the relative orientation of the Isotrak receiver and MTx sensors is needed but also the relative orientation of the global reference frames of the two systems. The inertial reference frame of MTx is defined as north-west-up. The inertial reference frame of Isotrak is defined by the actual fixed orientation and position of the Isotrak transmitter. The relative orientations specified by rotational matrices were estimated using a set of measurements in static conditions and different poses of the apparatus in the volume where later the tremor measurements were done. See section 6.2

for derivation of the alignment algorithm and more details about the alignment procedure.

The accuracy of the reference frame alignment was not comprehensively tested, but an estimate of the error from the data used for the alignment itself was made: The calculated alignment matrices were used to transform the mean attitudes estimated by Isotrak to the attitudes in the coordinate system of MTx. That was done for every quasi-static slice of the data used for the alignment procedure. The alignment error was calculated as the angle of the rotation between the two attitudes expressed in the two (as assumed) same coordinate systems. Additionally, there was determined the error of the alignment of verticals as the angle between vertical vectors as specified by the two estimated attitudes. For the errors, root mean square (RMS) was calculated from all the quasi-static slices in the data.

7.4.1.3 Attitude estimation

For the estimation of attitude and inclination of the IMU, the algorithms described in section 7.3 were used with the inputs described also there. For all the three above mentioned algorithms, similar settings were used. In all cases a single-run discrete extended Kalman filter was used which was constructed by a time discretization of (7.2). Though, when a_{red} was used, the algorithm was a single-run causal filter to be comparable to others, but it used the center of rotation estimated by a non-causal filter.

For the sake of simplicity, constant covariance matrices were used for the Kalman filter:

- The covariance of the assumed noise of the gyroscope measurement $0.0005\,\mathcal{I}_3$ $[(\mathrm{rad\,s^{-1}})^2]$ which was then used to determine the covariance of the virtual process noise in the same way as in sections 5.2.3 and 6.1.
- The covariance of the assumed noise of the measurement of the gravitational artifact $4\,\mathcal{I}_3$ $[(\mathrm{m\,s^{-2}})^2]$.
- The covariance of the assumed noise of the magnetic field measurement $0.04\,\mathcal{I}_3$.
- The covariance of the assumed noise of the measurement of the quaternion (in fact estimated from the acceleration and magnetic field) $0.04\,\mathcal{I}_4$.

Fixed covariances represent fixed weights of the outputs in the state observer. Though, the gains are never fixed because of the system and filter nonlinearity and the response of the initial state. The assumed covariance of the error of acceleration measurement as a measurement of the gravitational component is a compromise between the trust to the measurement in the case of statical conditions and the dis-trust to it in the case of a very severe tremor. In case of a usage of raw acceleration measurement in severe tremor, the chosen covariance may cause too high trust to the data very corrupted by the movement accelerations. Estimator construction omitted the non-whiteness and non-normality of the errors, especially of the acceleration measurement and of the quaternion estimate.

The initial state of the observer was same for all the three algorithms and it was determined as follows: Mean accelerometer and magnetometer measurements were computed for the first 0.25 sec of the data. The directions of the two mean measurements were determined and then they were subject to LS estimation of quaternion as described for algorithm M2 in section 7.3.4. The covariance of the initial quaternion was determined as an identity matrix times a constant. The constant was the maximum of the covariances of the magnetometer measurement [-] and of the accelerometer measurement [g^2] in the 0.25 sec

interval. The constant was limited to lie between 0.01 and 1. The lower limit was applied because if the covariance of the initial state was low, then the influence of the accelerometer and magnetometer measurement during the trial would be low and differences between the algorithms would be also low.

As was proposed in section 7.3.5, the algorithms were tested also with the acceleration measurements filtered by a low pass filter. The discrete Butterworth filter of 2^{nd} order and cut-off frequency of 1 Hz was used. The filter was run in both directions of the time axis to provide an estimate with zero lag.

7.4.1.4 Accuracy determination

The accuracy of the proposed algorithms on the data from tremor voluntary simulation by humans was assessed by the angle discrepancy (deg) of the inclination estimated from the IMU data by the algorithm from the inclination estimated by the magnetic system Polhemus Isotrak. By the inclination we mean the direction of the gravitational component of acceleration in the coordinates of IMU. Root mean square of the angle discrepancy was used to represent each measurement trial.

Both the static and dynamic errors of both the systems are included in RMS. To separate the dynamical errors that occur during the oscillations, the inclinations were also filtered by a low-pass filter to provide time-averaged inclination estimates. The obtained filtered inclinations from the two systems were also compared by means of RMS. The filter was a discrete Butterworth filter of 2^{nd} order and cut-off frequency of 1 Hz. The filter was run in both directions of the time axis to provide an estimate with zero lag. To remove the influence of the initial conditions of the filter, the first second of the data was not used for the comparison.

The RMS errors given by the different algorithms and acceleration measurements were compared by the means of Wilcoxon paired signed rank test.

7.4.2 Results

7.4.2.1 Alignment of the measurement systems

The measurements were conducted during three days. At the beginning of each day, the alignment procedure was done. Mean RMS attitude error from the three alignment procedures was 1.0 deg. Mean RMS error of the vertical (error of the determination of inclination) was 0.36 deg.

One possible source of the found alignment error was the mutual magnetic distortion of the two measurement systems: Distortion of Isotrak by the electronics of MTx and distortion of the magnetometer (electronic compass) in MTx by the alternating magnetic field of Isotrak.

In the case of a measurement different from the alignment measurement and moreover a dynamic one, following additional errors may occur:

- Additional alignment error due to the difference of the poses occurred in the measurement from the poses covered in the alignment procedure.
- Noise of the Isotrak measurement about 0.05 deg and 0.02 deg for the attitude and inclination, respectively.
- Dynamic error of the Isotrak measurement.

7.4.2.2 Amplitudes and frequencies of the tremor

Tremor amplitudes and frequencies were assessed from the measured angular rate ω as described in chapter 5 to provide some picture of what were the amplitudes and how do they compare to the tremor amplitudes of essential tremor assessed in chapter 5. The angular rate was chosen instead of acceleration or other quantities because it is the same for all the palm and therefore does not depend much on the way how was the subject holding the apparatus. Acceleration amplitude depends highly on the place of the accelerometer and therefore it would be hard to compare it between the trials and especially with the essential tremor study. For the peak detection in the tremor quantification algorithm, the lower frequency limit was lowered because some of the tremors simulated by the healthy subjects exhibited frequencies lower than the original limit 3.5 Hz.

Median computed amplitude of the simulated tremor in the 100 trials was $4.58\,\mathrm{rad\,s^{-1}}$, inter-quartile range (IQR) $3.05\,\mathrm{rad\,s^{-1}}$, range 0.58–$10.48\,\mathrm{rad\,s^{-1}}$. Comparing with section 5.3.1, the amplitudes were higher than most of the amplitudes found for the essential tremor patients involved in our study. Median frequency was 5.53 Hz, IQR 1.72 Hz, and range 2.92–8.53 Hz.

Because the amplitudes were very high and exceeded the range of tremor amplitudes seen in patients, part of the following cross-validation with the magnetic system was done also for a subset of the trials with the lowest amplitudes. Namely, 20 trials with the lowest found amplitudes of ω were selected. Median amplitude in this subset was $1.45\,\mathrm{rad\,s^{-1}}$, IQR $0.85\,\mathrm{rad\,s^{-1}}$, and range 0.58–$2.29\,\mathrm{rad\,s^{-1}}$. The upper end of the range corresponds approximately to the point where the regression of the visual tremor assessment by ω in section 5.3.6 estimated 3.5 points at the 0–4 point modified Fahn-Tolosa-Marín rating scale. Median frequency in the subset was 5.93 Hz, IQR 0.68 Hz, and range 5.24–7.30 Hz.

7.4.2.3 Validation of the inertial attitude estimate

The attitude estimation algorithms and their different measurements of acceleration were compared by their performance in estimating the inclination relative to vertical as described in section 7.4.1.4. Let us recall that the alignment error between the two measurement systems – IMU and Polhemus Isotrak used as the reference measurement – as found directly in the data used for the alignment was at least 0.36 degree. The results are listed in table 7.1 for the dynamical measurements. To reduce the influence of the dynamical errors of the two systems, also low-pass filtered inclinations were compared, see table 7.2. Minimum, maximum, median, and mean RMS differences between the inclinations estimated by the two systems are listed in the two tables. Inter-quartile ranges (IQR) are also shown. At the right sides of both the tables, there are listed the results for the subset of 20 trials with lowest tremor amplitudes. The different lines are described in the table captions, see below for more details.

Lines X_{MTx} represent the estimates by the Xsens proprietary algorithm "Human, high acceleration" applied to the recorded data. Its estimate is usually accurate comparably to the best of our algorithms except several cases, when a severe tremor was present already at the beginning of the measurement. In such a case, the algorithm has problems in determining the initial orientation. To be honest, such a state at the beginning of an inertial estimation is hard to be coped with and usually, near to static conditions at the beginning are part of the assumptions for general inertial estimation algorithms. See table 7.3 for the comparison of the X_{MTx} with a selection of our algorithms at the data from 74 trials when the subjects started simulating tremor after the beginning of recording IMU data. User

Performance of inclination estimate
against inclination from Isotrak
RMSE (°)

all measurements						lower tremors only				
min	median	mean	max	(IQR)		min	median	mean	max	(IQR)
11.8	51.2	53.1	102.1	(30.5)	$a.\ a_{\mathrm{n}}$	11.8	24.1	28.6	56.3	(21.3)
2.2	16.5	21.5	61.9	(23.1)	a_{red}	2.2	5.9	7.6	14.6	(3.5)
0.6	3.6	4.6	29.0	(3.2)	X_{MTx}	0.6	1.5	1.6	3.2	(1.0)
0.7	3.3	3.7	12.9	(2.5)	Sa_{red}	0.7	1.5	1.4	2.8	(0.8)
1.0	3.9	4.4	13.2	(3.0)	Aa	1.0	1.6	1.8	2.9	(1.0)
0.9	13.8	14.6	40.4	(12.2)	Aa_{n}	0.9	4.3	7.8	22.6	(8.6)
0.7	3.4	3.8	13.1	(2.4)	Aa_{red}	0.7	1.5	1.4	2.7	(0.7)
0.7	4.3	5.0	16.9	(4.1)	$Aa_{\mathrm{red,n}}$	0.7	1.5	1.6	3.2	(0.9)
1.0	3.7	4.2	12.9	(2.8)	M_1a	1.0	1.8	1.8	2.7	(1.0)
1.0	9.3	10.0	24.8	(7.0)	M_1a_{n}	1.0	3.6	6.2	21.6	(4.6)
0.7	3.4	3.8	12.9	(2.2)	M_1a_{red}	0.7	1.5	1.5	2.8	(0.7)
0.7	4.2	4.5	14.9	(3.3)	$M_1a_{\mathrm{red,n}}$	0.7	1.5	1.6	2.8	(0.7)
2.0	19.6	19.9	57.8	(12.9)	M_2a	2.0	6.9	9.7	26.8	(10.6)
0.7	5.0	6.0	20.2	(5.9)	M_2a_{red}	0.7	1.6	1.8	3.8	(1.0)
0.7	8.5	11.0	42.4	(8.3)	$Aa_{\mathrm{F,n}}$	0.7	2.0	2.0	3.8	(1.4)
0.6	3.6	4.0	12.1	(3.0)	$Aa_{\mathrm{red,F,n}}$	0.6	1.4	1.4	2.8	(0.8)
0.7	7.7	9.2	30.7	(6.9)	$M_1a_{\mathrm{F,n}}$	0.7	1.8	1.9	3.5	(1.0)
0.7	3.6	4.0	12.2	(2.8)	$M_1a_{\mathrm{red,F,n}}$	0.7	1.5	1.5	2.9	(0.8)
0.7	7.9	9.3	29.5	(7.2)	$M_2a_{\mathrm{F,n}}$	0.7	1.9	2.0	3.8	(1.0)
0.8	3.9	4.2	12.2	(3.1)	$M_2a_{\mathrm{red,F,n}}$	0.8	1.5	1.5	2.9	(0.8)

Table 7.1: RMS angular difference between the inclinations estimated from IMU and from the Isotrak system. **Notation:** a,a_{n}/a_{red}– direction of acceleration used directly as the estimated inclination: measured acceleration / measured acceleration with subtracted estimate of rotation accelerations; X_{MTx}– Xsens algorithm 'Human, high acceleration' applied to the recorded data; Sa_{red}– smoothed estimate of inclination by the algorithm of the estimation of the center of rotation (section 6.1); A – Algorithm A, M_1 – algorithm M1 (acceleration + magnetic field); M_2 – algorithm M2 (quaternion estimated from instantaneous acceleration + magnetic field); n – acceleration normalized; red – centripetal and tangential acceleration estimates removed from acceleration measurement; F – measured or reduced acceleration first filtered by the low-pass filter before passing to the algorithm.

Performance of low-pass filtered inclination estimate
against low-pass filtered inclination from Isotrak
RMSE (°)

all measurements						lower tremors only				
min	median	mean	max	(IQR)		min	median	mean	max	(IQR)
0.3	7.9	10.5	43.0	(9.1)	a	0.3	1.5	1.5	3.3	(1.4)
0.3	17.1	20.4	83.6	(14.9)	a_{n}	0.3	4.7	7.9	22.1	(9.0)
0.2	1.4	1.8	7.2	(1.7)	a_{red}	0.2	0.5	0.5	0.9	(0.3)
0.2	1.1	2.4	28.6	(1.8)	X_{MTx}	0.2	0.5	0.8	3.2	(0.3)
0.2	0.8	1.1	5.9	(0.9)	Sa_{red}	0.2	0.4	0.4	0.9	(0.3)
0.2	1.0	1.4	5.8	(1.3)	Aa	0.2	0.5	0.4	0.8	(0.2)
0.2	12.9	13.9	39.6	(12.8)	Aa_{n}	0.2	3.9	7.4	22.5	(8.8)
0.2	0.9	1.1	6.2	(0.8)	Aa_{red}	0.2	0.4	0.4	0.8	(0.3)
0.2	2.0	3.1	16.5	(3.6)	$Aa_{\mathrm{red,n}}$	0.2	0.6	0.7	1.8	(0.6)
0.3	1.2	1.4	5.6	(1.0)	M_1a	0.3	0.6	0.6	1.1	(0.3)
0.6	8.2	9.0	24.7	(7.7)	M_1a_{n}	0.6	3.2	5.9	21.5	(5.2)
0.2	1.0	1.3	6.0	(0.9)	M_1a_{red}	0.2	0.6	0.6	1.1	(0.3)
0.2	1.6	2.4	12.3	(2.6)	$M_1a_{\mathrm{red,n}}$	0.2	0.7	0.8	1.6	(0.4)
1.9	18.3	19.5	57.1	(12.9)	M_2a	1.9	6.7	9.5	26.8	(10.7)
0.4	2.9	4.6	19.9	(5.6)	M_2a_{red}	0.4	0.9	1.1	2.6	(0.9)
0.3	7.4	10.1	41.9	(9.1)	$Aa_{\mathrm{F,n}}$	0.3	1.4	1.4	3.3	(1.4)
0.2	1.5	1.8	7.0	(1.8)	$Aa_{\mathrm{red,F,n}}$	0.2	0.4	0.4	0.8	(0.3)
0.4	5.8	8.2	29.3	(7.8)	$M_1a_{\mathrm{F,n}}$	0.4	1.3	1.4	2.9	(0.9)
0.2	1.5	1.8	6.1	(1.5)	$M_1a_{\mathrm{red,F,n}}$	0.2	0.6	0.7	1.4	(0.3)
0.4	6.4	8.2	28.5	(8.0)	$M_2a_{\mathrm{F,n}}$	0.4	1.4	1.5	3.3	(1.0)
0.3	1.8	2.1	6.9	(2.0)	$M_2a_{\mathrm{red,F,n}}$	0.3	0.8	0.7	1.2	(0.3)

Table 7.2: RMS angular difference between low-pass filtered inclinations estimated from IMU and from the Isotrak system. **Notation:** a,a_{n}/a_{red}– direction of filtered acceleration used directly as the estimated inclination: measured acceleration / normalized acceleration / measured acceleration reduced by subtraction of the estimate of rotation accelerations; X_{MTx}– Xsens algorithm 'Human, high acceleration' applied to the recorded data; Sa_{red}– smoothed estimate of inclination by the algorithm of the estimation of the center of rotation (section 6.1); A – Algorithm A, M_1 – algorithm M1 (acceleration + magnetic field); M_2 – algorithm M2 (quaternion estimated from instantaneous acceleration + magnetic field); n – acceleration normalized; red – centripetal and tangential acceleration estimates removed from acceleration measurement; F – measured or reduced acceleration first filtered by the low-pass filter before passing to the algorithm.

Comparison of selected algorithms with X_{MTx}
at the data with no tremor at the beginning of the record

RMSE(°)						
min	median	mean	max	(IQR)		compare with X_{MTx}(%)
raw results						
0.6	3.1	3.5	13.4	(2.7)	X_{MTx}	
0.7	3.1	3.4	12.9	(2.5)	Sa_{red}	-
1.0	3.7	4.1	13.2	(2.8)	Aa	> 70
0.7	3.2	3.5	13.1	(2.6)	Aa_{red}	-
1.0	3.6	3.9	12.9	(2.5)	M_1a	> 70
0.7	3.2	3.5	12.9	(2.5)	M_1a_{red}	-
0.6	3.5	3.6	12.1	(2.7)	$Aa_{\mathrm{red,F,n}}$	-
0.7	3.4	3.6	12.2	(2.7)	$M_1a_{\mathrm{red,F,n}}$	-
0.8	3.4	3.8	12.2	(2.7)	$M_2a_{\mathrm{red,F,n}}$	> 66
low-pass filtered results						
0.2	0.9	1.2	6.3	(0.9)	X_{MTx}	
0.2	0.8	1.0	5.9	(0.8)	Sa_{red}	-
0.2	0.9	1.4	5.8	(1.3)	Aa	-
0.2	0.8	1.1	6.2	(0.7)	Aa_{red}	-
0.3	1.0	1.3	5.3	(1.0)	M_1a	-
0.2	1.0	1.2	6.0	(0.9)	M_1a_{red}	-
0.2	1.3	1.6	6.9	(1.7)	$Aa_{\mathrm{red,F,n}}$	> 72
0.2	1.3	1.6	4.8	(1.4)	$M_1a_{\mathrm{red,F,n}}$	> 76
0.3	1.6	1.9	6.5	(1.8)	$M_2a_{\mathrm{red,F,n}}$	> 81

Table 7.3: RMS angular difference between inclinations estimated from IMU and from the Isotrak system. Top: Direct calculation. Bottom: Low-pass filtered inclinations. **Notation:** See table 7.1 or 7.2. Symbol '-' in the last column means that there was no significant difference between the algorithm results and X_{MTx} according to Wilcoxon paired rank test (P 0.001). The numbers in the last column are the percentages (from the 74 trials) of cases when RMSE was greater (>) than for X_{MTx}.

manual (Xsens Technologies 2010) states that Xsens algorithms count with accelerometer instantaneous inclination (probably with its estimate) in the algorithm desing in a way that it is more close to average the movement acceleration in an Earth-fixed reference frame than in the sensor reference frame. Therefore, the deteriorating influence of the centripetal acceleration may be reduced. See section 7.3.6 above for a brief description of an algorithm with similar properties.

Lines Sa_{red} represent the attitude estimates which were obtained as side products of the algorithm for the estimation of the center of rotation (section 6.1). Compared to other estimates, these attitude estimates are smoothed – they utilize also future measurements. The initial quaternion estimate described above was not used in this algorithm and moreover, the initial quaternion estimate shall have little influence thanks to the smoothing.

By observing the tables 7.1 and 7.2, the direct usage of the instantaneous acceleration without fusing with the gyroscope measurement leads to the highest dynamical errors. When using the direction of the acceleration ($\ldots a_{\mathrm{n}}$, M_2a), the error is high even if the results are filtered: the mean inclination estimate is highly biased. The best algorithms (Sa_{red}, Aa,

Aa_{red}, M_1a, M_1a_{red}, $Aa_{\mathrm{red,F,n}}$, $M_1a_{\mathrm{red,F,n}}$, $M_2a_{\mathrm{red,F,n}}$) gave RMS inclination errors under 13.2 degrees (median under 4 deg) in all the measurements and under 3 deg (median under 1.8 deg) in 20 measurements with the lowest tremor amplitudes (but still high, see section 7.4.2.2 for more details about the amplitudes). The same results low-pass filtered due to the reduction of dynamical errors gave at the lower frequencies RMS errors under 7 degrees (median under 1.8 deg) in all the measurements and under 1.4 deg (median under 0.8 deg) in 20 measurements with the lowest tremor amplitudes.

Table 7.4 contains an excerpt from the results of the Wilcoxon paired rank tests applied to the RMS errors from the 100 trials. Due to the high number of the different estimates, all the results would occupy several pages. The excerpt contains several important comparisons:

a,b) Estimates using only the direction of acceleration usually produced greater errors than estimates using whole acceleration (a_{n} vs. a; $a_{\mathrm{red,n}}$ vs. a_{red}).

a,b) Estimates using the estimate of the center of rotation usually produced more accurate estimates than the ones without it (a_{red} vs. a; $a_{\mathrm{red,n}}$ vs. a_{n}).

c) Adding the magnetometer measurement to the raw acceleration measurement using the algorithm M1 tended to improve the accuracy.

d) When using only direction of acceleration / normalized acceleration, adding the magnetometer measurement using the algorithm M1 almost always improved the accuracy.

d) When using without additional preprocessing, the algorithm M2 usually gave worse results than algorithms A and M1.

e) When only the direction of acceleration / normalized acceleration was used, prefiltering the acceleration by the low-pass filter often improved the accuracy.

7.5 Discussion and conclusions

At the beginning of this part, let us to state the most important conclusion: When using a suitable estimation algorithm, the inclination estimate is relatively accurate although the accelerations caused by tremor motion may even exceed the size of the gravitational component of acceleration. After removing the dynamical errors which could be also at the side of the reference system, the RMS error was under 7 degrees (median under 1.8 deg) in all the measurements including simulations of very massive hand tremor and under 1.4 deg (median under 0.8 deg) in 20 measurements with the lowest tremor amplitudes in the validation study. Please note, that almost all the amplitudes got in the essential tremor study in chapter 5 were lower than the range of the 20 lowest tremor amplitudes in the validation study.

The algorithm used in chapter 5 was not tested in this study but it is close to algorithm M1 (M_1a) that provided relatively good estimates. The main differences of the algorithm from chapter 5 are the covariance settings which were data-driven there, and usage of the unscented Kalman filter (UKF) instead of EKF.

Let us list several recommendations for attitude estimation during severe tremor. The first two recommendations are rather general natural approaches which may be inferred intuitively:

1. If possible (for short-duration assessment trials), use stationary starting position of the measurement unit before the starts of the assessment trials, i.e. ensure that there is no tremor or only mild tremor present at the beginning of data acquisition. Have the rate gyroscopes well calibrated from biases. Do not rely much on the accelerometer measurements to estimate attitude during assessment trials, rather rely on the initial estimate and the gyroscope.

2. If possible, eliminate magnetic disturbance and use magnetometers to measure the Earth magnetic field and incorporate it to the attitude estimation scheme.

The next recommendations are the result of this study and/or derived from descriptions of referenced works:

3. If the movement has a rotational character with a stable or slowly changing center or axis of rotation (e.g. a static tremor without any other marked movement superposed), estimate the position of the axis or center of rotation and use that information to subtract the centripetal and tangential acceleration from the acceleration measurements. Alternatively, use the approach of Luinge and Veltink (2005) which may probably help also in situations, when a different movement is present.

4. Do not use algorithms which use only the direction of the accelerometer measurement, not the whole acceleration measurement.

5. If due to some reason an algorithm has to be used which does not comply to the previous point, prefilter the acceleration by a low-pass filter with the cut-off frequency below the frequency of tremor.

Possible direction of future studies may be more deep validation of the algorithms which model the acceleration caused by motion as a general dynamical model of low frequency noise in an Earth-fixed reference frame (Luinge and Veltink 2005). The validation shall contain a study of the sensitivity of accuracy to the parameters of the model and to the tremor frequency. Validation and comparison in situations where more significant movements are present together with tremor would be also of interest.

The inertial estimation generally may open a new approach to study human tremor – by properties of its attitude trajectories or even also displacement trajectories with the use of inertial sensors. That way, a more detailed insight may be given than by the raw measured signals or their simple time integrals or derivatives. Obtained trajectories would be also better interpretable because they are more close to visual observations than the raw signals.

Comparison of inclination estimation accuracies

	Estimated inclination			**Low-pass filtered estimate**			
a)	Effect of the measurement of gravitational component in algorithm A						
	Aa	< 95	> 83	-	Aa	< 97	> 73	< 79
		Aa_{n}	> 98	> 98		Aa_{n}	> 97	> 97
			Aa_{red}	< 88			Aa_{red}	< 88
				$Aa_{\mathrm{red,n}}$				$Aa_{\mathrm{red,n}}$
b)	Effect of the measurement of gravitational component in algorithm M1							
	M_1a	< 95	> 81	-	M_1a	< 98	-	< 73
		M_1a_{n}	> 95	> 92		M_1a_{n}	> 98	> 94
			M_1a_{red}	< 75			M_1a_{red}	< 76
				$M_1a_{\mathrm{red,n}}$				$M_1a_{\mathrm{red,n}}$
c)	Comparison of algorithms A and M1 with raw acceleration used							
		Aa	> 69	M_1a		Aa	-	M_1a
d)	Comparison of A, M1, and M2 with direction / normalization of accel.							
		Aa_{n}	> 97	< 78		Aa_{n}	> 97	< 78
			M_1a_{n}	< 98			M_1a_{n}	< 97
				M_2a				M_2a
e)	Effect of the filtering of the acceleration measurement							
	$Aa_{\mathrm{F,n}}$		< 74	Aa_{n}	$Aa_{\mathrm{F,n}}$		< 70	Aa_{n}
	$Aa_{\mathrm{red,F,n}}$		< 85	$Aa_{\mathrm{red,n}}$	$Aa_{\mathrm{red,F,n}}$		< 68	$Aa_{\mathrm{red,n}}$
	$M_1a_{\mathrm{F,n}}$		-	M_1a_{n}	$M_1a_{\mathrm{F,n}}$		-	M_1a_{n}
	$M_1a_{\mathrm{red,F,n}}$		< 76	$M_1a_{\mathrm{red,n}}$	$M_1a_{\mathrm{red,F,n}}$		-	$M_1a_{\mathrm{red,n}}$
	$M_2a_{\mathrm{F,n}}$		< 95	M_2a	$M_2a_{\mathrm{F,n}}$		< 95	M_2a
	$M_2a_{\mathrm{red,F,n}}$		< 87	M_2a_{red}	$M_2a_{\mathrm{red,F,n}}$		< 83	M_2a_{red}

Table 7.4: Comparison of RMS errors of different inclination estimates. Polhemus Isotrak was used as reference. **Notation:** $Aa < 95\ Aa_{\mathrm{n}}$ means that median difference of the RMS errors of the two estimates was nonzero according to Wilcoxon paired signed rank test ($P<0.001$) and that Aa had a lower RMSE than Aa_{n} in 95 cases of 100. Symbol '-' means that no significant difference was found.

Chapter 8

Conclusions and Suggestions for Future Work

8.1 Summary

In this thesis, I proposed several methods and documented studies in the field of accelerometer calibration for the use in humans and in the field of tremor quantification by means of inertial sensors.

The study of accelerometer calibration from in-use gathered quasi-static data brings a proposal to use other ellipsoid fitting methods and comparison of the methods in synthetic data. In tremor, attitude estimation was used to study different acceleration measurement components. The measurements were also successfully used to regress the tremor severity evaluation done by trained clinicians. Attitude estimation accuracy during tremor was the subject of a study bringing several conclusions about the estimator construction. As a tool used in the study, a method of finding mutual orientation of two attitude measurement systems was proposed.

Let me recapitulate the selected concrete thesis contributions, here accompanied by their placement in the thesis and publications.

- *Design of a new criterion for ellipsoid fitting to be used in a procedure for accelerometer calibration from data collected in nearly static conditions:*
  The criterion was proposed in chapter 4. It is the sum of squares of distances of the measured points to the intersections of the ellipsoid and lines going through the center of the ellipsoid and the measured point. Its minimization is called Method 4 in the chapter.
  [Šprdlík and Hurák (2007)]

- *Comparison of several ellipsoid fitting methods mainly in situations when the collected data have only a limited range – simulating the probable situation in in-use accelerometer calibration: that the sensor is positioned only in a limited range of possible inclinations:*
  That was done in chapter 4 on synthetic data. The above mentioned method gave very good results compared to other methods.
  [In preliminary extent and form Šprdlík and Hurák (2007)]

- *Finding that even during a severe hand tremor it is possible to estimate the attitude by the inertial estimation with a certain accuracy:*
  The accuracy was evaluated in chapter 7 in tremor mimicking by healthy humans and accompanied by several recommendations about the estimator construction.

- *Proposal to estimate the center of rotation during hand tremor and finding that it may increase the accuracy of inertial estimation compared to the situation when there is no model of the motion:*
  This was done also in chapter 7 and evaluated in the same data. The estimation method itself was described and shortly validated in chapter 6.1.

- *Experimental determination of how big is the gravitational artifact in the oscillatory tremor acceleration signal when measuring at hands:*
  That was done also in chapter 5 in the same data by comparing the amplitudes get from frequency spectra of different acceleration components in different directions. Attitude estimation was used to get the components.
  [Šprdlík et al. (2009, 2011)]

- *Accurate regression of a visual tremor scoring done by trained clinicians using features extracted from the data captured with inertial measurement units placed on hands:*
  That was done also in chapter 5 and evaluated in data from the same study. The accuracy was at least comparable to the results of other published studies where a visual scoring was regressed by data from motion-related sensors.
  [Šprdlík et al. (2011)]

- *According to my knowledge an original method to find the relative orientation of two attitude measurement systems:*
  The method was proposed in chapter 6.2. It was used in chapter 7 giving reliable estimates of the relative orientations.

8.2 Future research

Future research directions involving the use of the inertial sensors in the assessment of diseases can be many, including the assessment of other motion-related symptoms, improvements of existing methods, or utilization for other diseases. From the more specific fields developed in this thesis, the following topics may be the targets of the future research:

In the field of accelerometer calibration from in-use data, a possible future development may include development and tuning of adaptive procedures using the quasi-static states. The methods shall forget old and incorporate new data and enable estimation of time varying parameters during long measurement trials with patients. Some validation of the calibration accuracy in such trials would be needed.

In the field of tremor assessment using inertial sensors, the attitude estimate and decomposition of the acceleration to the motion and gravitational components may be used to reconstruct the motion trajectory. To have exact data about the motion of the hand or a finger (wherever the sensor is placed), a calibration of the sensor position on the segment will be needed. The acquired trajectories of the displacement or the orientation of the segment may be used to characterize the tremor in bigger detail than only by the amplitude and frequency. An example can be to describe if the tremor is more like flexion-extension or pronation-supination, or if it is characterized by circular motion or back-and-

forth motion. Such observations are used by clinicians to recognize the probable type and the source disease of the tremor. Inclusion of such an information may enhance automatic classification of tremors. An automatic classification was already studied by several teams, e.g. Spyers-Ashby et al. (1999), Ai et al. (2008).

The inertial estimation in tremor may be used also as a part of the measurement component of a feedback loop for active tremor attenuation. Tremor measurement by inertial sensors generally has a big potential in the feedback loops for tremor control. That includes the mentioned active attenuation, e. g. by means of FES (Bó et al. 2011, Zhang et al. 2011), and hypothetically also an automatic dosing of medication or tuning of deep brain stimulation.

Bibliography

L. Ai, J. Wang, and X. Wang. Multi-features fusion diagnosis of tremor based on artificial neural network and D-S evidence theory. *Signal Processing*, 88(12):2927–35, 2008.

W. T. Ang, P. K. Khosla, and C. N. Riviere. Design of all-accelerometer inertial measurement unit for tremor sensing in hand-held microsurgical instrument. In *Proceedings of the 2003 IEEE International Conference on Robotics and Automation*, pages 1781–6, 2003.

L. Bao and S. S. Intille. Activity recognition from user-annotated acceleration data. In *Pervasive Computing 2004*, pages 1–17. Springer, 2004.

P. Batista, C. Silvestre, P. Oliveira, and B. Cardeira. Accelerometer calibration and dynamic bias and gravity estimation: Analysis, design, and experimental evaluation. *IEEE Transactions on Control Systems Technology*, 19(5):1128–1137, 2011.

B. M. Bell. The iterated Kalman smoother as a Gauss-Newton method. *SIAM Journal on Optimization*, 4(3):626–636, 1994.

B. M. Bell, J. V. Burke, and G. Pillonetto. An inequality constrained nonlinear Kalman-Bucy smoother by interior point likelihood maximization. *Automatica*, 45:25–33, 2009.

A. L. Betker, Z. M. Moussavi, and T. Szturm. Center of mass approximation and prediction as a function of body acceleration. *IEEE Transactions on Biomedical Engineering*, 53(4): 686–693, 2006.

B. R. Bloem, K. I. Roon, G. J. Delleman, J. G. van Dijk, and R. A. C. Roos. Prolonged duration of standing up is an early dopa-sensitive abnormality in Parkinson's disease. *Journal of the Neurological Sciences*, 146:41–44, 1997.

A. P. L. Bó, P. Poignet, and C. Geny. Filtering voluntary motion for pathological tremor compensation. In *IEEE/RSJ International Conference on Intelligent RObots and Systems*, pages 55–60, 2009.

A. P. L. Bó, C. Azevedo-Coste, P. Poignet, C. Geny, and C. Fattal. On the use of fes to attenuate tremor by modulating joint impedance. In *50th IEEE Conference on Decision and Control and European Control Conference*, 2011.

S. Bonnet, C. Bassompierre, C. Godin, S. Lesecq, and A. Barraud. Calibration methods for inertial and magnetic sensors. *Sensors and Actuators A*, 156:302–311, 2009.

C. V. Bouten, K. R. Westerterp, R. Verduin, and J. D. Janssen. Assessment of energy expenditure for physical activity using a triaxial accelerometer. *Medicine and Science in Sports and Exercise*, 26(12):1516–23, 1994.

P. R. Burkhard, J. W. Langston, and J. W. Tetrud. Voluntarily simulated tremor in normal subjects. *Clinical Neurophysiology*, 32(2):119–126, 2002.

J. B. J. Bussmann, W. L. J. Martens, and J. H. M. Tulen. Measuring daily behaviour using ambulatory accelerometry: The activity monitor. *Behaviour Research Methods, Instruments, and Computers*, 33(3):349–356, 2001.

G. Calafiore. Approximation of n-dimensional data using spherical and ellipsoidal primitives. *IEEE Transactions on Systems, Man, and Cybernetics – Part A*, 32(2):269–278, 2002.

M. P. Caligiuri and R. M. Tripp. A portable hand-held device for quantifying and standardizing tremor assessment. *Journal of Medical Engineering and Technology*, 28(6):254–262, 2004.

R. Dai, R. B. Stein, B. J. Andrews, K. B. James, and M. Wieler. Application of tilt sensors in functional electrical stimulation. *IEEE Transactions on Rehabilitation Engineering*, 4 (2):63–72, 1996.

J. T. Davis, K. E. Lyons, and R. Pahwa. Freezing of gait after bilateral subthalamic nucleus stimulation for Parkinson's disease. *Clinical Neurology and Neurosurgery*, 108:461–464, 2006.

G. Deuschl, P. Krack, M. Lauk, and J. Timmer. Clinical neurophysiology of tremor. *Journal of Clinical Neurophysiology*, 13(2):110–121, 1996.

G. Deuschl, P. Bain, M. Brin, and Ad hoc scientific committee. Consensus statement of the Movement Disorders Society on tremor. *Movement Disorders*, 13(S3):2–23, 1998.

G. Deuschl, R. Wenzelburger, K. Löffler, J. Raethjen, and H. Stolze. Essential tremor and cerebellar dysfunction: Clinical and kinematic analysis of intention tremor. *Brain*, 123 (8):1568–80, 2000.

R. J. Dunnewold, C. E. Jacobi, and B. J. van Hilten. Quantitative assessment of bradykinesia in patients with Parkinson's disease. *Journal of Neuroscience Methods*, 74:107–112, 1997.

R. J. Dunnewold, J. I. Hoff, H. C. van Pelt, P. Q. Fredrikze, E. A. Wagemans, and B. J. van Hilten. Ambulatory quantitative assessment of body position, bradykinesia, and hypokinesia in Parkinson's disease. *Journal of Clinical Neurophysiology*, 15(3):235–242, 1998.

R. J. Elble. Characteristics of physiologic tremor in young and elderly adults. *Clinical Neurophysiology*, 114(4):624–635, 2003.

R. J. Elble. Gravitational artifact in accelerometric measurements of tremor. *Clinical Neurophysiology*, 116(7):1638–1643, 2005.

R. J. Elble, S. L. Pullman, J. Y Matsumoto, J. Raethjen, G. Deuschl, R. Tintner, and the Tremor Research Group. Tremor amplitude is logarithmically related to 4- and 5-point tremor rating scales. *Brain*, 129(10):2660–66, 2006.

S. Fahn, E. Tolosa, and C. Marín. Clinical rating scale for tremor. In J. Jankovic and E. Tolosa, editors, *Parkinson's disease and movement disorders*. Williams and Wilkins, Baltimore, second edition, 1993.

F. Ferraris, U. Grimaldi, and M. Parvis. Procedure for effortless in-field calibration of three-axis rate gyros and accelerometers. *Sensors and Materials*, 7(5):311–330, 1995.

A. Fitzgibbon, M. Pilu, and R. B. Fisher. Direct least square fitting of ellipses. *IEEE Transactions on Pattern Analysis and Machine Intelligence*, 21(5):476–480, 1999.

F. Foerster and J. Fahrenberg. Motion pattern and posture: Correctly assessed by calibrated accelerometers. *Behavior Research Methods, Instruments, and Computers*, 32(3):450–7, 2000.

F. Foerster and M. Smeja. Joint amplitude and frequency analysis of tremor activity. *Electromyography and clinical neurophysiology*, 39(1):13–19, 1999.

J. D. Frost. Triaxial vector accelerometry: a method for quantifying tremor and ataxia. *IEEE Transactions on Biomedical Engineering*, 25(1):17–27, 1978.

W. Gander, G. H. Golub, and R. Strebel. Least-square fitting of circles and ellipses. *BIT*, 43:558–578, 1994.

D. Gebre-Egziabher, G. H. Elkaim, J. D. Powell, and B. W. Parkinson. Calibration of strapdown magnetometers in magnetic field domain. *Journal of Aerospace Engineering*, 19(2):87–102, 2006.

D. Giansanti and G. Maccioni. Physiological motion monitoring: a wearable device and adaptive algorithm for sit-to-stand timing detection. *Physiological Measurement*, 27:713–723, 2006.

J. P. Giuffrida, D. E. Riley, B.N. Maddux, and D. A. Heldman. Clinically deployable Kinesia technology for automated tremor assessment. *Movement Disorders*, 24(5):723–730, 2009.

A. Godfrey, R. Conway, D. Meagher, and G. ÓLaighin. Direct measurement of human movement by accelerometry. *Medical Engineering and Physics*, 30(10):1364–86, 2008.

N. Grammalidis and M. G. Strintzis. Using 2-D and 3-D ellipsoid fitting for head and body segmentation and head tracking. In *Int'l Conference on Image and Multidimensional Digital Signal Processing*, Alpbach, Austria, 1998.

M. Hallet. Overview of human tremor physiology. *Movement Disorders*, 13(Supplement 3), 1998.

J. H. Han, W. J. Lee, T. B. Ahn, B. S. Jeon, and K. S. Park. Gait analysis for freezing detection in patients with movement disorder using threedimensional acceleration system. In *Proceedings of the 25' Annual lntemational Conference of the IEEE EMBS*, 2003.

J. M. Hausdorff, Y. Balash, and N Giladi. Time series analysis of leg movements during freezing of gait in Parkinson's disease: akinesia, rhyme or reason? *Physica*, A 321: 565–570, 2003.

Y. Higashi, K. Yamakoshi, T. Fujimoto, M. Sekine, and T. Tamura. Quantitative evaluation of movement using the timed up-and-go test. *IEEE Engineering in Medicine and Biology Magazine*, 27(4):38–46, 2008.

J. I. Hoff, E. A. Wagemans, and J. J. van Hilten. Ambulatory objective assessment of tremor in Parkinson's disease. *Clinical Neuropharmacology*, 24(5):280–283, 2001.

J. I. Hoff, V. van der Meer, and J. J. van Hilten. Accuracy of objective ambulatory accelerometry in detecting motor complications in patients with Parkinson disease. *Clinical Neuropharmacology*, 27(2):53–57, 2004.

R. A. Hyde, L. P. Ketteringham, S. A. Neild, and R. J. S. Jones. Estimation of upper-limb orientation based on accelerometer and gyroscope measurements. *IEEE Transactions on Biomedical Engineering*, 55(2):746–754, 2008.

InvenSense. ITG-3050 product specification, 2011. Revision 1.3.

W. G. Janssen, J. B. Bussmann, H. L. Horemans, and H. J. Stam. Validity of accelerometry in assessing the duration of the sit-to-stand movement. *Medical and Biological Engineering and Computing*, 46(9):879–887, 2008.

L. A. Johnston and V. Krishnamurthy. Derivation of a sawtooth iterated extended Kalman smoother via the AECM algorithm. *IEEE Transactions on Signal Processing*, 49(9): 1899–1909, 2001.

S. J. Julier and J. K. Uhlmann. A new extension of the Kalman filter to nonlinear systems. In *Proc. Int. Symp. Aerospace/Defense Sensing, Simul. and Controls*, 1997.

J. J. Kavanagh and H. B. Menz. Accelerometry: A technique for quantifying movement patterns during walking. *Gait and Posture*, 28(1):1–15, 2008.

N. L. W Keijsers, M. W. I. M. Horstink, and S. C. A. M. Gielen. Online monitoring of dyskinesia in patients with Parkinson's disease. *IEEE Medicine and Biology Magazine*, 22(3):96–103, 2003.

N. L. W Keijsers, M. W. I. M. Horstink, C. A. M. Stan, and S. C. A. M. Gielen. Ambulatory motor assessment in Parkinson's disease. *Movement Disorders*, 21(1):34–44, 2006.

Kionix. KGY13 series gyroscopes, 2011. Revision 1.

A. M. Kuncel, S. E. Cooper, B. R. Wolgamuth, and W. M. Grill. Amplitude- and frequency-dependent changes in neuronal regularity parallel changes in tremor with thalamic deep brain stimulation. *IEEE Transactions on Neural systems and rehabilitation engineering*, 15(2), 2007.

W. T. Latt, U. X. Tan, C. Y. Shee, C. N. Riviere, and W. T. Ang. Compact sensing design of a handheld active tremor compensation instrument. *IEEE Sensors Journal*, 9(12): 1864–71, 2009.

J. C. Lötters, J. Schipper, P. H. Veltink, W. Olthuis, and P. Bergveld. Procedure for in-use calibration of triaxial accelerometers in medical applications. *Sensors and Actuators*, 68: 221–8, 1998.

E. D. Louis and S. L. Pullman. Comparison of clinical vs. electrophysiological methods of diagnosing of essential tremor. *Movement Disorders*, 16(4):668–673, 2001.

H. J. Luinge and P. H. Veltink. Measuring orientation of human body segments using miniature gyroscopes and accelerometers. *Medical and Biological Engineering and Computing*, 43:273–282, 2005.

G. M. Lyons, T. Sinkjær, J. H. Burridge, and D. J. Wilcox. A review of portable FES-based neural orthoses for the correction of drop foot. *IEEE Transactions on Neural systems and rehabilitation engineering*, 10(4):260–279, 2002.

G. M. Lyons, K. M. Culhane, D. Hilton, P. A. Grace, and D. Lyons. A description of an accelerometer-based mobility monitoring technique. *Medical Engineering and Physics*, 27: 497–504, 2005.

R. Mahony, T. Hamel, and J.-M. Pflimlin. Nonlinear complementary filters on the special orthogonal group. *IEEE Transactions on Automatic Control*, 53(5):1203–1218, 2008.

F. L. Markley. Attitude determination using vector observations and the singular value decomposition. *Journal of the Astronautical Sciences*, 36(3):245–258, 1988.

F. L. Markley. Fast quaternion attitude estimation from two vector measurements. *Journal of Guidance Control and Dynamics*, 25(2):411–414, 2002.

I. Markovsky and B. De Moor. Linear dynamic filtering with noisy input and output. *Automatica*, 41(1):167–171, 2005.

I. Markovsky, A. Kukush, and S. Van Huffel. Consistent least squares fitting of ellipsoids. *Numerische Mathematik*, 98(1):177–194, 2004.

I. Markovsky, J. C. Willems, S. Van Huffel, and B. De Moor. *Exact and Approximate Modelling of Linear Systems: A Behavioral Approach*. SIAM, 2006.

M. Marschollek, G. Nemitz, M. Gietzelt, K. H. Wolf, H. Meyer Zu Schwabedissen, and R. Haux. Predicting in-patient falls in a geriatric clinic: a clinical study combining assessment data and simple sensory gait measurements. *Zeitschrift für Gerontologie und Geriatrie*, 42(4):317–321, 2009.

M. J. Mathie, A. C. F. Coster, N. H. Lovell, and B. G. Celler. Detection of daily physical activities using a triaxial accelerometer. *Medical and Biological Engineering and Computing*, 41:296–301, 2003.

J. Y. Matsumoto, D. W. Dodick, L. N. Stevens, R. C. Newman, P. E. Caskey, and W. Fjerstad. Three-dimensional measurement of essential tremor. *Movement Disorders*, 14(2): 288–294, 1999.

R. E. Mayagoitia, J. C. Lötters, P. H. Veltink, and H. Hermens. Standing balance evaluation using a triaxial accelerometer. *Gait and Posture*, 16(1):55–59, 2002.

M. Moakher. Means and averaging in the group of rotations. *SIAM Journal on Matrix Analysis and Applications*, 24:1–16, 2002.

R. Moe-Nilssen. A new method for evaluating motor control in gait under real-life environmental conditions. part 1: The instrument. *Clinical Biomechanics*, 13(4–5):320–7, 1998.

R. Moe-Nilssen and J. L. Helbostad. Trunk accelerometry as a measure of balance control during quiet standing. *Gait and Posture*, 16(1):60–68, 2002.

R. Moe-Nilssen and J. L. Helbostad. Estimation of gait cycle characteristics by trunk accelerometry. *Journal of Biomechanics*, 37(1):121–6, 2004.

S. T. Moore, H. G. MacDougall, J. M. Gracies, H. S. Cohen, and W. G. Ondo. Long-term monitoring of gait in Parkinson's disease. *Gait and Posture*, 26:200–207, 2007.

S. T. Moore, H. G. MacDougall, and W. G. Ondo. Ambulatory monitoring of freezing of gait in Parkinson's disease. *Journal of Neuroscience Methods*, 167:340–348, 2008.

S Morrison, J. Kavanagh, S. J. Obst, J. Irwin, and L. J. Haseler. The effects of unilateral muscle fatigue on bilateral physiological tremor. *Experimental Brain Research*, 167(4): 609–621, 2005.

G. Mostile, J. P. Giuffrida, O. R. Adam, A. Davidson, and J. Jankovic. Correlation between Kinesia system assessments and clinical tremor scores in patients with essential tremor. *Movement Disorders*, 25(12):1938–43, 2010.

K. A. Myers and B. D. Tapley. Adaptive sequential estimation with unknown noise statistics. *IEEE Transactions on Automatic Control*, 21(4):520–523, 1976.

B. Najafi, K. Aminian, F. Loew, Y. Blanc, and P. A. Robert. Measurement of stand–sit and sit–stand transitions using a miniature gyroscope and its application in fall risk evaluation in the elderly. *IEEE Transactions on Biomedical Engineering*, 49(8):843–851, 2002.

B. Najafi, K. Aminian, A. Paraschiv-Ionescu, F. Loew, C. J. Büla, and P. Robert. Ambulatory system for human motion analysis using a kinematic sensor: Monitoring of daily physical activity in the elderly. *IEEE Transactions on Biomedical Engineering*, 50(6): 711–723, 2003.

N.-O. Negård, R. Kauert, S. Andres, T. Schauer, and J. Raisch. Gait phase detection and step length estimation of gait by means of inertial sensors. In *The 3rd European Medical and Biological Engineering Conference (EMBEC'05)*, Prague, November 2005.

NOAA National Geophysical Data Center. Magnetic field calculators, 2012. `http://www.ngdc.noaa.gov/geomag-web`.

B. J. Odelson, A. Lutz, and J. B. Rawlings. The autocovariance least-squares method for estimating covariances: Application to model-based control of chemical reactors. *IEEE Transactions on Control Systems Technology*, 14(3):532–540, 2006.

OGI School of Science & Engineering. ReBEL: Recursive bayesian estimation library for Matlab. `http://choosh.csee.ogi.edu/rebel`, 2008.

M. O'Sullivan, C. Blake, C. Cunningham, G. Boyle, and C. Finucane. Correlation of accelerometry with clinical balance tests in older fallers and non-fallers. *Age and Ageing*, 38(3):308–313, 2009.

I. P. I. Pappas, T. Keller, S. Mangold, M. R. Popovic, V. Dietz, and M. Morari. A reliable gyroscope-based gait-phase detection sensor embedded in a shoe insole. *IEEE Sensors Journal*, 4(2):268–274, 2004.

D. Podsiadlo and S. Richardson. The timed "Up & Go": a test of basic functional mobility for frail elderly persons. *Journal of the American Geriatrics Society*, 39(2):142–8, 1991.

T Prill and J. Fahrenberg. Simultaneous assessment of posture and limb movements (e.g., periodic leg movements) with calibrated multiple accelerometry. *Physiological Measurement*, 27:N47–N53, 2006.

S. L. Pullman, B. Elibol, and S. Fahn. Modulation of parkinsonian tremor by radial nerve palsy. *Neurology*, 44(10):1861–4, 1994.

T. Pylvänäinen. Automatic and adaptive calibration of 3D field sensors. *Applied Mathematical Modelling*, 32(4):575–587, 2008.

E. Rocon de Lima, A. O. Andrade, J. L. Pons, P. Kyberg, and S. J. Nasuto. Empirical mode decomposition: a novel technique for the study of tremor time series. *Medical and biological engineering and computing*, 44(7):569–582, 2006.

D. Roetenberg, H. J. Luinge, C. T. M. Baten, and P. H. Veltink. Compensation of magnetic field disturbances improves inertial and magnetic sensing of human body orientation. *IEEE Transactions on Neural Systems and Rehabilitation Engineering*, 13(3), 2005.

J. Rueterbories, E. G. Spaich, B. Larsen, and O. K. Andersen. Methods for gait event detection and analysis in ambulatory systems. *Medical Engineering and Physics*, 32(6): 545–552, 2010.

A. Salarian. *Ambulatory monitoring of motor functions in patients with Parkinson's disease using kinematic sensors*. PhD thesis, EPFL, Laussane, 2006.

A. Salarian, H. Russmann, F. J. G. Vingerhoets, C. Dehollain, Y. Blanc, P. R. Burkhard, and K. Aminian. Gait assessment in Parkinson's disease: Toward an ambulatory system for long-term monitoring. *IEEE Transactions on Biomedical Engineering*, 51(8), 2004.

A. Salarian, H. Russmann, F. J. G. Vingerhoets, P. R. Burkhard, and K. Aminian. Ambulatory monitoring of physical activities in patients with Parkinson's disease. *IEEE Transactions on Biomedical Engineering*, 54(12):2296–9, 2007a.

A. Salarian, H. Russmann, C. Wider, P. R. Burkhard, F. J. G. Vingerhoets, and K. Aminian. Quantification of tremor and bradykinesia in Parkinson's disease using a novel ambulatory monitoring system. *IEEE Transactions on Biomedical Engineering*, 54(2):313–322, 2007b.

A. Salarian, F. B. Horak, C. Zampieri, P. Carlson-Kuhta, J. G. Nutt, and K. Aminian. iTUG, a sensitive and reliable measure of mobility. *IEEE Transactions on Neural Systems and Rehabilitation Engineering*, 18(3):303–310, 2010.

H. W. Sander, J. C. Masdeu, G. Tavoulareas, A. Walters, T. Zimmerman, and S. Chokroverty. Orthostatic tremor: An electrophysiological analysis. *Movement Disorders*, 13(4):735–738, 1998.

A. Saxena, G. Gupta, V. Gerasimov, and S. Ourselin. In use parameter estimation of inertial sensors by detecting multilevel quasi-static states. In *Knowledge-Based Intelligent Information And Engineering Systems: 9th International Conference, KES*. Springer-Verlag, 2005.

M. Šimandl and J. Duník. Derivative-free estimation methods: New results and performance analysis. *Automatica*, 45(7):1749–1757, 2009.

P. S. Slack and X. Ma. Tremor amplitude determination for use in clinical applications. *Measurement Science and Technology*, 18(11):3471–8, 2007.

O. Šprdlík and Z. Hurák. Ambulatory assessment in Parkinson's disease: Use of inertial sensors and identification and filtering techniques. In *Process Control*, Štrbské Pleso, Slovakia, 2007.

O. Šprdlík, Z. Hurák, M. Hoskovcová, and E. Růžička. Tremor analysis by decomposition of acceleration into gravity and inertial acceleration using inertial measurement unit. In *Proceedings of the 9th International Conference on Information Technology and Applications in Biomedicine*, Larnaca, Cyprus, 2009.

O. Šprdlík, Z. Hurák, M. Hoskovcová, O. Ulmanová, and E. Růžička. Tremor analysis by decomposition of acceleration into gravity and inertial acceleration using inertial measurement unit. *Biomedical Signal Processing and Control*, 6(3), 2011.

J. M. Spyers-Ashby, P. G. Bain, and S. J. Roberts. A comparison of fast Fourier transform (FFT) and autoregressive (AR) spectral estimation techniques for the analysis of tremor data. *Journal of Neuroscience Methods*, 83(1):35–43, 1998.

J. M. Spyers-Ashby, M. J. Stokes, P. G. Bain, and S. J. Roberts. Classification of normal and pathological tremors using a multidimensional electromagnetic system. *Medical Engineering and Physics*, 21(10):713–723, 1999.

B. Stevens and F. Lewis. *Aircraft Control and Simulation*. John Wiley & Sons, second edition, 2003.

J. Timmer. Modelling noisy time series: Physiological tremor. *International Journal of Bifurcation and Chaos*, 8:1505–16, 1998.

J. Timmer, M. Lauk, and G. Deuschl. Quantitative analysis of tremor time series. *Electroencephalography and Clinical Neurophysiology*, 101:461–468, 1996.

S. Umeyama. Least-squares estimation of transformation parameters between two point patterns. *IEEE Transactions on Pattern Analysis and Machine Intelligence*, 13:376–380, 1991.

R. van der Merwe and E. A. Wan. Sigma-point Kalman filters for integrated navigation. In *Proceedings of the 60th Annual Meeting of the Institute of Navigation (ION)*, pages 641–654, 2004.

E. J. W. van Someren, W. A. van Gool, B. F. M. Vonk, M. Mirmiran, J. D. Speelman, D. A. Bosch, and D. F. Swaab. Ambulatory monitoring of tremor and other movements before and after thalamotomy: a new quantitative technique. *Journal of the Neurological Sciences*, 117:16–23, 1993.

E. J. W. van Someren, R. H. C. Lazeron, B. F. M. Vonk, M. Mirmiran, and D. F. Swaab. Gravitational artefact in frequency spectra of movement acceleration: implications for actigraphy in young and elderly subject. *Journal of Neuroscience Methods*, 65:55–62, 1996.

E. J. W. van Someren, B. F. M. Vonk, W. A. Thijssen, J. D. Speelman, P. R. Schuurman, M. Mirmiran, and D. F. Swaab. A new actigraph for long-term registration of the duration and intensity of tremor and movement. *IEEE Transactions on Biomedical Engineering*, 45(3):386–395, 1998.

E. J. W van Someren, M. D. Pticek, J. D. Speelman, P. R. Schuurman, R. Esselink, and D. F. Swaab. New actigraph for long-term tremor recording. *Movement Disorders*, 21(8): 1136–43, 2006.

P. H. Veltink, E. G. O. Engberink, B. J. van Hilten, R. Dunnewold, and C. Jacobi. Towards a new method for kinematic quantification of bradykinesia in patients with Parkinson's disease using triaxial accelerometry. In *Proceedings of 17th International Conference of the Engineering in Medicine and Biology Society*, volume 2, pages 1303–04. IEEE EMBS, 1995.

P. H. Veltink, H. B. J. Bussmann, W. de Vries, W. L. J. Martens, and R. C. van Lummel. Detection of static and dynamic activities using uniaxial accelerometers. *IEEE Transactions on Biomedical Engineering*, 43:375–385, 1996.

VTI Technologies. CMR3000-d0x product family specification, 2011. Version A.03.

G. Wahba. A least squares estimate of satellite attitude. *SIAM Review*, 8(3):384–386, 1966.

E. A. Wan and R. van der Merwe. The unscented Kalman filter. In S. Haykin, editor, *Kalman Filtering and Neural Networks*, pages 221–280. John Wiley & Sons, 2001.

A. Weiss, T. Herman, M. Plotnik, M. Brozgol, I. Maidan, N. Giladi, T. Gurevich, and J. M. Hausdorff. Can an accelerometer enhance the utility of the Timed Up & Go test when evaluating patients with parkinson's disease? *Medical Engineering and Physics*, 32(2): 119–125, 2010.

S. L. Whitney, J. L. Roche, G. F. Marchetti, C.-C. Lin, Steed D. P., G. R. Furman, M. C. Musolino, and M. S. Redfern. A comparison of accelerometry and center of pressure measures during computerized dynamic posturography: A measure of balance. *Gait and Posture*, 33(4):594–9, 2011.

A. T. M. Willemsen, F. Bloemhof, and H. B. K. Boom. Automatic stance-swing phase detection from accelerometer data for peroneal nerve stimulation. *IEEE Transactions on Biomedical Engineering*, 37(12):1201–8, 1990.

R. Williamson and B. J. Andrews. Gait event detection for FES using accelerometers and supervised machine learning. *IEEE Transactions on Rehabilitation Engineering*, 8(3): 312–319, 2000.

Xsens Technologies. MTi and MTx user manual and technical documentation, 2005. Revision D.

Xsens Technologies. MTi and MTx user manual and technical documentation, 2010. Revision O.

C.-C. Yang and Y.-L Hsu. A review of accelerometry-based wearable motion detectors for physical activity monitoring. *Sensors*, 10(8):7772–88, 2010.

C. Zampieri, A. Salarian, P. Carlson-Kuhta, K. Aminian, J. G. Nutt, and F. B. Horak. The instrumented timed up and go test: potential outcome measure for disease modifying therapies in Parkinson's disease. *Journal of Neurology, Neurosurgery, and Psychiatry*, 81 (2):171–6, 2010.

D. Zhang, P. Poignet, F. Widjaja, and W. T. Ang. Neural oscillator based control for pathological tremor suppression via functional electrical stimulation. *Control Engineering Practice*, 19(1):74–88, 2011.

R. Zhu and Z. Zhou. A real-time articulated human motion tracking using tri-axis inertial/magnetic sensors package. *IEEE Transactions on Neural Systems and Rehabilitation Engineering*, 12(2):295–302, 2004.

W. Zijlstra and A. L. Hof. Assessment of spatio-temporal gait parameters from trunk accelerations during human walking. *Gait and Posture*, 18(2):1–10, 2003.

D. G. M. Zwartjes, T. Heida, J. P. P. van Vugt, J. A. G. Geelen, and P. H. Veltink. Ambulatory monitoring of activities and motor symptoms in Parkinson's disease. *IEEE Transactions on Biomedical Engineering*, 57(11):2778–86, 2010.

Appendix A

Estimation of Angular Rate from Orientation Data

This appendix describes how an estimate of angular rate as measured by a rate gyroscope can be get from orientation data provided by Polhemus Isotrak device. The quaternion representation of orientation of Isotrak receiver in Isotrak reference frame is used. If Euler angles are acquired from Isotrak, they are first transformed to quaternions.

The quaternion update equation is

$$\dot{q}(t) = \frac{1}{2} \begin{bmatrix} -q_1(t) & -q_2(t) & -q_3(t) \\ q_0(t) & -q_3(t) & q_2(t) \\ q_3(t) & q_0(t) & -q_1(t) \\ -q_2(t) & q_1(t) & q_0(t) \end{bmatrix} \omega_{\mathrm{Iso}}(t) \ , \tag{A.1}$$

where q is the quaternion of Isotrak receiver orientation and ω_{Iso} its angular rate in the local coordinate frame. At each sample the angular rate was estimated by solving (A.1) for ω_{Iso}. A numerical estimate (by the 5-point stencil method) of quaternion's time derivative was used as $\dot{q}$. The possibility to represent one orientation by two different unit quaternions was taken into account in the computation.

Then, to get an estimate of angular rate in IMU coordinates, the obtained values were transformed by (6.6).

Appendix B

Categorization of Publications with Tremor Quantification using Motion Measurement

This text expands the introductions to the tremor quantification based on inertial sensors given in the main text of the thesis. The expansion is especially in the number of papers referenced and partially also in technical details. Besides inertial sensors, the text refers also to works using other types of sensors of the quantities related to motion (e. g. displacement). The hand or arm tremor is of the interest. The provided references are many but still far from being complete, because the field of the intrumented tremor assessment is large, studied already for tens of years and the methods are still in usage and in progress. The layout of the appendix is such that several technical points of the methods are selected and then one-by-one they are briefly described and references to the published works are divided based on how they approached the specific point. The used points are

- sensor placement,
- frequency extraction,
- amplitude extraction,
- number of processed sensor axes,
- (for the non-inertial sensors for motion measurement): types of the sensors,

and several approaches to quantify the intention tremor are also listed.

One field was omitted because it is already a little far from the use of the inertial sensors: The tremor assessment in writing and drawing using digitizing tablets. Only one paper of our colleagues [Ulm07] was mentioned where appropriate, but the others from this quite large field were left out.

Some of the referenced papers are focused directly on the tremor quantification methods, while most of them are focused on the tremor itself, related disorders, or their treatment, and the tremor quantification methods are just part of the methods used in them.

Several works are referenced with asterisk (*) symbol. In such a case, some other publications usually by the same authors could be also referenced. See section B.8 for the inter-connected publications.

The appendix references to more works than the main text. Because most of the references were not needed for the thesis itself, a separate list of references is used for this appendix. It is located in section B.9.

B.1 Sensor placement

Most usual positions of motion sensors for hand or arm tremor assessment are

- hand dorsum [Mor75, Pul94*, Tim96, Foe99, Deu00*, Bur02, Sap03, Zeu03, Rae04, Stu05, Bir07, Kun07, Sla07, Ker08, Gal10, Spr11*],
- a finger, usually the index finger, [Ran73 (with fingers kept together), Elb94 (a finger strengthened by a splint), Hal95, Hal99, Cal04, Hon08, Ker08, Mor08, Giu09*].

Other used places are

- fingers in a fixed position relative to the palm [Elb96*],
- palm [Tim00],
- wrist as in [Som98, Som06, Sal07] and some other works dealing with ambulatory monitoring of tremor in daily life,
- a handled object [Ang03, Pel04 (beam end-point position of a laser pointer was measured), Her06*],
- more places at one extremity [Roc06, Gal10].

B.2 Preprocessing remarks

The measured data are often subjects of various ways of preprocessing. One typical example is high-pass filtering for removing the DC component caused mainly by the gravitational component. Such step is usually used in case of time-domain processing for detection and quantification of tremor. The cut-off frequency shall be below the range of the expected tremor frequencies. An alternative may be the empirical mode decomposition used by [Sla07]. Sometimes, also low-pass filtering is used for reduction of the measurement noise.

The measured or filtered data may be used directly to detect tremor and quantify its amplitude and frequency by the amplitude or power and frequency of the signal. Sometimes, for all the tasks or for some of them, a time derivative or integral of the signal is used. For example, double time integral of measured acceleration is a quantity with units of displacement. But it is not the actual displacement – it would need a more complicated calculations to be estimated. Similar holds for time integral of the angular rate measured by a gyroscope and angles of orientation.

For accelerometer, such an estimate of displacement cannot correctly remove the gravitational component of the measurement if the motion is (at least in part) rotational. Because all the joints in human body are more or less rotational, almost never is the motion purely translational. That holds also for tremor. This deficiency was omitted by many

authors [e. g. Pul94, Zeu03, Stu05, Sla07]. Though, they get sort of measure of the motion range which may under certain conditions correspond well to the actual spatial amplitude. This estimate may be quite accurate if the tremor does not cause large changes of the gravitational component in the processed sensor axes. Such a situation occurs if only one sensor axis is processed and it is approximately vertical. Of course, in this way only the amplitude in that direction is calculated. A typical example is the posture with arms extended forward [Ker08] or the forearms laid on an armrest and hands extended forward [Ran73, Zeu03] with palms facing down and sensors placed on fingers or hand dorsa and only the axes perpendicular to the palms are processed. Eventually, the motion may me moreover restricted to flexion and extension of the wrists. Usually, there are not given reasons for these choices in the papers where they are used. An analysis of the gravitational component and reasons for such choices are given in [Elb05].

On the other hand, with the use of sensors of displacement or velocity, it may be sometimes useful to calculate numerically time derivatives of the measured signals. See the next section.

B.3 Frequency

For frequency estimation, a frequency data processing is usually used, typically Power Spectral Density (PSD) estimate using Fast Fourier Transform (FFT). The major question is what signal to use as the input of the spectral analysis. In known studies using accelerometers or other sensors of movement, following signals are used:

- measured angular rate (ω) [Bur02, Sal07, Giu09*, Gal10, Spr11],
- angle [Spy99],
- measured acceleration (a) [Ran73, Mor75, Gre90, Gan92, Elb94*, Pul94*, Hal95, Deu96, Tim98, Foe99, Hal99, Deu00*, Mor01*, Oka01, Sap03, Zeu03, Stu05, Bir07, Kun07, Hon08, Ker08, Giu09*, Spr11*],

  or first time derivative of velocity, or second derivative of measured displacement [Mat99, Her06*],
- velocity, time-integrated acceleration, or first derivative of measured displacement [Leg10],
- position [Pel04], time-integrated velocity, or double integrated acceleration.
- alternatively to motion sensors, image intensity in a video recording [Uhr10*].

A special case is [OSu01], where the spectrum of positions was estimated, but *because spectra tend to have a "pink" noise component with a sloping baseline*, a derivative of the PSD was used to identify sharp peaks instead of searching for the highest peak.

The position or the time-integrated signals are less suitable for the frequency extraction because in them, the low frequency component is amplified and may embarrass the location of the spectrum peak corresponding to the tremor, especially if the position of none of the near joints is fixed and therefore there are more non-cyclical slow movements present. Probably because of that, the velocity or acceleration computed by numerical time derivative is often used when the motion is measured by a sensor of position [Mat99, Her06*, Leg10].

Frequency is determined as

- the position of the highest spectral peak (in most of the studies), or
- the centre of gravity of the spectrum or of its part surrounding the highest point [Elb94*] – the centre of gravity was found to be less inter-trially variable than just the highest point, or
- the position of the highest of the Gauss curves fitted to the spectrum [Bar09], or
- (as an alternative to PSD) using the approximation of the spectrum by an autoregressive (AR), moving average (MA) or ARMA model of a low order identified from the data and by subsequent analysis of the found model [using inertial sensors: Ran73, Tim98,98b,00, Oka01, Zha05, Sal07; using other sensors: Cap97, Spy99], or
- by identification of linear stochastic state-space model considering the measurement noise in contrary to ordinary AR model [Gan92, Tim98b].

A comparison of several methods for PSD estimation for tremor quantification and an adaptive parametrization of a PSD estimation method was given by [Tim96]. A kind of comparison of of FFT-based PSD estimation and by the approximation by an AR model was given by [Spy98].

The PSD estimation is commonly used also for preprocessed data of Electromyogram (EMG) [e. g. Elb00, Lau01]. Tremor frequency estimated from EMG is less sensitive to mechanical properties of the body part and to additional masses added to the mass of the body part than the frequency estimated from PSD of a signal coming from motion, see e. g. [Elb00].

As an alternative to the tremor frequency estimation from spectrum or its model, a time-domain processing is also possible. Several algorithms based on zero crossing detection were published [Som98, Cal04, Som06]. They are useful especially in case of long-term actigraphy thanks to a lower computational demand compared to PSD.

B.4 Amplitude

To get a measure of the tremor amplitude, the following approaches are usually used:

- Take the power or its square root in a neighborhood of the found frequency. The neighborhood may be fixed, as in [Spr11, partially also Bar09], or of fixed size but shifted such that the spectral power in it is maximum [Her06* with twice time-differentiated displacement], or in such extend that the spectral density in it is greater than half the spectral density at the highest point [Tim96].
- Often, the spectral power in all the assumed range of possible tremor frequencies is used [Deu96, Deu00, Rae04, Kun07, Uhr11].
- Sometimes, the power in a frequency range is not used but only the value of the highest point in the spectrum [Ker08, Giu09*, and some older works], but that may lead to a big underestimation of the tremor amplitude, especially if the spectral peak is broad [Tim96].
- Another approach to extract the amplitude from spectrum is the area under the highest of the Gauss curves fitted to the spectrum [Bar09].

- An alternative to PSD-based methods is to use time-domain processing for amplitude extraction instead of the frequency domain. Usually, the signal is filtered by a band-pass filter and then its root mean square (RMS) is used or its local minima and maxima are detected and their differences are used.
  - [Pul94*, Sal07] used a time-domain processing for amplitude extraction although the frequency was determined in the frequency domain.
  - In some works, e. g. [Mor75, Fro78, Sla07] there was not a spectrum used at all, the amplitude was determined as RMS of the signals or similarly.
  - In [Mor01*, Giu09*], such amplitude was determined besides the amplitude from the spectral peak.

For the amplitude extraction, the same signal or spectrum may be used as for the frequency extraction, but it may be helpful to use a different one. Typical motivation is that for the frequency extraction the acceleration and velocity signals are usually more useful, see the previous section, but the spatial amplitude is sometimes required. [Pul94*] used time processing of twice integrated accelerometer signal to get a rough estimate of the spatial amplitude. Estimate of the spectrum of a time-integrated signal may be get easily without the numerical integration of the signal: by dividing the points in spectrum by $(2\pi f_k)^2$ where f_k are the frequencies of points k in spectrum [Tim96], used e.g. in [Uhr11]. Another simple but sometimes less accurate way how to estimate the amplitude of a time-integrated (quasi-)periodic signal is to calculate first the amplitude of the original signal and then divide it by $2\pi f_d$ where f_d is the dominant frequency (or by the second power of the number if the power of the signal is used instead of amplitude). Similar calculation is used in [Elb03, Zeu03, Stu05]. This calculation is exact for purely sinusoidal signals, otherwise it is only an estimate.

B.5 Number of processed sensor axes

The works diverse a lot in the matter of how many sensor axes were used and if more than one was used, how the measurements from the axes were aggregated. In the literature, following variants were found:

- Usage of just one single-axis sensor or one axis of a multi-axis sensor,
  - predetermined axis, usually vertical (approximately) – [Ran73, Mor75, Hal95, Tim96*,98b, Foe99, Hal99, Deu00*, Elb00*, Mor01*, Oka01, Bur02, Zeu03, Stu05, Ker08, Mor08],
  - data-based selection of one axis of a multi-axis sensor – that one which gave the highest signal power or the highest measure of tremor amplitude [Pul94*, Her06*].
- Calculation of a one-dimensional signal from the more signals of a multi-axis sensor and then working only with this derived 1D signal:
  - Calculation of the size of the 3D vector of acceleration [Bir07, Kun07]. From it is then subtracted the size of the gravitational acceleration or the low-frequency component. Alternatively, calculation of the size of the 3D vector of the signal

given by a high-frequency filtration of the measured signals [Fro78]. These methods cause a high sensitivity of the amplitude estimation to the direction of the movement relative to the direction of the Gravity.

  - Blind source separation – estimation of the time course of an unknown source [Vin09].

- First processing the separate signals (sensor axes) and then aggregating the outputs of the processing or preprocessing:

  - Summing the spectra of the single signals and then detection and quantification of peaks in the composite spectrum [Spr11*, for spiral drawing similar approach used in Ulm07].
  - Amplitude and frequency extraction from the single axes separately and then using one of them or sometimes their (weighted) mean as the frequency of tremor and/or using an aggregation of the amplitudes extracted from the single axes as the tremor amplitude [Elb94,96, Mat99, Sal07]. If the common frequency is determined as a mean of the particular frequencies (in part [Elb96]), problems may potentially occur if in the different axes, the highest peaks are located at very different frequencies – then the mean of the frequencies is used which lies somewhere between the peaks, although using one of them would be more meaningful.

- Processing all axes separately and not aggregating them directly, but using them as multiple inputs of a following analysis, e. g. regression of a visual assessment [Giu09*].

Many studies deal also with quantitative analysis of the coherence of different signals using cross-spectral analysis, entropy, etc. That may be a study of different axes of one sensor, sensors from different body parts (e. g. left and right hand), or sensors of different quantities (e. g. accelerometer and EMG or posturograph) [Tim98,00, Hal99, Mor01,05,08, Hon08, Ker08]

B.6 Instrumented assessment of intention tremor

Intention tremor was measured by [Mor75, Lou98,01, Deu00*, Wend00, Bre02, Bir07, Giu09*] using several repetitions of a task of pointing to a target or catching an item. Usually, the nose-finger-nose motion or nose-fixed target-nose motion were used, sometimes catching of small items or simulation of drinking from a cup. Another possible tasks for the subject are static aiming at a static target [Mor01, Pel04, Leg10] and tracking of a moving target [Leg10].

If we understand well the not very detailed descriptions of data processing, [Lou98,01, Wend00, Giu09, Bre02, Bir07] processed at once all the measured data captured during whole session including several repetitions of the task.

[Mor75] used a button to capture the time when the subject reached the target. Only last 4 seconds before each reaching of the target were processed. The subjects were asked and trained to do the task in such a manner, that the duration of the movement from the base position to the target was about 4 seconds.

[Deu00*] assessed "reach-to-grasp" simply by using RMS of deviation of position from the mean curve. No PSD or anything similar was used. From these works, only in [Wenz00] the frequency was estimated. It was done by a time-domain processing. The

motion was measured by a 3D position measurement system, not by inertial sensors. Accelerometers were used only for assessment of postural tremor. The final phase of movement towards the target, where the intention tremor was assumed and assessed, was defined using relative position of the index finger and thumb which were used for grasping the target object (cylinder of diameter 1 cm).

In [Leg10], kinetic tremor was assessed via tracking of virtual target by a finger. Its position and the position of the target were shown at a screen. Healthy people were assessed with and without hypoxia. Median of PSD above 2 or 3 Hz and the powers in different frequency bands were studied. The median frequency, power in band 6-12 Hz and the ratio of the power in band 6-12 Hz to the power in band 3-20 Hz was higher at hypoxia.

In [Mor01, Pel04], tremor was assessed in healthy persons aiming to a target by a laser beam.

B.7 Other sensors for tremor measurement based on motion

- Laser sensor of velocity (1D) [Nor99, Tit01]
- Laser sensor of displacement
  - 1D [Nor99, Leg10],
  - 2D [Her06*].
- Laser beam end-point tracking (2D) [Pel04]
- Mechanical sensors of position using goniometers (3D) [Mat99]
- Data glove (angles of hand joints) [Vin09]
- Magnetic sensors of displacement and rotation (3D) [Spy99, Raj00, OSu01, Her07]
- Camera systems (3D) [Cap97 (only simulation of tremor by a mechanical device), Deu00*, Pel04]
- Image intensity in ordinary video recording (only for frequency extraction) [Uhr10*]
- Digitizing tablets for assessment of tremor in drawing and writing – this field was not in the main focus of this text, see e. g. [Elb90] for a pioneering work and [Elb96, Ulm07] for other examples.

B.8 Connections of publications

This paragraph gives a simple list of works and publications which are directly connected or use same methods to measure and quantify the tremor. Usually they have same coauthors. Where the publications listed below with asterisk (*) symbol are cited above also with the same symbol, the connected works may be also mentioned in the same context.

The same basic processing of accelerometer data as in [Pul94] was used for example also in [Tro94, Lou98, Lou00, Wend00, Lou01, Bre02, Coh03]:

$$[\text{Pul94*}] = [\text{Pul94, Tro94, Lou98, Lou00, Wend00, Lou01, Bre02, Coh03}]$$

Partially in same way as in [Elb94], accelerometers were used in [Elb96] and same as there in [Elb00], except the number of used sensor axes. The processing in [Elb03] was almost the same as in [Elb00]:

$$\begin{aligned} [\text{Elb00*}] &= [\text{Elb00,03}] \\ [\text{Elb96*}] &= [\text{Elb96,00,03}] \\ [\text{Elb94*}] &= [\text{Elb94,96,00,03}] \end{aligned}$$

Similar processing as in [Elb94] was used also in [Tim96].

The analyses described in [Tim96] and [Tim98] were used as base for software [Lau99], which was used for accelerometers and/or EMG in [Deu00, Wenz00, Lau01, Rae04].

[Tim98b] utilized [Gan92].

[Tim00] utilized [Tim96, Tim98, Tim98b].

In a big part the same processing as in [Mor01] was used also in [Mor05]:

$$[\text{Mor01*}] = [\text{Mor01,05}]$$

[Wenz00, Her07] used the same measurement and quantification of intention tremor and similar of postural tremor as in [Deu00]:

$$[\text{Deu00*}] = [\text{Deu00, Wenz00, Her07}]$$

The same measurement and quantification of tremor with the use of a laser as in [Her06] was used also in [Par06]:

$$[\text{Her06*}] = [\text{Her06, Par06}]$$

Methods of the processing of ordinary video recordings from [Uhr10] and methods for accelerometer measurements and their processing similar to [Spr11] were used in [Uhr11]:

$$[\text{Uhr10*}] = [\text{Uhr10, Uhr11}]$$

$$[\text{Spr11*}] = [\text{Spr11, Uhr11}]$$

B.9 The list of publications

Ran73 J. E. Randall. A stochastic time series model for hand tremor. *J Appl Physiol*, 1973.

Mor75 M.H. Morgan, R.L. Hewer, and R. Cooper. Intention tremor: a method of measurement. *J Neurol Neurosur Ps*, 1975.

Fro78 J.D. Frost, Jr. Triaxial vector accelerometry: A method for quantifying tremor and ataxia. *IEEE T Biomed Eng*, 1978.

Elb90 R.J. Elble, R. Sinha, and C. Higgins. Quantification of tremor with a digitizing tablet. *J Neurosci Meth*

Gre90 M. Gresty and D. Buckwell. Spectral analysis of tremor: understanding the results. *J Neurol Neurosur Ps*, 1990.

Gan92 C. Gantert, J. Honerkamp, and J. Timmer. Analyzing the dynamics of hand tremor time series. *Biol Cybern*, 1992.

Elb94 R.J. Elble, C. Higgins et al. Factors influencing amplitude and frequency of essential tremor. *Movement Disord*, 1994.

Pul94 S.L. Pullman, B. Elibol, and S. Fahn. Modulation of parkinsonian tremor by radial nerve palsy. *Neurology*, 1994.

Tro94 R.M. Trosch and S.L. Pullman. Botulinum toxin A injections for the treatment of hand tremors. *Movement Disord*, 1994.

Hal95 D.M. Halliday, J.R. Rosenberg et al. A framework for the analysis of mixed time series/point process data – theory and application to the study of physiological tremor, single motor unit discharges and electromyograms. *Progress in Biophysics and Molecular Biology*, 1995.

Deu96 G. Deuschl, P. Krack et al. Clinical neurophysiology of tremor. *J Clin Neurophysiol*, 1996.

Elb96 R.J. Elble, M. Brilliant et al. Quantification of essential tremor in writing and drawing. *Movement Disord*, 1996.

Tim96 J. Timmer, M. Lauk, and G. Deuschl. Quantitative analysis of tremor time series. *Electroen Clin Neuro*, 1996.

Cap97 A. Cappello, A. Leardini et al. Application of stereophotogrammetry to total body three-dimensional analysis of human tremor. *IEEE T Rehabil Eng*, 1997.

Lou98 E.D. Louis, K.J. Wendt et al. Is essential tremor symmetric? *Arch Neurol*, 1998.

Spy98 J.M Spyers-Ashby, P.G. Bain, and S.J. Roberts. A comparison of fast fourier transform (FFT) and autoregressive (AR) spectral estimation techniques for the analysis of tremor data. *J Neurosci Meth*, 1998.

Som98 E.J.W. van Someren, B.F. Vonk et al. A new actigraph for long-term registration of the duration and intensity of tremor and movement. *IEEE T Biomed Eng*, 1998.

Tim98 J. Timmer, M. Lauk et al. Cross-spectral analysis of physiological tremor and muscle activity: I Theory and application to unsynchronized electromyogram; II Application to synchronized electromyogram. *Biol Cybern*, 1998.

Tim98b J. Timmer. Modeling noisy time series: Physiological tremor. *Int J Bifurcat Chaos*, 1998.

Foe99 F. Foerster and M. Smeja. Joint amplitude and frequency analysis of tremor activity. *Electromyo Clin Neur*, 1999.

Hal99 D.M. Halliday, B.A. Conway et al. Load-independent contributions from motor-unit synchronization to human physiological tremor. *J Neurophysiol*, 1999.

Lau99 M. Lauk, J. Timmer et al. A software for recording and analysis of human tremor. *Comput Meth Prog Bio*, 1999.

Mat99 J.Y. Matsumoto, D.W. Dodick et al. Three-dimensional measurement of essential tremor. *Movement Disord*, 1999.

Nor99 K.E. Norman, R. Edwards, and A. Beuter: The measurement of tremor using a velocity transducer: comparison to simultaneous recordings using transducers of displacement, acceleration and muscle activity. *J Neurosci Meth*, 1999.

Spy99 J.M. Spyers-Ashby, M. J. Stokes et al. Clasification of normal and pathological tremors using a multidimensional electromagnetic system. *Med Eng Phys*, 1999.

Deu00 G. Deuschl, R. Wenzelburger et al. Essential tremor and cerebellar dysfunction: Clinical and kinematic analysis of intention tremor. *Brain*, 2000.

Elb00 R.J. Elble. Essential tremor frequency decreases with time. *Neurology*, 2000.

Lou00 E.D. Louis, E. Yousefzadeh et al. Validation of a portable instrument for assesing tremor severity in epidemiologic field studies. *Movement Disord*, 2000.

Raj00 V. Rajaraman, D. Jack at al. A novel quantitative method for 3D measurement of Parkinsonian tremor. *Clin Neurophysiol*, 2000.

Tim00 J. Timmer, M. Lauk et al. Cross-spectral analysis of tremor time series. *Int J Bifurcat Chaos*, 2000.

Tim00b J. Timmer, S. Häussler et al. Pathological tremor: Deterministic chaos or nonlinear stochastic oscilators? *Chaos*, 2000.

Wend00 K.J. Wendt, S.M. Albert et al. Columbia University Assesment of Disability in Essential Tremor (CADET): methodological issues in essential tremor research. *Parkinsonism Relat D*, 2000.

Wenz00 R. Wenzelburger, J. Raethjen et al. Kinetic tremor in a reach-to-grasp movement in Parkinson's disease. *Movement Disord*, 2000.

Lau01 M. Lauk, J. Timmer et al. Variability of frequency and phase between antagonistic muscle pairs in pathological human tremors. *Muscle Nerve*, 2001.

Lou01 E.D. Louis and S.L. Pullman. Comparison of clinical vs. electrophysiological methods of diagnosing of essential tremor. *Movement Disord*, 2001.

Mor01 S. Morrison and J. Keogh. Changes in the dynamics of tremor during goal-directed pointing. *Hum Movement Sci*, 2001.

Oka01 K. Okada, S. Hando et al. Analysis of pathological tremors using the autoregression model. *Frontiers of Medical & Biological Engineering*, 2001.

Tit01 M.S. Titcombe, L. Glass et al. Dynamics of parkinsonian tremor during deep brain stimulation. *Chaos*, 2001.

Bre02 K.C. Brennan, E.C. Jurewicz et al. Is essential tremor predominantly a kinetic or a postural tremor? A clinical and electrophysiological study. *Movement Disord*, 2002.

Bur02 P.R. Burkhard, J.W. Langston, and J.W. Tetrud. Voluntarily simulated tremor in normal subjects. *Neurophysiol Clin*, 2002.

Ang03 W.T. Ang, P.K. Khosla, and C.N. Riviere: Design of all-accelerometer inertial measurement unit for tremor sensing in hand-held microsurgical instrument. In *IEEE International Conference on Robotics and Automation*, 2003.

Coh03 O. Cohen, S. Pullman et al. Rest tremor in patients with essential tremor: Prevalence, clinical correlates, and electrophysiologic characteristics. *Arch Neurol*, 2003.

Elb03 R.J. Elble. Characteristics of physiologic tremor in young and elderly adults. *Clin Neurophysiol*, 2003.

Sap03 N. Sapir, R. Karasik et al. Detecting scaling in the period dynamics of multimodal signals: Application to Parkinsonian tremor. *Phys Rev*, 2003.

Zeu03 K.E. Zeuner, F.M. Molloy et al. Effect of ethanol on the central oscilator in essential tremor. *Movement Disord*, 2003.

Cal04 M.P. Caligiuri and R.M. Tripp. A portable hand-held device for quantifying and standardizing tremor assessment. *J Med Eng Tech*, 2004.

Pel04 B. Pellegrini, L. Faes et al. Quantifying the contribution of arm postural tremor to the outcome of goal-directed pointing task by displacement measures. *J Neurosci Meth*, 2004.

Rae04 J. Raethjen, M. Lauk et al. Tremor analysis in two normal cohorts. *Clin Neurophysiol*, 2004.

Elb05 R.J. Elble. Gravitational artifact in accelerometric measurement of tremor. *Clin Neurophysiol*, 2005.

Mor05 S. Morrison, J. Kavanagh et al. The effects of unilateral muscle fatigue on bilateral physiological tremor. *Exp Brain Res*, 2005.

Stu05 M.M. Sturman, D.E. Vaillancourt, and D.M. Corcos. Effects of aging on the regularity of physiological tremor. *J Neurophysiol*, 2005.

Zha05 J. Zhang and F. Chu. Real-Time Modeling and Prediction of Physiological Hand Tremor. *Proceedings of IEEE Int Conf Acoust Spee*, 2005.

Her06 M.E. Héroux, S.L. Parisi et al. Upper-extremity disability in essential tremor. *Arch Phys Med Rehabil*, 2006.

Par06 S.L. Parisi, M.E. Héroux et al. Functional mobility and postural control in essential tremor. *Arch Phys Med Rehabil*, 2006.

Som06 E.J.W. van Someren, M.D. Pticek et al. New actigraph for long-term tremor recording. *Movement Disord*, 2006.

Bir07 M.J. Birdno, S.E. Cooper et al. Pulse-to-pulse changes in the frequency of deep brain stimulation affect tremor and modeled neuronal activity. *J Neurophysiol*, 2007.

Her07 J. Herzog, W. Hamel et al. Kinematic analysis of thalamic versus subthalamic neurostimulation in postural and intention tremor. *Brain*, 2007.

Kun07 A.M. Kuncel, S.E. Cooper et al. Amplitude- and Frequency-Dependent Changes in Neuronal Regularity Parallel Changes in Tremor With Thalamic Deep Brain Stimulation. *IEEE T Neur Sys Reh*, 2007.

Sal07 A. Salarian, H. Russman et al. Quantification of tremor and bradykinesia in Parkinson's disease using a novel ambulatory monitoring system. *IEEE T Biomed Eng*, 2007.

Sla07 P.S. Slack and X. Ma. Tremor amplitude determination for use in clinical applications. *Meas Sci Technol*, 2007.

Ulm07 O. Ulmanová, C. N. Homann et al. Tremor magnitude: A single index to assess writing and drawing in essential tremor. *Parkinsonism Relat D*, 2007.

Hon08 S.L. Hong, E.G. James, and K.M. Newell. Coupling and irregularity in the aging motor system: tremor and movement. *Neurosci Lett*, 2008.

Ker08 G. Kerr, S. Morrison, and P. Silburn. Coupling between limb tremor and postural sway in Parkinson's disease. *Movement Disord*, 2008.

Mor08 S. Morrison, G. Kerr et al. Differential time- and frequency-dependent structure of postural sway and finger tremor in Parkinson's disease. *Neurosci Lett*, 2008.

Bar09 A. Bartolić, M. Šantić, and S. Ribarič. Automated tremor amplitude and frequency determination from power spectra. *Comput Meth Prog Bio*, 2009.

Giu09 J.P. Giuffrida, D.E. Riley et al. Clinically deployable Kinesia technology for automated tremor assessment. *Movement Disord*, 2009.

Pow09 H.C Powel, jr., M.A. Hanson, and J. Lach. On-body inertial sensing and signal processing for clinical assessment of tremor. *IEEE T Biomed Circuits Syst*, 2009.

Vin09 R. Vinjamuri, D.J. Crammond et al. Extraction of sources of tremor in hand movements of patients with movement disorders. *IEEE T Inf Technol B*, 2009.

Gal10 J.A. Gallego, E. Rocon et al. Real-time estimation of pathological tremor parameters from gyroscope data. *Sensors*, 2010.

Leg10 A. Legros, H.R. Marshall et al. Effects of acute hypoxia on postural and kinetic tremor. *Eur J Appl Physiol*, 2010.

Uhr10 Z. Uhríková, E. Růžička et al. TremAn: A tool for measuring tremor frequency from video sequences. *Movement Disord*, 2010.

Spr11 O. Šprdlík, Z. Hurák et al. Tremor analysis by decomposition of acceleration into gravity and inertial acceleration using inertial measurement unit. *Biomed Signal Process Control*, 2011.

Uhr11 Z. Uhríková, O. Šprdlík et al. Validation of a new tool for automatic assessment of tremor frequency from video recordings *J Neurosci Meth*, 2011.